DISSERTATION

HEAVY FERMION BEHAVIOR IN SELECTED CE-BASED COMPOUNDS: MAGNETISM AND SUPERCONDUCTIVITY

Submitted by
A.D. Christianson
Department of Physics

In partial fulfillment of the requirements
For the Degree of Doctor of Philosophy
Colorado State University
Fort Collins, Colorado
Spring 2003

ProQuest Information and Learning Company
300 North Zeeb Road
P.O. Box 1346
Ann Arbor, MI 48106-1346

COLORADO STATE UNIVERSITY

March 20, 2003

WE HEREBY RECOMMEND THAT THE DISSERTATION PREPARED UNDER OUR SUPERVISION BY A.D. CHRISTIANSON ENTITLED HEAVY FERMION BEHAVIOR IN SELECTED CE-BASED COMPOUNDS: MAGNETISM AND SUPERCONDUCTIVITY BE ACCEPTED AS FULLFILING IN PART REQUIREMENTS FOR THE DEGREE OF DOCTOR OF PHILOSOPHY.

Committee on Graduate Work

Adviser

Department Head

ABSTRACT OF DISSERTATION
HEAVY FERMION BEHAVIOR IN SELECTED CE-BASED COMPOUNDS:
MAGNETISM AND SUPERCONDUCTIVITY

$CeRhIn_5$ is a member of the recently discovered series of heavy fermion superconductors $CeMIn_5$ (M = Co, Rh, Ir). Initial investigations showed that $CeRhIn_5$ undergoes an antiferromagnetic transition at 3.8 K, but that application of pressure induces a superconducting state with the unusually high T_c of 2.1 K. With the discovery that the other members of the $CeMIn_5$ family were ambient pressure superconductors it became apparent that this series offered an exceptional opportunity to explore systemically the unconventional magnetic and superconducting heavy fermion ground states.

The objective of this dissertation is to explore in further detail the nature and relation of the heavy fermion magnetic and superconducting ground states in $CeMIn_5$ with particular emphasis on the properties of antiferromagnetic $CeRhIn_5$. Information about these systems will be extracted using two techniques: (1) measurements of the electrical resistivity of single crystals in applied magnetic fields to 18 T; and (2) measurements of inelastic neutron scattering response of powdered single crystals.

Magnetotransport studies reveal a high temperature regime characteristic of single impurity Kondo interactions and a low temperature regime characteristic of a Kondo lattice. Moreover, the anisotropic behavior of the resistivity of $CeRhIn_5$ as well as experimental and theoretical investigations of other workers indicate that crystalline electric fields strongly influence the properties of the $CeMIn_5$ family. To further elucidate the role of crystalline electric field effects in the $CeMIn_5$ series we have determined the energy level splittings and wave functions of $CeRhIn_5$ with inelastic neutron scattering. Using these results, along with estimations of the contribution due to the Kondo effect and magnetic interactions, reasonable fits are obtained to the measured magnetic susceptibility and specific heat. Moreover, we show that our proposal of the crystal field level splitting in $CeRhIn_5$ can account for the magnitude of the ordered moment observed by neutron diffraction, while those of previous work

cannot. Taken together these studies indicate that any detailed understanding of the properties of these materials must account for interactions due to the Kondo effect and magnetic interactions, as well as crystalline electric field effects.

Andrew D. Christianson
Physics Department
Colorado State University
Fort Collins, CO 80523
Spring 2003

ACKNOWLEDGEMENTS

I would like to acknowledge the great number of people who have contributed scientifically to the work presented in this dissertation: My advisors Alex Lacerda and Sanford Kern, J.M. Lawrence, M.F. Hundley, J.L. Sarrao, N.O. Moreno, P.G. Pagliuso, W. Bao, E.A. Goremychkin, P.S. Riseborough, J.D. Thompson, and R.J. McQueeney. My friends and colleges S. Patamia and B. Gamble have contributed much in the way of suggestions and encouragement. In addition, I have had a number of fruitful discussions with G.H. Lander regarding the material in this dissertation as well as other projects that I had occasion to be involved in. Furthermore, I have had productive interactions with virtually all of the National High Magnetic Field laboratory staff. Of particular importance, was the technical support provided by M. Pacheco and J. Betts.

I am grateful for the enormous amount of support and encouragement given by my family and friends in this endeavor. Most importantly, my wife, Dina, for all of her love and support. My family (Gayle, Delmar, Renee, and Nathan) has provided love and encouragement from the very beginning. I have had the privilege of many friendships throughout my life, specifically I thank J. Welton and J. Ludwig for their continued friendship these many years. During my time at Colorado State University I have had the privilege to know a number of students and faculty that have had a profound influence upon me. Of particular importance are J. Atteberry, E. Birath, S. Kalarickal, and R. Komara. Finally, I thank all of those who supported me after the fire which took nearly all of my material possessions.

During my tenure at Los Alamos National Laboratory financial support has been provided by the Department of Energy and the National Science Foundation. I had the opportunity to be stationed at two national user facilities, the Los Alamos Neutron Science Center and the National High Magnetic Field Laboratory. The scientific work of collaborators has been supported financially as follows: Work at UC Irvine was supported by UCDRD funds provided by the University of California for the conduct of discretionary research by the Los Alamos National Laboratory and by the

UC/LANL Personnel Assignment Program. Work at Los Alamos and Argonne was performed under the auspices of the DOE. Work at Temple University was supported by the Department of Energy, award DE-Fg02-01ER45827.

Los Alamos, New Mexico
March 20, 2002

Andrew Christianson

To Dina.

Table of Contents

List of Tables

List of Figures

Chapter 1

Introduction

The purpose of this dissertation is to contribute to the understanding of the properties of heavy fermion systems. We have chosen to focus on understanding aspects of the properties of a new series of heavy fermion superconductors, namely $CeMIn_5$ (M = Co, Rh, Ir). This series is subset of a larger series of heavy fermion materials based upon $CeIn_3$. The similarities and peculiarities of each member within the $CeMIn_5$ series and the close relationship to a number of other heavy fermion systems offer the opportunity for systematic comparisons that were previously possible in only limited cases. We have elected to take advantage of this unique opportunity through experimental investigations employing two probes: magnetotransport and inelastic neutron scattering. A central theme in both types of experiments will be the influence of the Kondo effect, the Ruderman-Kittel-Kasuya-Yosida (RKKY) exchange interaction, and crystal field effects upon the physical properties of $CeMIn_5$. In the following introductory section, we briefly review relevant aspects of the field of heavy fermion physics and outline the contributions of this dissertation; following that, we introduce important theoretical concepts. The final section contains information relating to the specific properties of the $CeMIn_5$ family.

1.1 General Overview

The unique physics occurring in strongly correlated electron systems has sparked intense interest within the condensed matter physics community. Stated simply, a strongly correlated electron system is one in which the interactions between electrons may not be neglected. Like many of the problems at the frontiers of modern physics, the properties of strongly correlated electron systems are intimately related to the many body physics present. Strongly correlated electron behavior is found to lead to a large number of diverse physical phenomena: from the superconductivity found in molecular conductors and the high T_c cuprates, to the colossal magnetoresistance found in the manganites, to the Kondo physics and the exotic magnetic and superconducting ground states in the mixed valence and heavy fermion materials, etc. This dissertation will address aspects of the strongly correlated electron behavior present in heavy fermion materials. What follows, is a brief summary of the status of the field of heavy fermion physics as well as a description of the problems and discussions to which this dissertation seeks to contribute.

In 1975 experimental investigations of the specific heat and resistivity in $CeAl_3$ revealed interesting behavior at low temperature. As anticipated for a metal at low temperature, the specific heat displayed a region linear in temperature while the electrical resistivity followed a T^2 behavior [7]. Remarkably, the coefficients of the linear term in the specific heat and of the T^2 in the resistivity were enormous when compared to those observed in other metallic systems. At that time, the large enhancement of the low temperature coefficients was considered unusual, but did not stimulate great interest within the condensed matter physics community. However, in 1979, the discovery that $CeCu_2Si_2$ is superconducting at 0.5 K [8] launched the

field of heavy fermion physics. The importance of this discovery lies in the identification of the charge carriers participating in the superconductivity as the same as those responsible for the huge linear term in the specific heat. This follows from the interpretation of the large linear term in the specific heat being due to heavy fermions (large effective mass charge carrier quasiparticles)and the jump in the in the specific heat at the superconducting transition being proportional to the linear term in the specific heat and the superconducting transition temperature. Notably, the conventional wisdom was that in a material such as $CeCu_2Si_2$ the strong magnetic interactions thought to be present would preclude the formation of a superconducting state. This was an early indication that the mechanism responsible for heavy fermion superconductivity was magnetic in origin rather than being due to electron phonon coupling.

Subsequently, an intense search began for other materials which displayed superconductivity coupled with a large enhancement of the specific heat (the so called heavy fermion superconductors). The next examples of heavy fermion superconductivity were UBe_{13} [9] and UPt_3 [10]. Both materials were found to be superconducting at temperatures similar to that of $CeCu_2Si_2$ with transition temperatures of 0.85 K and 0.54 respectively. One important similarity among these three materials is that all appeared to have localized f-electrons which were expected to exhibit strong magnetic interactions.

While magnetic interactions were thought to be strong in both $CeCu_2Si_2$ and UBe_{13}, UPt_3 not only exhibits strong magnetic interactions [10], but antiferromagnetic order at 5 K [11] as well. Neutron scattering investigations of UPt_3 [11] found that the magnetic state ceases to evolve at the onset of superconductivity. This result

establishes a close relationship between magnetism and superconductivity in UPt_3. Another heavy fermion system which exhibits both magnetism and superconductivity is URu_2Si_2 [12]. URu_2Si_2 bears some similarity to UPt_3 in that the magnetic transition occurs at higher temperature than the superconducting transition. However, the situation appears to be somewhat more complex in URu_2Si_2 as the magnetism appears to be coupled to some other undiscovered hidden order [13].

Further evidence for the need to consider the magnetic interactions in heavy fermion systems is given by examining heavy fermion behavior under the influence of applied magnetic fields. A prime example of this is the metamagnetic transitions found in a number of heavy fermion systems including: $CeRu_2Si_2$ [14, 15], URu_2Si_2 [16], and UPt_3 [17]. In particular, the observation of a metamagnetic transition in UPt_3 reinforces the notion that magnetic interactions play a crucial role. While not all heavy fermion materials appear to exhibit a metamagnetic transition (e.g., UBe_{13} [18]), the field-induced evolution of the properties of heavy fermion systems provide important information on the type of ground states present.

Another important class of superconductors where magnetic interactions are thought to be important are the so-called high T_c superconductors. These materials are particularly interesting because of the high superconducting transition temperatures observed (e.g., $YBa_2Cu_3O_7$ with a $T_c = 90$ K [19, 20]). As in heavy fermion materials, magnetic interactions are important to the properties of high T_c materials [21]. This fact has lead to a number of theoretical attempts to describe the pairing mechanism as being mediated by magnetic fluctuations in both heavy fermion and high T_c materials. [22, 23, 24] Another similarity between the high T_c and heavy fermion systems is the linear temperature dependence of the electrical resistivity above the

superconducting transition(e.g., [25] and [2]). The high transition temperatures observed in the high T_c materials as opposed to the much lower transition temperatures observed in the heavy fermion systems may be due, in part, to the higher degree of anisotropy/lower dimensionality observed in the high T_c materials [26]. In fact, theoretical predictions indicate the superiority of 2-dimensional over 3-dimensional fluctuations in enhancement of T_c [27]. The effect of anisotropy/dimensionality has not yet been fully explored in heavy fermion systems.

The unique physics present in heavy fermion superconductors, coupled with possible carryover toward understanding the high T_c materials, is motivation to examine additional examples of heavy fermion superconductivity. The importance of magnetic interactions in heavy fermion superconductors suggests examining the relationship of magnetism with heavy fermion superconductors. Further impetus arises from the fact that sample quality is an important issue [8, 28, 29] for many heavy fermion superconducting materials. However, finding new examples of heavy fermion superconductivity has proven extremely difficult. Until recently, the only Ce-based heavy fermion superconductor at ambient pressure was $CeCu_2Si_2$. Even among U-based compounds where there are several more examples, the choices are limited.

One avenue for pursuing heavy fermion superconductivity in Ce-based systems has been to induce superconductivity with the application of pressure. Several examples have been found, including $CeCu_2Ge_2$ [30], $CeRh_2Si_2$ [31], $CePd_2Si_2$ [2], and $CeIn_3$ [2]. In these materials an antiferromagnetic transition is suppressed with increasing pressure and at some critical pressure superconductivity appears. It is interesting to note that not all heavy fermion antiferromagnets are amenable to inducing superconductivity by suppressing a magnetic transition. In some materials, such as $Ce_3Pt_4In_{13}$,

the Néel temperature increases with application of experimentally accessible pressures [32]. In some cases, another means of applying pressure is available, namely chemical pressure. The pressure in this instance is provided by substituting either larger or smaller ions into a material. A larger ion will expand the lattice, corresponding to a negative pressure, while a smaller ion will compress the lattice, corresponding to a positive pressure. However, complications may arise from disorder and other effects causing difficulty in interpreting data obtained in this way. As an example of the usefulness of chemical pressure consider $CeRu_2Si_2$. With a small amount of La substitution the magnetic fluctuations present in the parent compound lock in and long range antiferromagnetic order is established[33]. The dramatic difference in the behavior of Ce-based heavy fermion antiferromagnets under pressure underscores the need for further understanding of the complex interactions present in heavy fermion materials.

$CeIn_3$ provides an interesting example of a material in which superconductivity exists on the border of antiferromagnetic order. At ambient pressure at 10 K $CeIn_3$ undergoes an antiferromagnetic transition. Upon application of pressure the antiferromagnetic transition is smoothly suppressed toward zero[2, 34] (Fig 1.1a). After the magnetic order apparently disappears at the critical pressure, superconductivity is observed. This leads to the following argument due to ref. [2]: since the superconducting state borders a magnetic state, strong magnetic fluctuations must occur within the superconducting state and that these are the fluctuations responsible for creating the superconducting state. These arguments have lead to the proposal of a phase diagram where magnetic fluctuations are responsible for the formation of a superconducting state (Fig. 1.1b). Unfortunately, the experimental limitations

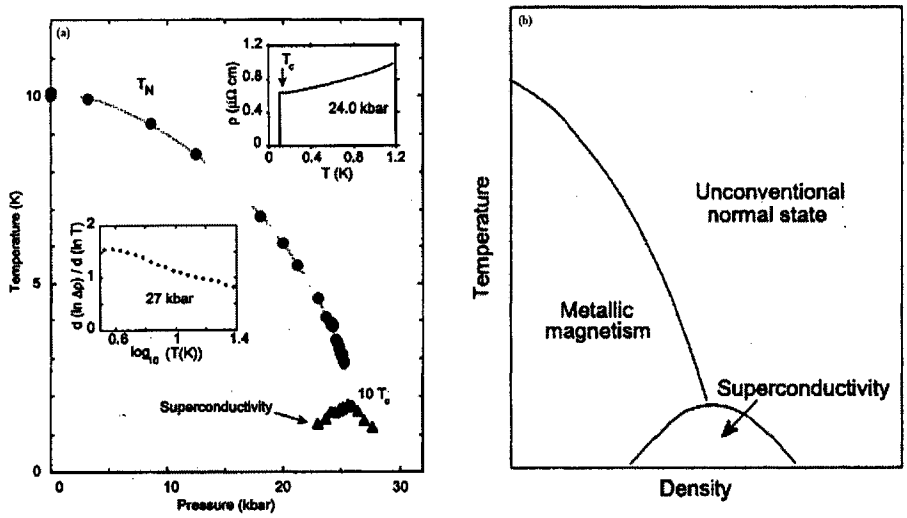

Figure 1.1: Figures from ref. [2] (a) Displays the phase diagram of high-purity single-crystal $CeIn_3$ as determined by resistivity (ρ) measurements for various applied pressures. Notice the smooth depression of T_N with increasing pressure. The upper inset displays the resistivity (ρ) versus temperature at a pressure of 24 kbar. The superconducting transition is the sharp drop in ρ. (b) Proposed phase diagram for a magnetic material in which superconductivity may be induced by the strong magnetic fluctuations present on the border of the magnetic transition.

imposed by the presence of a pressure cell make extensive systematic study of the general relevance of this phase diagram difficult.

A new family of Ce-based heavy fermions related to $CeIn_3$ was recently discovered that exhibits a complex phase diagram which challenges our understanding of correlated electron physics and provides new opportunities for exploration of the interplay of magnetism and superconductivity in heavy fermion systems. [3, 35, 36] This family has a generalized chemical formula, $Ce_mM_nIn_{3m+2n}$, where M is Rh, Ir, or Co. All compounds investigated to date (m = 1, 2 and n = 1), except cubic $CeIn_3$, crystallize in a tetragonal structure (space group P4/mmm)[37]. The most notable properties in this series of compounds include ambient-pressure magnetic order (T_N

= 3.8 K) and pressure-induced superconductivity (T_c = 2.1 K at 16 kbar pressure) in $CeRhIn_5$ [3, 38, 39] and unconventional [40] ambient-pressure superconductivity in both $CeIrIn_5$ (T_c = 0.4 K) and CeCoIn5 (T_c = 2.3 K); the transition temperature for $CeCoIn_5$ is the highest ambient-pressure T_c reported to date for a heavy fermion superconductor. The sample dependencies in the $Ce_mM_nIn_{3m+2n}$ family seem to be less important than in $CeCu_2Si_2$, and this coupled with the fact that large (as big as 1 cm^3) single crystals are available lends these materials to a systematic investigation of the interplay of superconductivity and magnetism in heavy fermion materials.

The objective of this dissertation is to explore in further detail the nature and relation of the heavy fermion magnetic and superconducting ground states in $CeMIn_5$ (M = Rh, Ir, Co) with particular emphasis on the properties of $CeRhIn_5$. The remainder of chapter 1 will be devoted to additional background material including basic theoretical notions in the field of heavy fermion physics and general properties of the $Ce_mM_nIn_{3m+2n}$ family.

1.2 Theoretical Overview

1.2.1 General Properties of a Heavy Fermion

The term heavy fermion arises from the identification of the large low temperature specific heat with massive (heavy) charge carriers (Fermions). This may be seen from simple arguments based on the Sommerfeld theory of metals [41]. The essence of the Sommerfeld model is to treat the conduction electrons in a solid as a degenerate Fermi gas. This yields the electronic (EL) term in the specific heat as:

$$C_{EL} = \frac{\pi^2}{3} k_B^2 T g(\varepsilon_F) \tag{1.2.1}$$

where k_B is Boltzmann's constant, T is the temperature, and $g(\varepsilon_F)$ is the density of states at the Fermi energy, and is given by

$$g(\varepsilon_F) = \frac{mk_F}{\hbar^2\pi^2}. \tag{1.2.2}$$

where k_F is the Fermi wave vector and m is the charge carrier effective mass. By combining equations 1.2.1 and 1.2.2 we obtain

$$C_{EL} = \frac{mk_F k_B^2}{3\hbar^2}T. \tag{1.2.3}$$

In addition to an electronic term in the low temperature specific, there is a term due to phonons which varies as T^3. The low temperature specific heat of a metal is then written as

$$C = \gamma T + aT^3, \tag{1.2.4}$$

where γ is the coefficient of T in eq. 1.2.3 and a is a constant which depends on the phonon modes present in the material.

Within the framework of the Sommerfeld model an experimental observation of a large linear term in the specific heat implies a large density of states at the Fermi surface, which in turn implies a large effective mass for the charge carriers. The charge carriers are not single electrons or holes, but are collective excitations often referred to as quasiparticles [1]. However, the issue of assigning a material the name heavy fermion is more complex than just observing a large specific heat at low temperature. An enhancement to the specific heat can be due to several factors including the presence of a phase transition. The presence of a phase transition in the same temperature region as the appearance of a band of heavy quasiparticles at the Fermi surface leads to difficulty in interpreting the real enhancement due to heavy fermion behavior and

[1] for a definition of a quasiparticle see section 1.2.2 and references therein

not just the cooperative phenomena of a phase transition. In addition, closely spaced crystal field levels can lead to enhancement of the specific heat and has produced the erroneous designation of heavy fermion in some materials [42]. Even among heavy fermion materials there are deviations from eq. 1.2.4. In UPt_3, eq. 1.2.4 must be modified to fully account for the behavior of the low temperature specific heat. The specific heat [10] for UPt_3 is given by

$$C = \gamma T + aT^3 + C_{SF} \tag{1.2.5}$$

where

$$C_{SF} = \gamma^3 T + \delta T^3 \ln\left[\frac{T}{T_{SF}}\right] \tag{1.2.6}$$

The extra contribution (eq. 1.2.6) to the specific heat is due to spin fluctuations. The spin fluctuation contribution was originally calculated to explain the properties of ^{3}He [43]. In fact, certain properties of heavy fermion materials bear a remarkable similarity to those of ^{3}He. This will be explained in more detail in the following section.

1.2.2 Fermi Liquid Theory

In 1957, Landau formulated Fermi liquid theory[44, 45] to explain the properties of liquid ^{3}He. Fermi liquid theory was later extended to the case of electrons in solid materials.[2] The essence of the theory is to treat a strongly interacting system as a system of heavy quasiparticles with weak residual interactions, where by quasiparticle we mean a real particle plus the disturbed particles due to the interaction.[3] A question

[2]for more detail see references [41], [46], or *The Theory of Quantum Liquids I*, D. Pines and P. Nozieres, W.A. Benjamin, Menlo Park, CA, 1966.

[3]for a whimsical, but useful introduction to the concept of a quasiparticle see *A guide to Feynmann Diagrams in the Many Body Problem*, Richard D. Mattuck, New York, McGraw-Hill, 1976 2ed.

immediately arises from the above definition: How strong can the interactions be for Fermi Liquid theory to still apply? A qualitative, but dramatic answer is yielded from comparison of the magnitude of the Sommerfeld parameters of normal metals such as sodium or copper (both ~1 mJ/mole K^2) to those of heavy fermion materials (e.g., 8000 mJ/K^2 for YbBiPt[47] and 1620 mJ/K^2 $CeAl_3$[7]). Clearly, the strength of the interactions can be quite large.

Several experimental quantities which are characteristic of materials which exhibit Fermi liquid behavior are given below.

$$C = \gamma T \tag{1.2.7}$$

$$\chi = \chi_o \tag{1.2.8}$$

$$\rho = AT^2 \tag{1.2.9}$$

The electronic specific heat depends only on the Sommerfeld parameter γ, the magnetic susceptibility, χ, is temperature independent; and the resistivity varies as T^2. These results are quite striking, for this behavior is observed in materials with weakly interacting electrons as well as in the heavy fermion materials where strong interactions are present among the electrons. The source of this agreement is that the properties for both are governed by low lying excitations of the electron fluid. Evidently, in the strongly interacting case it is sufficient for the quasiparticles to behave as Fermions. In which case, the Pauli exclusion principle applies so that the number of low lying excitations is severely restricted in a similar manner to that of the weakly interacting electron fluid. Yet, not all their properties are the same. While the temperature dependence of the quantities from equations 1.2.7,1.2.8, and 1.2.9 is the same for the interacting case and the noninteracting case, the coefficients γ, χ_o, and A are greatly enhanced in the interacting case.

A better understanding of the limits of validity of Fermi liquid theory may be gained by carefully considering the nature of the interactions and the quasiparticles that are created. Consider the weakly interacting case and slowly turning on the interactions: Initially in the noninteracting case the Pauli exclusion principle limits the number of low lying excitations near the Fermi surface. As the interactions are turned on, the single electron states are modified such that it becomes natural to think of the resulting electronic states as consisting of an electron plus the disturbed electronic distribution associated with it due to the interactions (quasiparticles). If the quasiparticles behave as Fermions, then the Pauli principle limits the number of low lying excitations. In this sense, a one-to-one correspondence exists between the low lying excitations of the noninteracting case with the interacting case. If the interactions are such that a one to one correspondence between the electronic states of the noninteracting case and the interacting case is no longer valid Fermi liquid theory does not apply. Any interaction which changes the symmetry of the problem necessarily violates this condition. Thus, in cases where the electron fluid is near a phase transition one would not expect Fermi liquid theory to apply. In fact, an area of great interest among the condensed matter physics community is the study of nonFermi liquid behavior. However, rather than being due to the proximity of a classical phase transition, it appears that in this instance the breakdown of Fermi liquid theory is due to the presence of a quantum critical point.[4] The fluctuations due to the presence of a quantum phase transition persist much farther from the location of the transition than in a classical phase transition, which has led to speculation of

[4]for an introduction to this expanding topic see *Quantum Phase Transitions*, Subir Sachdev, New York, Cambridge University Press, 1999 and G.R. Stewart, "Non-Fermi-liquid Behavior in d- and f-electron metals", Rev. Mod. Phys., vol 73, p. 797, 2001

the importance of the presence of a quantum critical point in explaining the behavior of both the high T_c and the heavy fermion superconductors. Continuing with our discussion of the limits of validity of Fermi liquid theory; as mentioned above, a simple way to visualize a quasiparticle is to imagine it as the real particle plus the cloud of disturbed particles that the interaction has generated. That the lifetime of the quasiparticles be long enough such that they exist for the lifetime of the excited states in the system is crucial-if this is not the case a quasiparticle in an excited state may decay leaving only a bare electron. Then the concept of the quasiparticle is no longer valid and the one to one correspondence ceases to exist for the low lying excitations of the interacting and noninteracting cases. Having now identified the means by which the low temperature specific and other physical quantities are enhanced, we are now left with the question: What are the interactions responsible for quasiparticle formation?

1.2.3 Local Moment Conduction Electron Interactions

The electronic interactions which lead to the exotic behavior observed in heavy fermion systems are the interactions between local moments and conduction electrons. These interactions are due to the localized nature of the f-electrons in the rare earth elements, as opposed to the more delocalized nature of the d-electrons in the transition metals. This explains the lack of examples of heavy fermion materials in d-electron systems [5]. In heavy fermion materials, the most important interactions are the Kondo effect [49] and the Ruderman-Kittel-Kasuya-Yosida (RKKY) [50] exchange interaction. These two interactions have significantly different character and

[5] a notable exception is LiV_2O_4 [48]

each favors a different type of ground state.

The Kondo Effect

The Kondo effect is thought to contain the essential physics necessary to describe the large effective masses in heavy fermion materials. The Kondo effect was first explored in the context of dilute magnetic impurities in a host metal (the single impurity Kondo effect). The hallmark of the single impurity Kondo effect is a minimum in the resistivity of a metal at low temperature. The first observation of a minimum in the resistivity of a metal was seen in gold [51]. Subsequently, it was found that the temperature of the minimum could be affected greatly by the amount and type of impurity present in a metal. It wasn't until 1963 that a significant theoretical formulation was achieved by J. Kondo.

Kondo treated the case of magnetic impurities in a host metallic lattice perturbatively [52]. However, rather than stopping at leading order as previous investigations had done, he found that all higher orders diverged, yielding an infinite resistance. This is in sharp contrast to the temperature independent effect of nonmagnetic impurities [6]. The origin of the minimum in the resistivity at low temperature is the shrinking of the contribution due to phonons while the contribution due to scattering of the conduction electrons by a local magnetic moment of the magnetic impurity ions increases. The key ingredients in the Kondo hamiltonian[7] are a background conduction band of width D; a magnetic impurity which supplies the local moment, which can be either transition metal, a rare earth, or an actinide element; and the local moment conduction electron exchange, J, which determines the strength of the

[6] see section 2.1.1 and references therein.

[7] for more details see ref. [49]

interaction between the local moments and the conduction electrons.

The result of the interaction between the conduction electrons and the local moment is that the conduction electrons screen the local moment on the energy scale T_K, the Kondo temperature. The screening occurs as follows: For $T \gg T_K$ the antiferromagnetic coupling between the conduction electrons and the dilute magnetic impurities is largely disrupted due to thermal randomization; as $T \rightarrow T_K$ the interactions lock in and a virtual bound state forms where the local moment is completely screened by the conduction electrons. It is this screening of the local moment that produces the large number of low lying scattering states that leads to the divergence of the resistivity. Crudely speaking, it is as if the screening of the magnetic impurity has resulted in a larger scattering center and is thus more effective at scattering the conduction electrons. In order to calculate the properties below T_K, appeals must be made to renormalization group methods. The solution of the Kondo problem in this regime is one of the triumphs of many body physics. The Kondo temperature depends on the strength of the exchange interaction and this dependence for small $Jg(\epsilon_F)$ [46] is given by

$$T_K = \frac{1}{g(\epsilon_F)} e^{\left(-\frac{1}{Jg(\epsilon_F)}\right)} \tag{1.2.10}$$

When contemplating the possibility that the Kondo effect may be important to the physical behavior of heavy fermion materials, it is immediately apparent that heavy fermion materials don't simply contain a small number of dilute magnetic impurities but a lattice of localized magnetic moments. This situation calls for consideration of the Kondo lattice model. An important difference between the single impurity Kondo effect and the Kondo lattice is that the density of the local moments in the Kondo lattice allow for interaction among the local moments mediated by the conduction

electrons. This gives rise to such effects as coherence, where the interactions among the impurities yield a periodic condition for the scattering of conduction electrons that results in a decrease in the resistivity. In addition, in the case of the Kondo lattice more careful consideration must be given to the concept of screening as the number of conduction electrons may not be sufficient to fully screen the local moments.

RKKY Interaction

Up to this point we have only considered the onsite conduction electron local moment interaction (Kondo effect), however the prospect of a Kondo lattice suggests the need to consider intersite interactions among the local moments which, in contrast to the Kondo effect, favors a magnetically ordered ground state. One such interaction is the Ruderman-Kittel-Kasuya-Yosida (RKKY) magnetic exchange interaction[50]. The essence of the RKKY interaction is that a local moment polarizes the conduction electrons, which in turn interact with another local moment. The resulting indirect coupling between magnetic moments may be antiferromagnetic or ferromagnetic depending on the distance between the the magnetic moments (Fig. 1.2 and eq. 1.2.11). The conduction electron polorazation is given by

$$F(x) = \frac{xcos(x) + sin(x)}{x^4} \tag{1.2.11}$$

where x = $2k_F r$ and k_F is the Fermi wave vector and r is the distance between local moments.

As mentioned above the polarization of the conduction electrons has a periodicity depending on the Fermi wave vector and the distance between magnetic impurities. Thus the nature of the RKKY exchange interaction can lead to a situation where the local moments are pointing in many different directions. As with the Kondo effect,

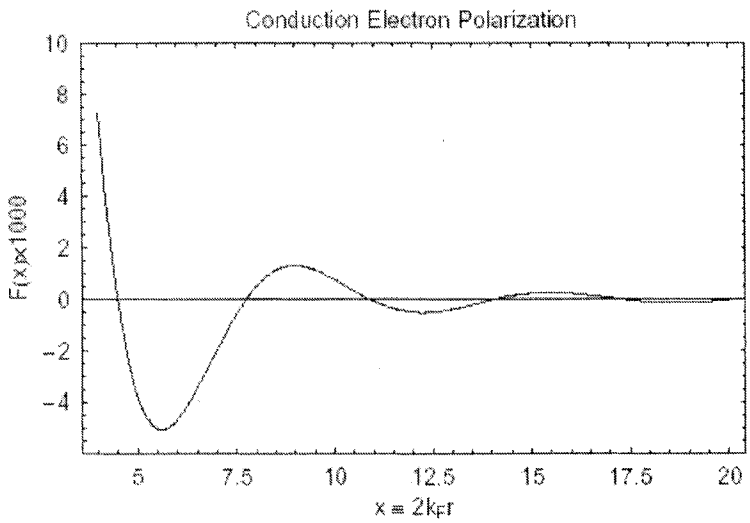

Figure 1.2: Conduction electron polarization for the RKKY exchange interaction given by eq. 1.2.11.

the RKKY interaction depends on the strength of J. However, this dependence takes a different form

$$T_{RKKY} = J^2 g(\epsilon_F) \tag{1.2.12}$$

The significance of the different functional dependence on the conduction electron-local moment exchange interaction (J) is discussed within the framework of the Doniach model in the next section.

The Doniach Model

The Doniach model [53, 54] proposes that the ground state of a heavy fermion material is ultimately determined by the competition between the RKKY magnetic exchange interaction and the Kondo effect. The basic idea is that the same conduction electrons responsible for the Kondo effect and thus the ground state Kondo singlet are also the mediators of the RKKY exchange interaction, which favors a magnetically ordered ground state. The realization of a particular ground state is governed by the different functional dependencies of the Kondo effect (eq. 1.2.10) and the RKKY exchange interaction (eq. 1.2.12) on the density of states at the Fermi level and the conduction electron local moment interaction strength.

Doniach proposed a simple model based in 1-dimension with periodic boundary conditions (a Kondo necklace). Fig. 1.3 displays the functional dependence of the RKKY interaction and the Kondo effect on the exchange interaction. By tuning J, for example by applying pressure or through chemical substitution, there are regions of the Doniach phase diagram where a magnetic ground state is favored (low J values) and regions where a nonmagnetic ground state is favored (high J values).

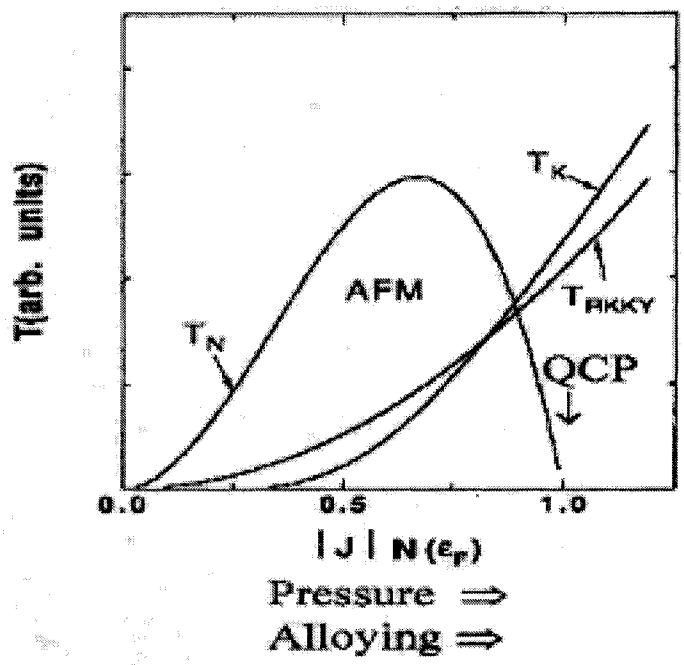

Figure 1.3: The Doniach phase diagram.

The Anderson Hamiltonian

While the single impurity Kondo model and the Kondo lattice provide general insight into the problem of the Kondo effect, they are special cases of the Anderson impurity model and the periodic Anderson model.[8] Additionally, the Anderson lattice model should contain the essential physics to explain the properties of the heavy fermions. However, the complications of the model have thus far prevented detailed theoretical understanding. In light of this fact we discuss the Anderson impurity model in more detail, due to its possible relevance to explaining the crystal field level schemes in $CeMIn_5$.[9]

The Hamiltonian for the Anderson impurity model is given by

$$H = \sum_{\sigma} E_f a^{\dagger}_{f\sigma} a_{f\sigma} + U a^{\dagger}_{f\uparrow} a_{f\uparrow} a^{\dagger}_{f\downarrow} a_{f\downarrow} + \sum_{\mathbf{k}\sigma} \epsilon_{k\sigma} a^{\dagger}_{k\sigma} a_{k\sigma} + \sum_{k\sigma} (V_{\mathbf{k}f} a^{\dagger}_{\mathbf{k}\sigma} a_{f\sigma} + V_{fk} a^{\dagger}_{f\sigma} a_{\mathbf{k}\sigma}) \tag{1.2.13}$$

The first two terms represent the energy cost of placing electrons upon the impurity site. E_f is the energy of the level of local moment, U is the Coulomb repulsion for a doubly occupied level, and a's are the Fermi operators with subscripts $\mathbf{k}$ and σ which denote wave vector and the spin state ($\uparrow$ and $\downarrow$) respectively. The third term represents conduction band states with energies $\epsilon_{k\sigma}$. The final term captures the hybridization, $V_{\mathbf{k}d}$, between the conduction electrons and the impurity. In particular, it is interesting to consider certain limits. The first when $U \gg V$, is the case where the Coulomb repulsion dominates the hybridization which is known as the Kondo limit, in this limit the f-electron occupation is one. The second is for $U \ll V$, when the hybridization dominates the Coulomb repulsion. This situation results in an

[8] see refs. [55, 49, 50].

[9] More details will be given in chapter 5.

f occupation of less than one which is the behavior observed for the intermediate valence compounds.

The Kondo limit is an appropriate limit to consider for heavy fermion systems. It is possible to simplify the situation even further by applying an approximation scheme known as the non-crossing approximation[56, 57]. Here one takes advantage of degeneracy (N) in the problem and expands in $1/N$. In the case of a heavy fermion system the degeneracy is the orbital degeneracy of the localized spin.

1.2.4 Crystal Field Effects

In addition to the conduction electron local moment interactions discussed above, one must consider the perturbation of the local electronic states by the electrostatic potential of the surrounding ions (crystalline electric field (CEF)). As an example of the importance of the crystal fields to the properties of rare earth materials consider the relation between the intermediate valence materials and the heavy fermions. A rough way to make the distinction is that in the intermediate valence materials the Kondo coupling is so large that it smears out each crystal field split level in a multiplet so much that the separate energy levels are no longer distinguishable, giving only a very broad response to probes such as inelastic neutron scattering. In the case of the heavy fermions, the Kondo effect acts on each energy level, but does not cause much smearing between energy levels, giving rise to broadened peaks in the inelastic neutron scattering spectra. It is the latter case that we expect to observe for the $CeMIn_5$ family. Further impetus to consider the effect of crystal fields on the ground state properties of $CeMIn_5$ comes from both experiment[58] and theory[59].

In rare earth materials, the most important splitting of the free ion states is spin-orbit coupling (fig. 1.4). In Ce this splitting is typically of order 300 meV, so for the low temperature properties only the ground state manifold need be considered. In heavy fermion materials, as mentioned above, the effect of the crystal electric field (CEF) must be considered for the ground state manifold. In the case of an insulating materials it is sometimes possible to employ a point charge model [60, 61] that will yield approximate crystal field parameters. However, in metals the situation is much more difficult owing to such effects as screening by the conduction electrons. Nevertheless, a point charge model will still capture the essential symmetry of the problem and allow the selection of the proper terms in the crystal field Hamiltonian.

A concise and useful way to write the CEF Hamilton is in terms of the Stevens operator equivalents [62]. The Stevens operator equivalent method simplifies calculating the matrix elements for the crystal field Hamiltonian by combining the appropriate angular momentum operators into a single operator whose matrix elements are tabulated. Using this notation the CEF Hamiltonian in cubic symmetry can be written as[60]

$$H_{CEF} = B_4^0 \left[O_4^0 + 5O_4^4\right] + B_6^0 \left[O_6^0 - 21O_6^4\right] \tag{1.2.14}$$

where the B_l^m may be determined experimentally or calculated from physical considerations and the O_l^m are the Stevens operator equivalents. The B_l^m account for the strength of the CF interaction as expressed through the symmetry imposed by the operators, O_l^m, where l is limited to, i)to be even and ii) no larger than 6 for f-electrons. More generally for a 4f-electron the Hamiltonian may be written

$$H_{CEF} = \sum_{l,m} B_l^m O_l^m \tag{1.2.15}$$

Now let us return to eq. 1.2.14 for the case of Ce^{3+}. We have stated that we need

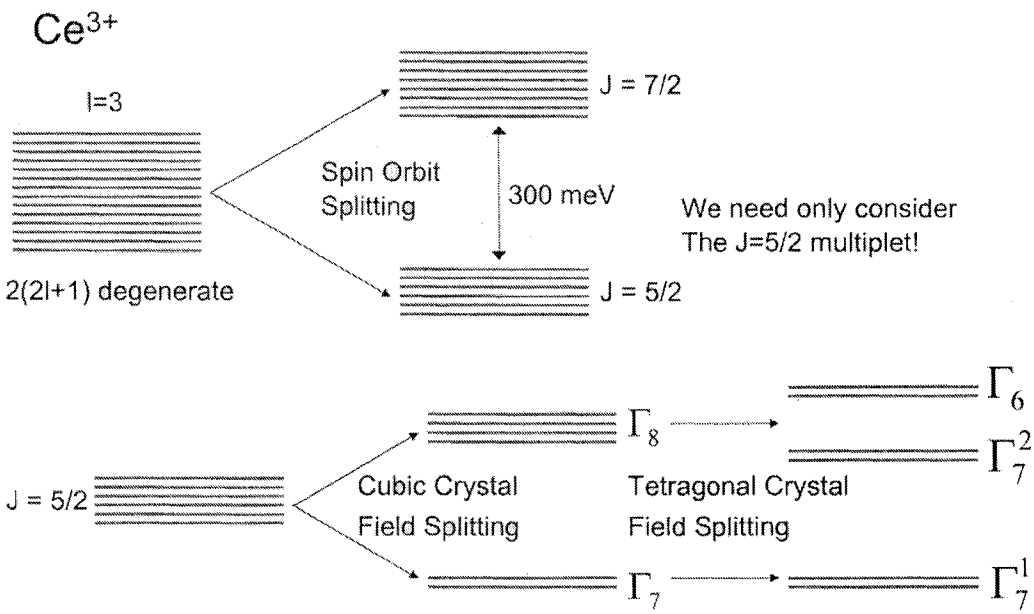

Figure 1.4: Schematic diagram of the effect of the spin orbit and crystal field splitting for Ce^{3+}. J is used here to denote the total angular momentum. Note: For the case of crystal field splitting the symmetry of the environment determines only whether splitting does or does not occur and not the relative energies of the levels to one another.

only consider the $J = \frac{5}{2}$ multiplet (J is used here to denote the total angular momentum) of the $4f^1$ configuration. The sixth order Stevens operators may be neglected because the matrix elements are zero for $J = \frac{5}{2}$ states[60]. The perturbatively split eigenfunctions for all J's have been tabulated in ref. [61]. The wave functions for $J = \frac{5}{2}$ in a cubic environment are

$$|\Gamma_7\rangle = \sqrt{\frac{1}{6}}\left|\pm\frac{5}{2}\right\rangle - \sqrt{\frac{5}{6}}\left|\mp\frac{3}{2}\right\rangle \tag{1.2.16}$$

$$|\Gamma_8\rangle = \begin{cases} \left|\pm\frac{1}{2}\right\rangle \\ \sqrt{\frac{5}{6}}\left|\pm\frac{5}{2}\right\rangle + \sqrt{\frac{1}{6}}\left|\mp\frac{3}{2}\right\rangle \end{cases} \tag{1.2.17}$$

where the kets are labelled by the z component of the total angular momentum, J_z.

For Ce^{3+} there is only 1 f-electron and due to the theory of Kramers [63] for odd-order electron systems the electronic levels must be at least doubly degenerate. However, in the case of cubic symmetry, the Γ_8 contains an accidental degeneracy so its degeneracy is four rather than two as in the case of the Γ_7 (see fig. 1.4). When the symmetry of the problem is changed to tetragonal this degeneracy is lowered with the result that the tetragonal crystal field scheme for $J = \frac{5}{2}$ consists of 3 doublets. The Hamiltonian in this case becomes[64]

$$H_{cef} = B_2^0 O_2^0 + B_4^0 O_4^0 + B_4^4 O_4^4 \tag{1.2.18}$$

Diagonalizing this Hamiltonian results in the following tetragonal-symmetry wave functions.

$$|\Gamma_7^1\rangle = a\left|\pm\frac{5}{2}\right\rangle - b\left|\mp\frac{3}{2}\right\rangle \tag{1.2.19}$$

$$|\Gamma_7^2\rangle = b\left|\pm\frac{5}{2}\right\rangle + a\left|\mp\frac{3}{2}\right\rangle \tag{1.2.20}$$

$$|\Gamma_6\rangle = \left|\pm\frac{1}{2}\right\rangle \tag{1.2.21}$$

The effect of the tetragonal symmetry is to lift the degeneracy of the Γ_8. The Γ_8 splits into a Γ_7 and a Γ_6 in tetragonal symmetry(see fig. 1.4). In addition, the lower symmetry allows for different admixtures of the $\left|\pm\frac{5}{2}\right\rangle$ into the $\left|\mp\frac{3}{2}\right\rangle$ states and will depend on the relative magnitudes of B_2^0, B_4^0 and B_4^4.

There are a number of techniques available for the determination of the the CEF splittings and wave functions in a given system. There are several considerations which eliminate the possibility of calculating the CEF splittings and wave functions through simple means such as the point charge model for the $CeMIn_5$ family. Two of the most noteworthy are: the screening due to conduction electrons and the perturbation of the crystal field levels due to the Kondo effect[65, 66]. Calculations applying density functional theory have been partially successful at calculating the crystal field splitting in simple metallic systems[67]. Such calculations would be particularly interesting in that they may be of use to separate out the effect of Kondo spin fluctuations in $CeMIn_5$; however, including the Kondo effect in these calculations would be a difficult task. We therefore must determine the CEF splittings and wave functions experimentally[10].

1.3 Properties of the $Ce_mM_nIn_{3m+2n}$ Series

1.3.1 General Properties

The discovery that $CeRhIn_5$ is superconducting under pressure [3] and that the phase diagram apparently did not follow that expected from the Doniach model (compare fig. 1.5 to fig. 1.3) indicated the need for further investigations of $CeRhIn_5$ and

[10] see section 2.2.2 for details

related materials. Subsequent efforts to synthesize related materials revealed a surprising array of possibilities [68, 35, 36, 69]. Despite the great diversity of materials discovered, the different members of the family are related through a simple relation, namely, the number of rare earth/In_3 layers separated by a transition metal/In_2 layer.

Fig. 1.6 depicts the structures for the different members of the $Ce_mM_nIn_{3m+2n}$ family. An instructive way to understand the relationship between the various members of the family is as follows: Cubic $CeIn_3$ may be considered to be made of an infinite number of $CeIn_3$ layers. The next group, $CeMIn_5$, is made of alternating layers of $CeIn_3$ and MIn_2. The so called 218 materials, Ce_2MIn_8, can be thought of as being made up of 2 layers of $CeIn_3$ alternating with a layer of MIn_2. Thus, the 218 members should be viewed as an intermediary step between $CeIn_3$ and $CeMIn_5$. The remainder of this thesis will restrict discussion to the single layer 115 materials, with occasional comparisons to the other variants where useful. One of the attractive properties of these materials is the fact that large high quality single crystals can be grown. The method of growth is the self flux growth technique [70, 71, 37].

In the case of $CeRhIn_5$, the single crystal growth procedure is as follows [37]: Ce,Rh, and In with purity better than 99.95 % are combined in the ratio 1:1:20 and placed within an quartz tube. The contents of the quartz tube are then heated to $\sim$1400 K and maintained at that temperature until they reach thermal equilibrium. They are then slowly cooled until $\sim$1000 K, where a centrifuge is used to remove excess In flux. The resulting single crystals can be as large as one cm^3. The crystal structure is tetragonal. The quality of the single crystals can be inferred from a number of different measurements. The residual resistivity ratio is large ($\sim$100 [72, 73]), which indicates that a only small amount of temperature independent disorder scattering

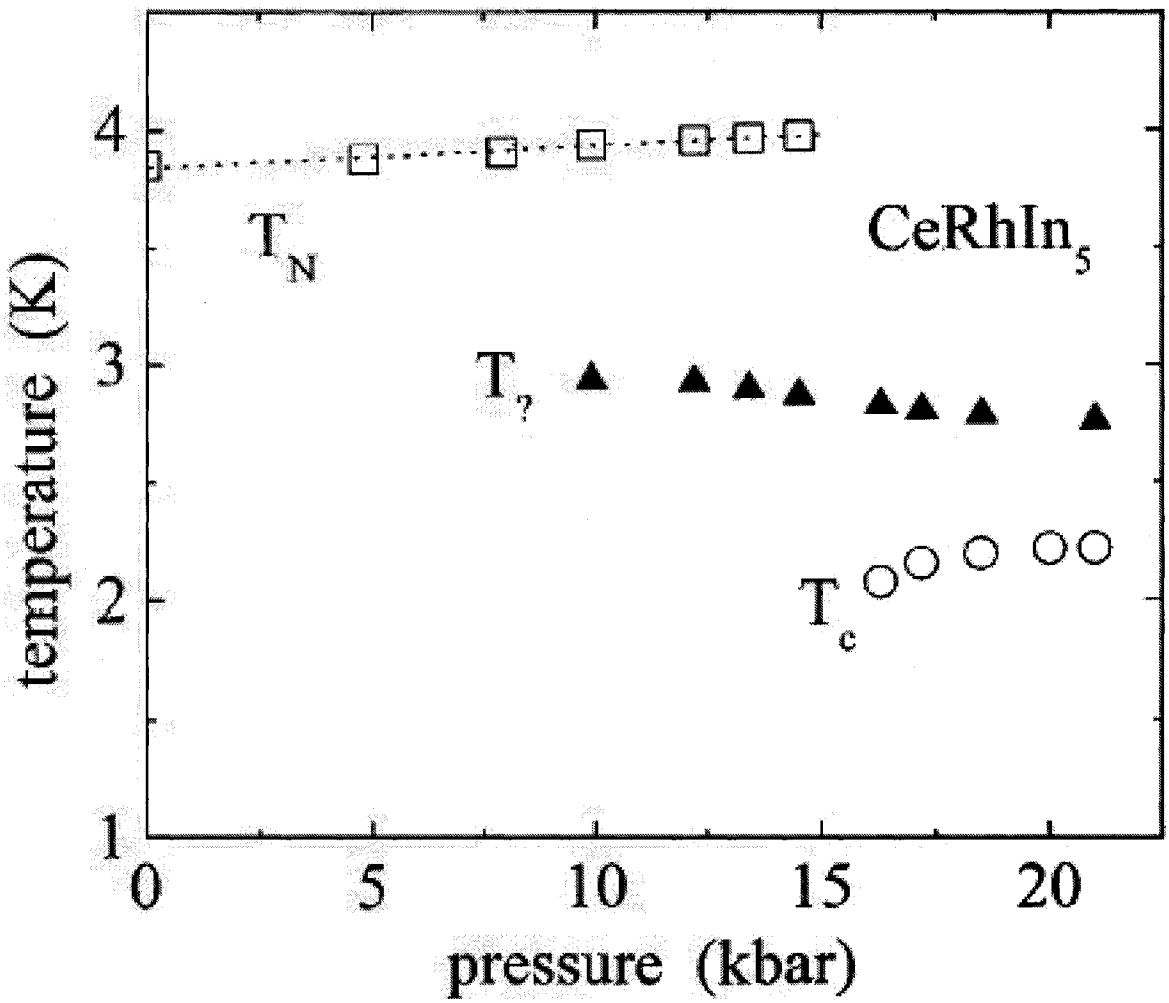

Figure 1.5: From ref. [3]. Temperature-pressure phase diagram for $CeRhIn_5$ determined from resistivity measurements under pressure. Squares represent the antiferromagnetic transition, circles represent the superconducting transition, and triangles represent features in the resistivity of unknown origin. At the time of these measurements the superconducting transition appeared to be first order.

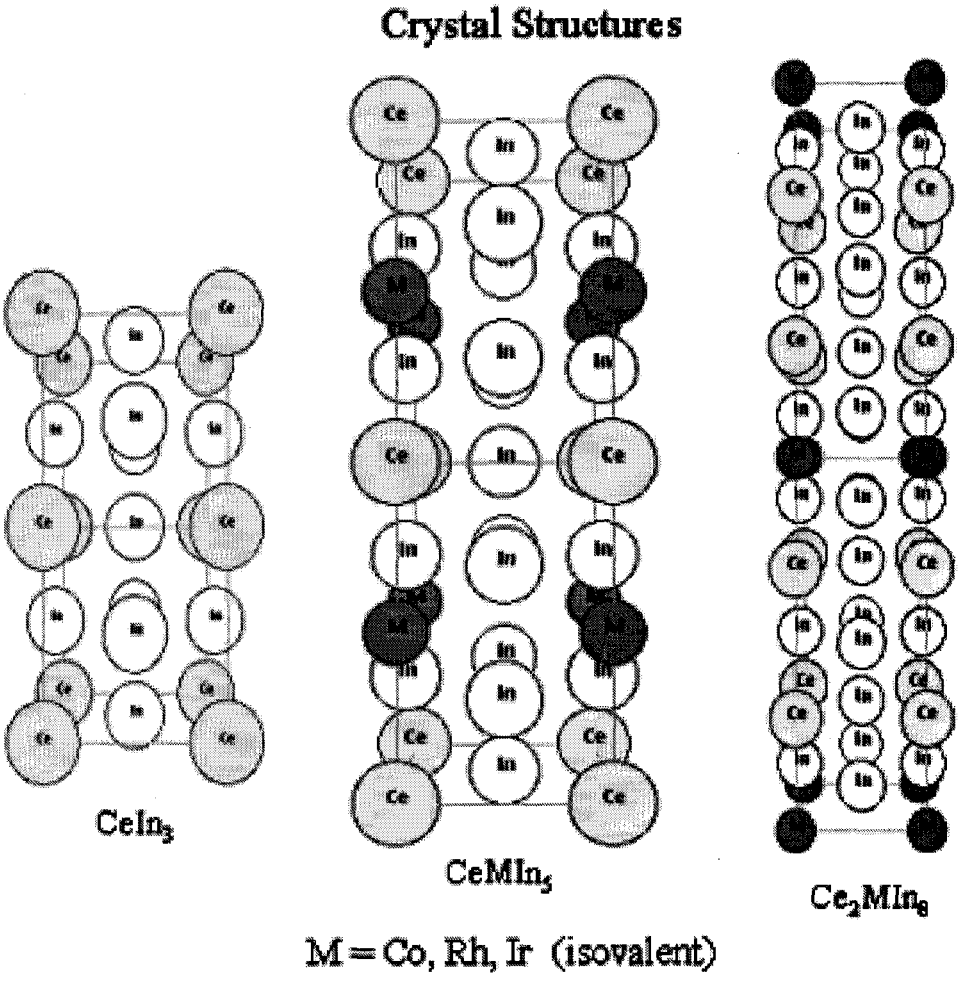

Figure 1.6: The $Ce_mM_nIn_{3m+2n}$ series of heavy fermion superconductors.

is present. X-ray and neutron scattering indicate sharp well formed peaks and no impurity peaks[37]. Electron diffraction studies observe no superlattice peaks[37].

An open question in the realm of heavy fermion physics is the relevance of dimensionality and/or anisotropy to the heavy fermion ground state. As mentioned previously, the lower dimensionality present in the high T_c materials may be relevant to the high transition temperatures. The terms dimensionality and anisotropy can have several different meanings relative to a particular material. We will classify the different types of dimensionality and anisotropy in three, not necessarily independent, ways as follows: electronic, magnetic, and crystallographic. Electronic anisotropy is that anisotropy that pertains to electronic properties of a material; experimental probes are Fermi surface studies and electron transport. Magnetic anisotropy can either be related to anisotropy in magnetic structure or fluctuations or with respect to applied magnetic fields. Crystallographic anisotropy is that anisotropy related to the crystal structure of a material. In $CeMIn_5$, in contrast to $CeIn_3$, it is apparent that the $CeIn_3$ layers are now separated by a layer containing no f-electrons ions which may enhance the 2-dimensionality or anisotropy in $CeMIn_5$.

Though the crystallographic anisotropy is apparent in $CeMIn_5$ relative to $CeIn_3$ it is important to consider the electronic dimensionality as shown by the Fermi surface. The Fermi surface of all members of the $CeMIn_5$ bear some similarity. The basic picture is that there are three bands which cross the Fermi energy yielding 3 distinct Fermi surfaces (see fig. 1.7. One of these surfaces is ellipsoidal and the other two are undulating cylinders [74, 4, 75, 76]. A purely cylindrical Fermi surface is expected for a 2-dimensional material, while a spherical Fermi surface is expected in 3-dimensions. The cylindrical Fermi surfaces in $CeMIn_5$ are not perfect cylinders but

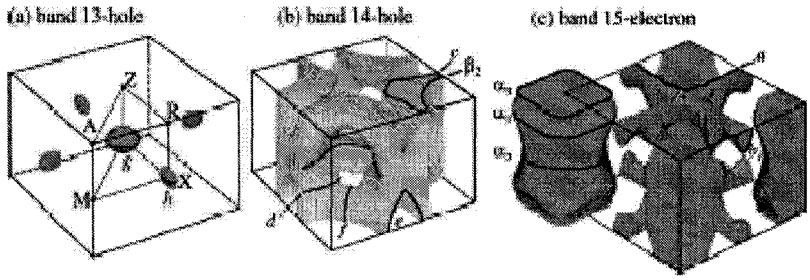

Figure 1.7: From Ref. [4]. Calculated Fermi surfaces for $CeIrIn_5$.

are warped, indicating some degree of 3-dimensional behavior. Furthermore, there are hole pockets which are more spherical in nature than the undulating cylinders. The most 2-dimensional member of $CeMIn_5$, as viewed from Fermi surface studies, is $CeCoIn_5$. The magnetic anisotropy will be discussed in the next section. An important question which arises from the above considerations is: To what degree are the $CeMIn_5$ materials influenced by the anisotropic nature of the fermi surface? Or more importantly, if anisotropy strongly influences the formation of the exotic heavy fermion ground states observed in $CeMIn_5$ what is the origin of this anisotropy?

1.3.2 Magnetism

The magnetic structure of $CeRhIn_5$ was determined by nuclear quadrupolar resonance and neutron diffraction [1, 77]. In comparison to $CeIn_3$ the magnetic structure of $CeRhIn_5$ is more complex. In $CeIn_3$, antiferromagnetic order sets in at 10 K [78] with a simple 3-d magnetic structure [79, 80]. In the case of $CeRhIn_5$ (see fig. 1.8), antiferromagnetic order sets in at 3.8 K with a spiral structure with ordered moments of 0.75 μ_B only upon the Ce atoms. The spiral structure has the magnetic moments on the Ce atoms antiferromagnetically aligned in the basal plane of the tetragonal

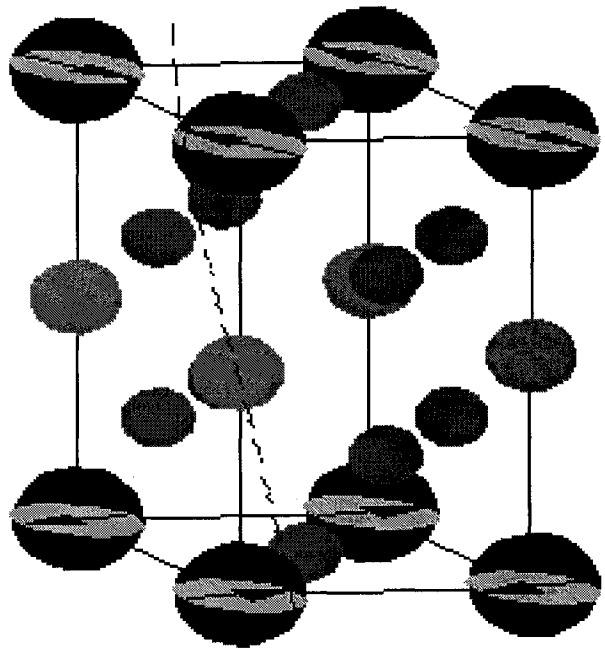

Figure 1.8: The magnetic structure of $CeRhIn_5$. The magnetic moments on the Ce atoms lie in the basal plane and are antiferromagnetically ordered.

structure with the angle between the moments in the next $CeIn_3$ plane of 107° [1].

To clarify the nature of the magnetic to superconducting transition in $CeRhIn_5$ there have been several studies of the resistivity and specific heat under applied pressures [3, 81, 82]. Other studies such nuclear quadrupolar resonance and neutron diffraction under pressure have been performed as well. Nuclear quadrupolar resonance studies[39] under pressure indicate that there is either a moment reduction as a function of pressure or that the moments are tilting out of the basal plane toward the c-axis. However, neutron scattering measurements under pressure seem to be in conflict with this[83], indicating that at 3.8 kbar the structure and magnetic moment remain essentially unchanged. More studies are needed to clarify the details of the

evolution of the magnetic structure of $CeRhIn_5$. Another means of probing the nature of the interactions in $CeMIn_5$ is through doping studies. There have been several single crystal neutron scattering studies of the the evolution of the magnetic structure of $CeRhIn_5$ [84, 85] with chemical substitution. In addition, there have been studies of $CeRhIn_5$ with application of magnetic fields.[6, 86, 87] These studies provide further motivation to examine the complex behavior of $CeMIn_5$ in greater detail.

1.3.3 Superconductivity

All three members of the $CeMIn_5$ series become superconducting at low temperature. $CeRhIn_5$, undergoes a superconducting transition at 2.1 K near 16 kbar [3]. In addition the $CeIrIn_5$ and $CeCoIn_5$ undergo superconducting transitions at 0.4 and 2.3 K respectively at ambient pressure. Several studies of the nature of the superconductivity in $CeIrIn_5$ and $CeCoIn_5$ show strong evidence for the unconventional nature of the superconductivity including the observation of lines of nodes in the superconducting gap function [40, 88, 38]. Further indication of the uniqueness of the superconductivity found in $CeMIn_5$ is the robustness of the superconducting transition as a function of chemical doping when compared to other heavy fermion materials[89, 90]. For example, in $CeRh_{1-x}Ir_xIn_5$ superconductivity is found for $0.3 \leq x \leq 1$[89], which in this sense makes $CeRh_{1-x}Ir_xIn_5$ more similar to the high T_c materials than many heavy fermion superconductors where very small amounts of impurities are sufficient to destroy superconductivity. Ultimately the question arises: What is the mechanism which determines that one member of the $CeMIn_5$ family is an ambient pressure antiferromagnetic and the others ambient pressure superconductors with T_cs which are more than a factor of 5 different?

1.3.4 Dissertation Organization

The objective of this dissertation is to explore in further detail the nature and relation of the heavy fermion magnetic and superconducting ground states in $CeMIn_5$ (M = Rh, Ir, Co) with particular emphasis on the properties of $CeRhIn_5$. Information about these systems will be extracted using two techniques: (1) measurements of the electrical resistivity of single crystals in applied magnetic fields to 18 T; and (2) measurements of inelastic neutron scattering response of powdered single crystals. The organization of this dissertation is as follows: Chapter 1 has been devoted to a description of background material including basic theoretical notions in the field of heavy fermion physics and general properties of the $Ce_mM_nIn_{3m+2n}$ family. Chapter 2 will explain the apparatus and techniques employed when performing magnetoresistance and inelastic neutron scattering measurements, as well as the theoretical response expected for these probes. In Chapter 3, we will discuss the details of magnetotransport in the $CeRhIn_5$. The results of these studies indicate only a modest degree of anisotropy present, as well as three distinct regimes in the magnetotransport; a high temperature regime where single impurity Kondo behavior is observed, an intermediate temperature regime where a crossover to Kondo lattice behavior is observed, and finally a low temperature region within the antiferromagnetically ordered state where a positive magnetoresistance is observed. Additionally, evidence is presented suggesting the importance of crystal field effects in explaining the magnetotransport properties of $CeRhIn_5$. The magnetotransport response of the superconducting members of $CeMIn_5$ will be described in chapter 4. The results of these studies will be contrasted and compared to the properties of $CeRhIn_5$. The results, show similar behavior in that once again two Kondo regimes are observed: one at high temperature

where the single impurity Kondo effect dominates; and the other at low temperature where Kondo lattice effects dominate. The inelastic neutron scattering response of $CeRhIn_5$ and $CeIrIn_5$ specifically aimed at determining the crystal field level splitting will be described in Chapter 5. We discuss a crystal field level scheme which explains the inelastic neutron scattering spectra of $CeRhIn_5$, as well as show fits to the magnetic susceptibility and specific heat. In addition, non-crossing approximation calculations to the Anderson impurity model have been performed which further emphasizes the role of Kondo physics in $CeRhIn_5$. A discussion will be given concerning plausible crystal field schemes for $CeIrIn_5$ and suggestions for further experimentation that will likely yield results which would allow for a accurate determination of the crystal field level scheme in this material. Finally, the summary of the results of this thesis will be given in Chapter 6, as well as proposals for the direction for future work. The conclusions will stress that the Kondo effect, the RKKY exchange interaction, and crystal field effects must be considered for any detailed understanding of both the magnetotransport properties and inelastic neutron scattering response of $CeMIn_5$.

Chapter 2

Experimental Techniques

In this chapter we describe the experimental techniques of magnetotransport and inelastic neutron scattering. The chapter starts with description of electron scattering mechanisms in a normal metal as well as the contributions due to crystal field effects and the Kondo effect. The discussion will be expanded to include the behavior of heavy fermion systems when large magnetic fields are applied. Following this, a description is given of magnetotransport techniques with specific details relating to the experimental apparatus utilized in the studies presented in the following chapters. The final section will explain basic aspects of neutron scattering before entering into a discussion of inelastic neutron scattering as it pertains to specifically elucidating crystal field levels. The discussion will be augmented by a description of the relation of the results of neutron scattering to those of specific heat and magnetic susceptibility. Finally, details are given of the experimental apparatus employed in acquiring the results presented in chapter 5.

2.1 Magnetotransport

2.1.1 Scattering Mechanisms

Magnetotransport techniques are important tools within the suite of those available to the condensed matter physicist. Unlike specific heat and magnetic susceptibility, the electrical resistivity is not a thermodynamic quantity. It is a percolative measurement, which means that a resistivity measurement does not always probe the whole sample. The virtue of a resistivity measurement is that it probes the conduction electron scattering rate in solids and thus provides information about abrupt changes in scattering rate (a phase transition) as well as more gradual changes in scattering such as in the Kondo effect. In many cases, where complex sample environments are required, measuring the resistivity provides the simplest (in some cases resistivity is one of the few options available) means for probing the behavior of a particular system. However, owing to the numerous complex scattering mechanisms present in materials, quantitative calculations are often impossible.

While the scattering mechanisms are often complex, there are some general ideas which allow information to be extracted [46, 41]. The resistivity of a simple metal is dominated by three scattering mechanisms. The first is scattering due to lattice vibrations or phonons. Since the population of the various phonon modes in a material follows Bose-Einstein statistics it is natural to expect a temperature dependence of the electron phonon scattering. This is in fact the case, and below the Debye temperature[1] the temperature dependence of the resistivity for a simple 3-dimensional metal is given

[1]The Debye temperature is simply related to the maximum allowed phonon frequency for a particular material

by

$$\rho \sim T^5 \tag{2.1.1}$$

The second scattering method arises from the scattering of impurities in the material. A simple model which displays the characteristic temperature dependence of impurities may be constructed by assuming that the impurities behave as hard sphere scatters with concentration n_i with each impurity possessing a cross section of σ_i. The mean free path is then given by

$$l = (n_i \sigma_i)^{-1} \tag{2.1.2}$$

and placing this in the expression for the resistivity derived for the free electron gas[46] yields

$$\rho \sim \frac{mv}{n_e e^2 l} \sim \frac{mv\sigma_i n_i}{n_e e^2} \tag{2.1.3}$$

where v is the average electronic speed, n_e is the density of conduction electrons, and e is the charge of an electron. Thus the scattering due to impurities is found to be temperature independent. The temperature independence of impurity scattering provides a convenient way to characterize the quality of samples. The simplest comparison is simply to measure the low temperature resistivity, which is known as the residual resistivity. Small values[2] may indicate that a sample has high purity. Another means to estimate the purity of the samples is to compute the ratio of the resistivity at 300 K to a value at lower temperature; in most cases 4 K is chosen. This ratio is known as the residual resistivity ratio (RRR). Larger values indicate higher quality samples[3].

[2]In heavy fermion materials a residual resistivity of $\sim 1\mu\Omega cm$ is a good value

[3]For heavy fermion materials values of 100 or more are generally good however, for materials such as Potassium values as high as 10000[91]have been observed.

The third scattering mechanism is electron-electron scattering. Here the temperature dependence of the scattering rate can be estimated by examining the process where a single electron excited above the fermi energy interacts with an electron below the fermi level. The probability of this interaction or scattering event depends upon the temperature as the phase space for the interaction increases with the thermal rounding of the Fermi-Dirac distribution. Roughly, we have a factor of T from the conduction electrons and another factor of T from the Fermi distribution[46]. The resistivity is then given by

$$\rho \sim T^2 \tag{2.1.4}$$

Here it is interesting to note that the proportionality constant in front of the T^2 term depends upon the effective mass of the charge carriers and is thus more important in the heavy fermion materials.

If we now consider all of the above scattering mechanisms together it is not completely clear that the the scattering processes should proceed completely independent of one another. However, in the simplest approximation, the scattering probabilities may be considered to be independent and the resistivities of the various contributions should be additive (Matthiessen's rule). The resistivity of a simple metal should then be of the form

$$\rho = a + bT^2 + cT^5 \tag{2.1.5}$$

To complicate matters further, there are several other scattering mechanisms which are observed in metals. We restrict discussion of these mechanisms to two of magnetic origin, namely scattering due to the thermal population of crystal field levels and that due to the Kondo effect.

From section 1.2.4 it is evident that the degeneracy of a local moment in a crystalline environment will be lessened due to electrostatic considerations. This lifting of the degeneracy results in different thermal occupations of the split energy levels. To understand the contribution to the resistivity due to CEF effects we start by considering the scattering due to static randomly orientated local moments[4]. The Hamiltonian for the nth local moment at position $\vec{R}_n$ is[92]

$$H_n = -2J_{ex}\delta(\vec{r} - \vec{R}_n)(g-1)\vec{S}_e \cdot \vec{J}_n \tag{2.1.6}$$

where the spin of a conduction electron, $\vec{S}_e$, at position $\vec{r}$ is coupled to the spin of a local moment, $\vec{J}_n$, at position $\vec{R}_n$. To avoid confusion between the total angular momentum and the conduction electron local moment exchange the latter has been denoted by $J_e x$. To calculate the resistivity, we note that the relaxation time is given by[92]

$$\tau^{-1} = \frac{\hbar k_F N}{m} A_t \tag{2.1.7}$$

where N is the density of local moments participating in the scattering process and A_t is the transport cross-section per scattering center. The resistivity can then be written as[46].

$$\rho = \frac{m}{ne^2\tau} = \frac{\hbar k_F N}{ne^2} A_t \tag{2.1.8}$$

where n is the density of conduction electrons. A_t can then be calculated under the Born approximation using eq. 2.1.6. Physically, the situation is as follows: a conduction electron with spin S_e ($m_e = \pm\frac{1}{2}$) scatters from state $\vec{k}$ to $\vec{k'}$ by a local moment with angular momentum J. This yields matrix elements of the form

$$-2J_{ex}(g-1)\left\langle m'_e, m'_j \left| \int exp\left[i\left(\vec{k} - \vec{k'}\right)\cdot\vec{r}\right]\delta(\vec{r})\, d\vec{r}\left(\vec{S}_e \cdot \vec{J}\right)\right| m_e, m_j \right\rangle \tag{2.1.9}$$

[4]For complete details of this derivation see [92]

The important point is that each value of m_j is equally occupied and thus A_t reduces to

$$A_t = 4\pi \left(\frac{m}{2\pi\hbar^2}\right)^2 J_{ex}^2 (g-1) j(j+1) \tag{2.1.10}$$

The spin disorder (sd) resistivity is then given by eqs. 2.1.8 and 2.1.10 as

$$\rho_{sd} = \left(\frac{2\pi N m}{2\hbar e^2 \epsilon_F}\right) J_{ex}^2 (g-1)^2 j(j+1) \tag{2.1.11}$$

Equation 2.1.11 is only valid for equal occupation of all of the angular momentum states of the local moment of a given multiplet. When crystal field effects are included the matrix elements of eq. 2.1.9 must be modified to be between the appropriate eigenstates and to include the thermal occupation of the local moment states[93]. The thermal occupation is given by Boltzman statistics as

$$p_i = \frac{N_i}{N} = \frac{e^{\left(\frac{-E_i}{k_B T}\right)}}{\sum_j e^{\left(\frac{-E_j}{k_B T}\right)}} \tag{2.1.12}$$

where N_i is the occupation of the ith level. The spin disorder resistivity in the presence of CEF effects is then given by[93]

$$\rho_{sd} = \left(\frac{2\pi N m}{2\hbar e^2 \epsilon_F}\right) J_{ex}^2 (g-1)^2 \sum_{m_e, m_e', i, i'} \langle m_e', i' \left| \vec{S} \cdot \vec{J} \right| m_s, i \rangle^2 p_i f_{ii'} \tag{2.1.13}$$

where i references a particular crystal field eigenstate and the factor $f_{ii'}$ is given by

$$f_{ii'} = \frac{2}{1 + e^{\left(\frac{-E_{ii'}}{k_B T}\right)}} \tag{2.1.14}$$

Eq.2.1.13 gives the contribution to the resistivity in the absence of magnetic correlations or the Kondo effect. To further understand the magnetotransport behavior of heavy fermion systems we now examine the influence of the Kondo effect on the resistivity.

We consider the Kondo effect in two forms, the single impurity and the Kondo lattice. Let us first consider the single impurity case. Here there is a magnetic impurity immersed in a host metallic lattice. The screening of the magnetic impurity by the conduction electrons[5] causes additional terms to appear in the resistivity which are given by the following expression[49].

$$\rho = n_i\rho_0 - n_i\rho_1 ln\left(\frac{k_BT}{D}\right) \tag{2.1.15}$$

where n_i is the concentration of magnetic impurities and ρ_0 and ρ_1 are term proportional to the conduction electron local moment exchange and the spin of the impurity. If the impurity carried no magnetic moment (zero spin) then there would be no Kondo effect, which is exactly what is observed for nonmagnetic impurities. If we now make the assumption that the only impurities are magnetic and that the electron-electron scattering term proportional to T^2 is negligible when compared to the other scattering mechanism, the resistivity may be written as the sum of the Kondo terms (eq. 2.1.15) and the phonon scattering term (eq. 2.1.1) as.

$$\rho = cT^5 + n_i\rho_0 - n_i\rho_1 ln\left(\frac{k_BT}{D}\right) \tag{2.1.16}$$

Not only does this form reproduce the logarithmic divergence of the resistivity, but the minimum in the resistivity is also predicted to occur at

$$T_m = \left(\frac{\rho_1}{5c}\right)^{\frac{1}{5}} n_i^{\frac{1}{5}} \tag{2.1.17}$$

which is in agreement with experiment[52].

The Kondo lattice presents a much more complicated situation. Instead of isolated magnetic impurities there is now a periodic array of local magnetic moments. An

[5]see section 1.2.3 and reference therein for details

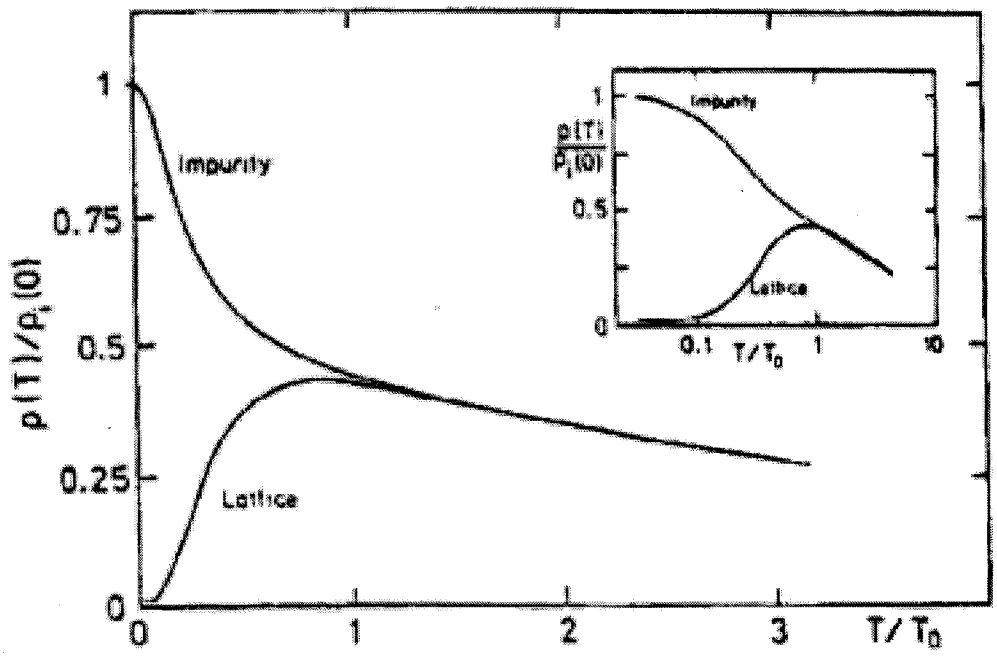

Figure 2.1: From ref. [5]. Calculations based upon the Anderson lattice. Notice above the coherence temperature (T_o) both the impurity and lattice behave in a similar manner, while below T_o the lattice exhibits a sharp drop in the resistivity characteristic of a Kondo coherent state.

additional feature here is that the impurities are now close enough to begin to interact with one another. The interaction among the impurities is termed coherence. Above a certain temperature, often termed the onset of coherence, the Kondo lattice often behaves as a single impurity material. Below the coherence temperature behavior associated with coherence effects is observed in the physical properties of Kondo lattice materials. A consequence of the interaction among the local moments is a sharp drop in the resistivity observed below the coherence temperature. No exact calculation has been performed; however, approximate calculations based upon the Anderson lattice[5] (see fig 2.1.1) display behavior due to coherence. The sharp drop in the resistivity below the coherence temperature is due to the interactions among the magnetic impurities establishing a periodic condition for the conduction electrons

and the scattering rate goes to zero.

2.1.2 Magnetoresistance

Studies of the behavior of materials under the influence of applied magnetic fields provide a wealth of information. They can differentiate between different ground states, provide information about field induced magnetic states, allow the normal state of superconductors to be examined at low temperatures, explore anisotropy, etc. In this section we will concentrate upon the influence of applied magnetic fields as observed in the resistivity of materials. We will first discuss the behavior expected for a normal metal followed by that expected for the Kondo effect.

The topic of magnetoresistance will appear repeatedly. The magnetoresistance is defined as follows:

$$\frac{\Delta\rho}{\rho_o} = \frac{\rho(T,H) - \rho(T,0)}{\rho(T,0)} \tag{2.1.18}$$

Therefore a material which has a positive value of $\frac{\Delta\rho}{\rho_o}$ is said to have a positive magnetoresistance while a negative value indicates a negative magnetoresistance. As a first step in understanding magnetoresistance phenomena in real materials let us consider the simple case of a free electron gas. The following arguments are found in greater detail in ref. [94]. Consider a magnetic field ($\vec{B}$) applied perpendicular to the current density ($\vec{J}$). Under steady state conditions, collisions and the effect of the magnetic field yield the following expression

$$ne\vec{E} = \frac{m^*\vec{J}}{e\tau} - \vec{J} \times \vec{B} \tag{2.1.19}$$

The salient feature here is that the component of the current parallel to electric field ($\vec{E}$) is unchanged by the magnetic field. Thus the resistivity is unchanged as well.

Evidently deeper considerations are necessary to explain the widespread observation of magnetoresistance in materials.

Contrary to the free electron case above the magnetoresistance for a normal metal is expected to be positive and at low fields to vary as H^2. In order to explain the widespread observation of magnetoresistance found in metals, a model which includes the periodic potential of a crystal lattice must be used[41]. However, it is possible to estimate the effect of an applied magnetic field on the resistivity by simpler means. Before we begin it is important to define the cyclotron frequency which is given by

$$\omega_c = \frac{eH}{cm} \tag{2.1.20}$$

where H is the magnetic field and m is the effective mass of the charge carriers. The relaxation time (τ) multiplied by ω_c determines the relative importance of the applied magnetic field and scattering processes upon electronic motion. In these terms, a low magnetic field is one for which $\omega_c\tau \ll 1$ and a high magnetic field is one for which $\omega_c\tau \gg 1$. We now consider the low field case. The effect of the magnetic field is to cause curvature of electron motion, which in turn decreases the mean free path. The correction to the resistivity may then be estimated by[46]

$$\Delta\rho \sim \rho\left(\frac{l}{r_L}\right)^2 \tag{2.1.21}$$

where l is the mean free path and the radius of the electron orbit (r_L) as determined by ω_c is given by $r_L \sim \frac{v}{\omega_c}$. The correction to the resistivity is then

$$\Delta\rho \sim \rho\left(\omega_c\tau\right)^2 \sim \rho\left(\frac{eH}{cm}\tau\right)^2 \tag{2.1.22}$$

In the high field case, the topology of the Fermi surface becomes important. The electrons now travel through significant portions of orbits around the Fermi surface

before being scattered. Thus the details of the magnetoresistance depend on the Fermi surface of the material, and in some cases, where sample purity is high enough and temperatures low enough, the magnetoresistance will show oscillations (Shubnikov - de Haas oscillations) which are periodic in $\frac{1}{H}$, and from which the shape of the Fermi surface may be extracted.

There are other mechanisms which result in an observable magnetoresistance in solids. For example, as detailed above, local magnetic moments can give rise to resistivity. An application of a magnetic field can align the magnetic moments (a Zeeman term is introduced to change the population of the local moment eigenstates) which results in the observation of a negative magnetoresistance. Another mechanism in heavy fermion materials which leads to an observable magnetoresistance is the Kondo effect.

In the case of the single impurity Kondo effect there is numerous experimental evidence and theoretical calculations for the magnetoresistance to be negative [95, 96, 97, 98, 99, 100, 101]. This may be envisioned by considering that the local moments are screened by the conduction electrons leading to a larger resistivity than were the screening not taking place. The application of a magnetic field disrupts the screening leading, to a lower resistivity and hence a negative magnetoresistance. From this point of view it is natural that the destruction of the Kondo screening process should be related to the magnetization. This fact is observed experimentally [99] as well as theoretically [100, 101] where it is found that

$$\rho \propto M^2 \tag{2.1.23}$$

In the case of the Kondo Lattice, there is less experimental evidence and the

theoretical calculations are somewhat meager. Experimentally a low-T positive magnetoresistance has been reported in both $CeAl_3$ [102, 103] and $CeRu_2Si_2$ [104] at low temperatures, and in UBe_{13} under pressure. [105]. The interpretation of the positive magnetoresistance is hampered by the close proximity of field induced states in many heavy fermion materials. However, in the mixed valence Kondo lattice materials (which have much higher Kondo temperatures than heavy fermion materials) positive magnetoresistance is also observed at temperatures below the coherence temperature in such canonical examples as $CePd_3$[106] and $YbAl_3$ [107]. Despite a number of attempts, there is no satisfactory theoretical description of the positive magnetoresistance in observed in the coherence regime, although a number of studies predict positive magnetoresistance for certain cases [108, 109, 110].

2.1.3 Resistance Measurement

The most common method of measuring electrical resistance in the laboratory is to employ a four-probe AC technique. This method has several advantages. The first is that a four probe method avoids measuring the resistance of the leads and contacts. A second is that the AC technique allows the use of phase sensitive detection. Phase sensitive detection methods are well known for their capability of extracting small signals from relatively large amounts of noise.

A typical sample geometry is shown in fig. 2.2. Leads are attached to the sample with silver epoxy which gives contact resistances of 1-2 Ω. A current (I) is supplied and the resulting voltage (V) drop is measured. The resistance (R) is then given by Ohm's law.

$$V = IR \tag{2.1.24}$$

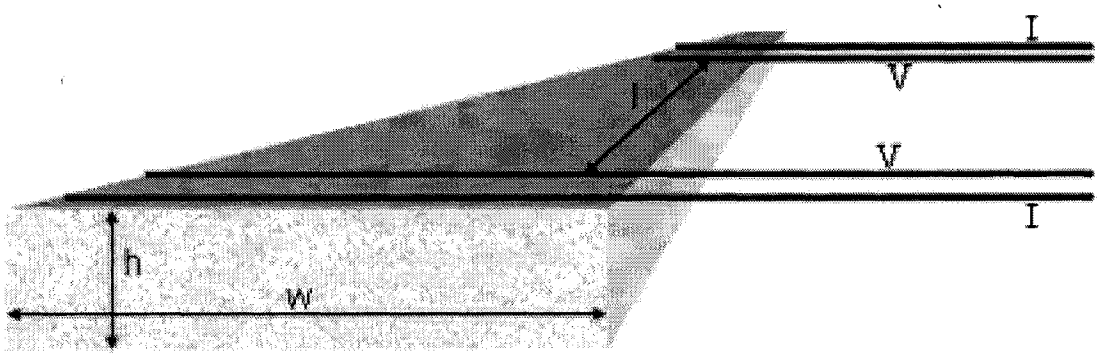

Figure 2.2: A typical sample geometry. The Current leads are labelled I and the voltage leads are labelled V. l, w,and h are the relevant physical dimensions for calculation of ρ from the measured R

To obtain ρ, a purely geometrical quantity must be applied. ρ is given by

$$\rho = R\frac{A}{l} \tag{2.1.25}$$

where A is the cross section the current flows through and l is the length between the voltage electrodes.

The resistance measurement can be accomplished in a number of ways. The method used to obtain the results in chapters 3 and 4 is to use a LR-700 resistance bridge with a frequency of 18 Hz. The resulting resistance is read by computer with local Labview software as a function of another parameter, such as temperature or magnetic field. The magnetic field is supplied by an 18 T superconducting magnet at the National High Magnetic Field Laboratory - Los Alamos campus. The temperature range of 1.4 to 300 K is supplied by a variable flow cryostat and measured by a cernox resistance thermometer.

mass	1.675×10^{-27} kg
charge	0
spin	$\frac{1}{2}$
magnetic dipole moment (μ_n)	-1.913 μ_N
nuclear magneton (μ_N)	$5.051\times10^{-27}\frac{J}{T}$

Table 2.1: Properties of the neutron

2.2 Neutron Scattering

The unique properties of the neutron make it an excellent probe of the properties of condensed matter.[6] Consider a thermal neutron ($\frac{E}{k_B}$ = 293 K), which corresponds to an energy of 25.3 meV, a velocity of 2.2 kms^{-1}, and a wavelength of 1.8 Å as seen in eq. 2.2.1.

$$E = \frac{1}{2}mv^2 = \frac{3}{2}k_BT = \frac{h^2}{2m\lambda^2} = \frac{\hbar^2k^2}{2m} \tag{2.2.1}$$

Other properties of the neutron are summarized in table 2.1 The wavelength of a thermal neutron is of the same scale as the lattice spacings in solids, making thermal neutrons ideal for probing the crystal structure of solids. In addition, the energy of a thermal neutron is of the same order as many of the excitations in solids, so that experiments can be conducted which determine the excitations present. In the case of x-rays the energy of the photons is so high (keV) that an exchange of energy with an excitation constitutes only a small fraction of the x-rays' energy, making these types of experiments difficult. A neutron also possesses an intrinsic spin so that it may interact with magnetic moments in solids, so that both magnetic structures and excitations may be studied.

[6] for a more complete introduction see refs. [111] and [112].

Neutrons are produced at two different types of facilities. The traditional method is the use of a nuclear reactor. In this case, high fluxes of neutrons may be generated that are constant in time[7]. The other common method used to produce neutrons is called spallation. In contrast to the nuclear reactions used to produce neutrons in the case of a nuclear reactor, a spallation source consists of an accelerator which directs a beam of protons into a heavy target, such as tungsten or depleted uranium, yielding approximately 10 neutrons for each incident proton. A spallation, or pulsed source, has higher peak fluxes but generally lower time averaged fluxes than a reactor. Most pulsed source neutron scattering experiments take advantage of the timing introduced by the particle accelerator and use the time of flight method, whereby essentially all neutron wavelengths can be collected for each pulse during an elastic scattering experiment and a wide range of energy transfers can be collected for each pulse during an inelastic scattering experiment. An additional advantage of a spallation source is that much greater number of epithermal neutrons are available than at a reactor source.

For the following discussion of neutron scattering to be understandable it is necessary to introduce some of the terminology and concepts germane to neutron scattering. Fundamentally, every neutron scattering experiments sets out to measure the neutron scattering cross-section, σ, for some property of the material under study. In neutron scattering experiments there are two quantities of particular importance. The first is the momentum transfer which is given by

$$\vec{Q} = \vec{k_f} - \vec{k_i} \tag{2.2.2}$$

where $\vec{k_i}$ ($\vec{k_f}$) is the incident (final) neutron wavevector given by eq. 2.2.1. The

[7]An exception to this is the pulsed reactor at Dubna in Russia

second, energy transfer is given by

$$\hbar\omega = E_f - E_i \tag{2.2.3}$$

where $\hbar\omega$ is the energy transferred to the sample and E_i (E_f) is the incident (final) neutron energy.

2.2.1 Elastic Scattering

Elastic neutron scattering provides a means of determining crystalline structures of materials. When performing a structural determination the preferred method is to use x-ray diffraction. This is due to the the higher intensities available from x-ray sources (greater than an order of magnitude)and the lower cost of producing x-rays relative to that of neutrons. However, there are some instances where neutron diffraction provides a superior means of structural determination. Three of the most important advantages are: (1) the scattering lengths of the elements differ depending on the isotope and not on the number of electrons as for x-rays (this makes possible diffraction experiments with elements such as hydrogen); (2) the significant neutron scattering cross section due to magnetically ordered materials. (3) and bulk penetration of heavy elements such as rare earths and actinides where photons are essentially limited to being surface probes.

For elastic scattering the the energy transfer is zero. In a crystalline solid this constrains Q to be equal to a reciprocal lattice vector, $\vec{K}$[41]. This condition can be restated in terms of the well know Bragg law

$$\lambda = 2dsin(\theta) \tag{2.2.4}$$

where d, the d-spacing, is given by $|\vec{K}| = \frac{2\pi}{d}$ and θ may be found by finding the magnitude of $\vec{Q}$ via eq. 2.2.2.

The coherent elastic scattering cross-section is given by[112]

$$\frac{d\sigma}{d\Omega} = N\frac{(2\pi)^3}{v_o}\sum_{\vec{K}}\delta(\vec{Q}-\vec{K})\left|F_N(\vec{K})\right|^2 \tag{2.2.5}$$

where

$$F_N(\vec{K}) = \sum_j \overline{b}_j e^{i\vec{K}\cdot\vec{d}_j}e^{-W_j} \tag{2.2.6}$$

N is the number of unit cells, v_o is the volume of the unit cell, and the quantity $F_N(\vec{K})$ is known as the nuclear structure factor, where $\overline{b}_j$ is the average value of the scattering length for a element j (the scattering length depends on the specific isotope), d_j is the position of the jth atom, and e^{-W_j} represents the decreased intensity in the Bragg peaks due to atomic displacement and is known as the Debye-Waller factor. An important difference is evident between x-ray and neutron diffraction in that in the case of neutrons the scattering center is the nucleus and is a point source so that the structure factor only contains a scattering length and does not require an atomic form factor which depends on momentum transfer.

The case of magnetic neutron diffraction illustrates the need to consider an atomic form factor in neutron scattering experiments where the scattering is from unpaired electrons and not from the nucleus. In the case of a magnetically ordered solid the coherent elastic cross-section is given by[112]

$$\frac{d\sigma}{d\Omega} = N_M\frac{(2\pi)^3}{v_M}\sum_{\vec{K}_M}\delta(\vec{Q}-\vec{K}_M)\left|F_M(\vec{K}_M)\right|^2 \tag{2.2.7}$$

where

$$F_M(\vec{K}_M) = \sum_j f_j(|\vec{Q}|)\vec{J}_{\perp j}e^{i\vec{K}_M\cdot\vec{d}_j}e^{-W_j} \tag{2.2.8}$$

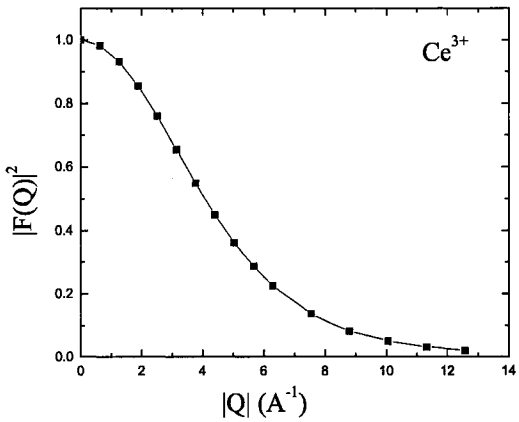

Figure 2.3: Ce^{3+} magnetic form factor.

where the M subscript denotes the analogous magnetic quantity to the elastic quantity in eq. 2.2.5 and $f_j(|\vec{Q}|)\vec{J}_{\perp j}$ takes the place of the nuclear scattering length. $\vec{J}_{\perp j}$ denotes the portion of the atomic magnetic moment which is perpendicular to the momentum transfer and $f_j(|\vec{Q}|)$ is the magnetic form factor which is the Fourier transform of the magnetization density. The magnetic form factor for Ce^{3+} is shown in fig. 2.3[113].

While elastic scattering provides interesting information, to obtain the crystal field excitation spectrum, another technique is needed.

2.2.2 Inelastic Neutron Scattering

Inelastic neutron scattering is a useful tool for probing excitations in solids. There are a number of different methods for measuring the inelastic response of a material. Traditionally, the most widely used at reactor sources is the triple axis method; it is especially useful for measurements of excitations as a function of both energy and

momentum transfer for single crystals. However, because crystal field excitations are local, the dependence of the scattering intensity is only dependent on the magnitude of the momentum transfer through the magnetic form factor. Thus there is a distinct advantage of studying polycrystalline materials with the time of flight method where many different momentum transfers and energy transfers can be collected simultaneously in a bank of detectors and summed appropriately to augment the signal. Fig. 2.4 displays a schematic diagram of the low resolution medium energy chopper spectrometer (LRMECS) at the Intense Pulse Neutron Source at Argonne National Laboratory. The instrument operates as follows: Neutrons produced by spallation are moderated and travel down the beam tube. They first encounter the frame definition chopper, or T_0 chopper. This chopper suppresses unwanted high energy neutrons and gamma-rays. Further down the beam tube, the neutrons encounter an energy selecting chopper, or Fermi chopper. The Fermi chopper only allows neutrons with a specified energy to pass. The remaining neutrons are then collimated before passing into the sample chamber. The neutrons are then either scattered, absorbed, or simply pass through the sample. The neutrons which are scattered are counted by ^3He detectors from angles of -10 to 120°.

From fig. 2.3 it is evident that the magnetic scattering will be strongest at low momentum transfers or low scattering angles. In addition the contributions of non-magnetic scattering such as phonons will be largest at high angles[111]. This allows us to differentiate the contributions of these two sources of information by following their change in intensity as a function of $\vec{Q}$, or scattering angle. The scattering

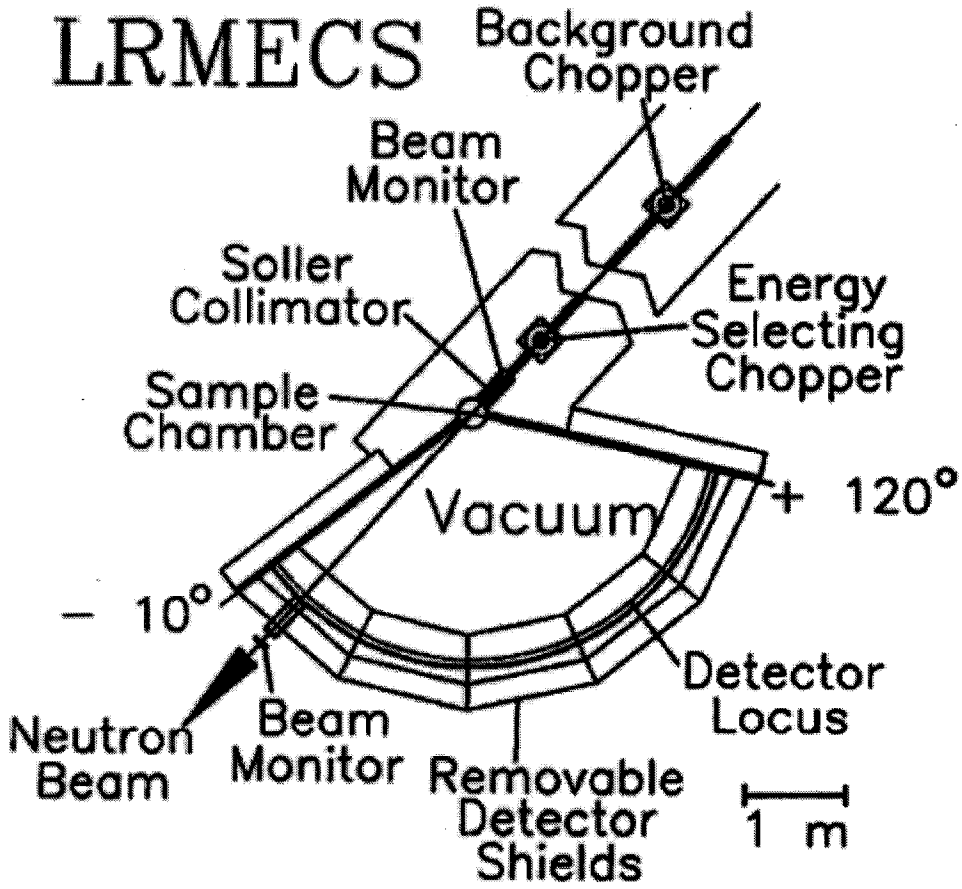

Figure 2.4: The low resolution medium energy chopper spectrometer (LRMECS) at Argonne National Laboratory

cross-section for crystal field excitations is given by[114]

$$\frac{\partial^2\sigma}{\partial\Omega\partial\omega} = exp(-2W)\frac{k_f}{k_i}\left(\frac{\frac{\mu_n}{\mu_N}e^2}{2mc^2}g_j\right)^2 |f(\vec{Q})|^2 \sum_{\Gamma,\Gamma'} \rho_\Gamma |\langle\Gamma|\vec{J}_\perp|\Gamma'\rangle|^2 \delta\left(\frac{E_\Gamma - E_{\Gamma'}}{\hbar} - \omega\right) \tag{2.2.9}$$

where ρ_Γ is the thermal population (eq. 2.1.12) of the crystal field level denoted by Γ and the rest of the symbols have their previously defined meanings.

2.2.3 Bulk Measurement of Crystal Field Excitations

While neutron scattering provides one of the most detailed means of probing crystal field excitations, crystal field splittings affect a number of other physical quantities including specific heat, magnetic susceptibility, and thermal expansion. The following will restrict discussion to specific heat and magnetic susceptibility. In contrast to neutron scattering, specific heat and magnetic susceptibility do not measure the crystal field excitations directly, making crystal field effects somewhat difficult to separate from other effects such as the Kondo effect and magnetic exchange.

Specific Heat

For Ce^{3+} compounds the splitting of the degeneracy of the $J = \frac{5}{2}$ multiplet gives rise to a contribution to the specific heat know as the Schottky effect for a two level system. The contribution to the specific heat may be derived by considering the free energy[115]

$$F = -k_B T Log(Z) \tag{2.2.10}$$

where Z is the partition function and is given by

$$Z = \sum_n exp\left(-\frac{E_n}{k_B T}\right) \tag{2.2.11}$$

where E_n is the energy of the nth CEF level. The specific heat can then be calculated from

$$C_p = -T\left(\frac{\partial^2 F}{\partial T^2}\right)_p \tag{2.2.12}$$

For a two level system with a levels at $E_0 = 0$ and $E_1 = \epsilon$, with no degeneracy the expression for the specific heat becomes,

$$C_p = \frac{1}{k_B}\left(\frac{\epsilon}{T}\right)^2 \frac{e^{\left(-\frac{\epsilon}{k_B T}\right)}}{\left[1 + e^{\left(-\frac{\epsilon}{k_B T}\right)}\right]^2} \tag{2.2.13}$$

For the three doublet crystal field levels found in $CeMIn_5$ (with energy levels $E_0 = 0$, $E_1 = \epsilon_1$, and $E_2 = \epsilon_2$) the specific heat becomes

$$C_p = \frac{\epsilon_1^2 e^{\left(\frac{-\epsilon_1}{k_B T}\right)} + \epsilon_2^2 e^{\left(\frac{-\epsilon_2}{k_B T}\right)} + (\epsilon_1^2 + \epsilon_2^2)\, e^{\left(\frac{-(\epsilon_1+\epsilon_2)}{k_B T}\right)} - 2\epsilon_1\epsilon_2 e^{\left(\frac{-(\epsilon_1+\epsilon_2)}{k_B T}\right)}}{k_B T^2 \left[1 + e^{\left(\frac{-\epsilon_1}{k_B T}\right)} + e^{\left(\frac{-\epsilon_2}{k_B T}\right)}\right]^2} \tag{2.2.14}$$

In contrast to neutron scattering, and as we show in the next section for the magnetic susceptibility, the specific heat is only sensitive to the energy splitting and not the wave functions.

Magnetic Susceptibility

The magnetic susceptibility reflects CEF splitting by anisotropy and Curie behavior. To calculate the magnetic susceptibility we first assume that the energy in an applied magnetic field can be expanded as follows[8].

$$E = E_0 + E_1 H + E_2 H^2 + ... \tag{2.2.15}$$

The magnetic moment per atom can then be calculated by

$$\mu = -\frac{\partial E}{\partial H} = -E_1 - 2E_2 H - ... \tag{2.2.16}$$

[8]For full details of this derivation see ref. [116]

The magnetic susceptibility is then given by

$$\chi = \frac{M}{H} = -\frac{N}{H}\frac{\sum \frac{\partial E}{\partial H} e^{\left(-\frac{E}{k_B T}\right)}}{\sum e^{\left(-\frac{E}{k_B T}\right)}} \tag{2.2.17}$$

Where the summation is taken over all states. Now substituting in eqs. 2.2.15 and 2.2.16 into eq. 2.2.17 and making the additional assumptions that H is small and that $\frac{E_1 H}{k_B T} \ll 1$ we obtain

$$\chi \cong N\frac{\sum \left(\frac{E_1^2}{k_B T} - 2E_2\right) e^{\left(-\frac{E_0}{k_B T}\right)}}{\sum e^{\left(-\frac{E_0}{k_B T}\right)}} \tag{2.2.18}$$

Where E_0 is the bare crystal field level and from perturbation theory we know that

$$E_1 = \left\langle i \left| \vec{L} + 2\vec{S} \right| i \right\rangle \tag{2.2.19}$$

$$E_2 = \frac{\left| \left\langle i \left| \vec{L} + 2\vec{S} \right| j \right\rangle \right|^2}{E_i - E_j} \tag{2.2.20}$$

where the states denoted by i and j are the now eigenstates referenced by the z component of the total angular momentum, and as in the case of the rare earths, for strong spin-orbit coupling $\vec{L} + 2\vec{S}$ may be replaced by $g_J \vec{J}$. Thus, the magnetic susceptibility may be written as

$$\chi \cong N\frac{\sum \left[\frac{\langle i | g_J \vec{J} | i \rangle^2}{k_B T} - 2\frac{\left| \langle i | \vec{L}+2\vec{S} | j \rangle \right|^2}{E_i - E_j} \right] e^{\left(-\frac{E_0}{k_B T}\right)}}{\sum e^{\left(-\frac{E_0}{k_B T}\right)}} \tag{2.2.21}$$

Thus the susceptibility may be calculated by inserting the appropriate energies and eigenfunctions for the problem at hand. Note that the temperature dependence enters only through the thermal population and the $\frac{1}{T}$ term. The term that is independent of temperature (aside from the thermal population factor) is known as the van Vleck term and the term proportional to $\frac{1}{T}$ is known as the Curie term. For the

$CeMIn_5$ family the appropriate eigenfunctions are those of tetragonal symmetry (eq. 1.2.19). Moreover, for tetragonal symmetry the magnetic susceptibility is found to be anisotropic. Thus the expression for the magnetic susceptibility for the magnetic field applied parallel ($||$) or perpendicular ($\perp$) to the c-axis is given by eq. 2.2.21 with the operator $g_J\vec{J}$ replaced by

$$|| \quad g_J\vec{J}_z \tag{2.2.22}$$

$$\perp \quad \frac{g_J}{2}\left(\vec{J}_+ + \vec{J}_-\right) \tag{2.2.23}$$

where $\vec{J}_z$ is given by the standard definition and acts as follows

$$\langle J, m \left| g_J J_z \right| J, m\rangle = g_J m \tag{2.2.24}$$

and the combination $\frac{g_J}{2}\left(\vec{J}_+ + \vec{J}_-\right)$ is given by the standard definition and acts as

$$\left\langle J, m \left| g_J \frac{1}{2}\left(\vec{J}_+ + \vec{J}_-\right) \right| J, m \pm 1 \right\rangle = \frac{g_J}{2}\left[(J \pm m + 1)(J \mp m)\right]^{\frac{1}{2}} \tag{2.2.25}$$

The matrix elements for the crystal field split wave functions of Ce^{3+} can be constructed by considering the matrix elements for the pure angular momentum states below. The nonzero matrix elements of J_z are

$$\begin{aligned}
\left\langle \frac{5}{2}, \pm\frac{5}{2} \right| J_z \left| \frac{5}{2}, \pm\frac{5}{2} \right\rangle &= \pm\frac{5}{2} \\
\left\langle \frac{5}{2}, \pm\frac{3}{2} \right| J_z \left| \frac{5}{2}, \pm\frac{3}{2} \right\rangle &= \pm\frac{3}{2} \\
\left\langle \frac{5}{2}, \pm\frac{1}{2} \right| J_z \left| \frac{5}{2}, \pm\frac{1}{2} \right\rangle &= \pm\frac{1}{2}
\end{aligned} \tag{2.2.26}$$

The nonzero matrix elements of $\vec{J}_+ + \vec{J}_-$ for Ce^{3+} can be constructed as follows from the matrix elements of J_+ and J_-

$$\begin{aligned}
\left\langle \frac{5}{2}, \frac{5}{2} \right| J_+ \left| \frac{5}{2}, \frac{3}{2} \right\rangle &= \sqrt{5} \\
\left\langle \frac{5}{2}, \frac{3}{2} \right| J_+ \left| \frac{5}{2}, \frac{1}{2} \right\rangle &= 2\sqrt{2} \\
\left\langle \frac{5}{2}, \frac{1}{2} \right| J_+ \left| \frac{5}{2}, -\frac{1}{2} \right\rangle &= 3 \\
\left\langle \frac{5}{2}, -\frac{1}{2} \right| J_+ \left| \frac{5}{2}, -\frac{3}{2} \right\rangle &= 2\sqrt{2} \\
\left\langle \frac{5}{2}, -\frac{3}{2} \right| J_+ \left| \frac{5}{2}, -\frac{5}{2} \right\rangle &= \sqrt{5} \\
\left\langle \frac{5}{2}, \frac{3}{2} \right| J_- \left| \frac{5}{2}, \frac{5}{2} \right\rangle &= \sqrt{5} \\
\left\langle \frac{5}{2}, \frac{1}{2} \right| J_- \left| \frac{5}{2}, \frac{3}{2} \right\rangle &= 2\sqrt{2} \\
\left\langle \frac{5}{2}, -\frac{1}{2} \right| J_- \left| \frac{5}{2}, \frac{1}{2} \right\rangle &= 3 \\
\left\langle \frac{5}{2}, -\frac{3}{2} \right| J_- \left| \frac{5}{2}, -\frac{1}{2} \right\rangle &= 2\sqrt{2} \\
\left\langle \frac{5}{2}, -\frac{5}{2} \right| J_- \left| \frac{5}{2}, -\frac{3}{2} \right\rangle &= \sqrt{5}
\end{aligned} \tag{2.2.27}$$

Chapter 3

Magnetotransport studies of $Ce_{1-x}La_xRhIn_5$

In section 3.1 we report measurements of the temperature-dependent anisotropic resistivity and in-plane magnetoresistance on single crystals of the tetragonal heavy-fermion antiferromagnet (T_N = 3.8 K) $CeRhIn_5$. The measurements are reported in the temperature range 1.4 K to 300 K and in magnetic fields to 18 tesla. The resistivity is moderately anisotropic, with a room-temperature c-axis to in-plane resistivity ratio $\rho_c/\rho_a(300\text{ K}) = 1.7$. $\rho(T)$ measurements on the non-magnetic analog $LaRhIn_5$ indicate that the anisotropy in the $CeRhIn_5$ resistivity stems predominantly from anisotropy in Kondo-derived magnetic scattering. In the magnetically ordered regime, an applied field H reduces T_N only slightly due to the small ordered moment ($0.75\mu_B$) and the effects of magnetic anisotropy. The magnetoresistance (MR) below T_N is positive and shows little sign of saturating in fields to 18 T. In the paramagnetic state, a positive MR is present below 7.5 K, while a high-field negative contribution is evident at higher temperatures. The positive contribution decreases in magnitude with increasing temperature. Above 40 K the positive contribution is no longer observable, and the MR is negative. The low-T positive MR results from interactions

with the Kondo-coherent state, while the high-T negative MR stems from single-impurity effects. In general, these results indicate that $CeRhIn_5$ exhibits a modest degree of transport anisotropy not atypical among heavy fermion compounds.

In section 3.2 we report on magnetotransport measurements between 1.4 and 300 K and in applied magnetic fields to 18 T on the $Ce_{1-x}La_xRhIn_5$ series of compounds. The results are discussed in terms of a positive contribution in the magnetoresistance due to the coherent Kondo regime and a negative contribution due to a more localized single impurity regime and serve to put the conclusions from the magnetotransport of $CeRhIn_5$ on firmer ground.

3.1 $CeRhIn_5$

3.1.1 Introduction

Transport measurements in high applied magnetic fields provide an exceptionally useful means of probing the electronic and thermodynamic properties of heavy fermion compounds. This stems from the magnetic origin of the interactions responsible for the mass-enhanced ground state [117, 118]. As such, the resistivity of a heavy fermion system is altered by an applied magnetic field in fundamentally different ways when the compound is in a magnetically ordered, Kondo-coherent or single-impurity regime. Field-dependent measurements can also provide information regarding the importance of magnetic fluctuations and the proximity to low-temperature magnetic instabilities in the coherent regime. Although no complete microscopic theory is available to model the transport and thermodynamic properties of a heavy fermion system, a number of theoretical treatments are available that qualitatively describe the key

features of a system's field-dependent behavior [108, 109]. From the experimental point of view, a wide range of phenomena can be observed when applying a magnetic field at low temperature [119]. Among archetype heavy fermion compounds, UPt_3 and $CeRu_2Si_2$ exhibit highly anisotropic magnetotransport behavior and remarkable field-induced metamagnetic transitions at 20 T [17], and 8 T [14, 15], respectively, while UBe_{13} exhibits negative magnetoresistance above its superconducting transition temperature [120]. Ultimately, a heavy fermion system's field-dependent properties are determined by RKKY and Kondo interactions [53], with the relative importance of these two interactions influenced by magnetic and structural anisotropies as well as the anisotropies and level splittings due to crystal field effects.

$CeRhIn_5$ has attracted considerable attention due to its unusual pressure-temperature phase diagram[3]. Ce heavy fermion systems that order antiferromagnetically typically exhibit a P-T phase diagram wherein applied pressure acts to smoothly reduce the Néel temperature, T_N, to zero at a critical pressure P_c, with superconductivity occurring over a range of pressure centered at P_c. The P-T phase diagram of the cubic member of the $Ce_mM_nIn_{3m+2n}$ series ($CeIn_3$) displays this behavior, with an ambient-pressure ordering temperature $T_N = 10$ K, a slightly enhanced Sommerfeld coefficient of 100 mJ/mole-K^2, and a critical pressure $P_c = 23$ kbar [2, 34]. The $CeRhIn_5$ P-T phase diagram is quite different. At ambient pressure, $CeRhIn_5$ orders antiferromagnetically at 3.8 K. Applied hydrostatic pressure acts to very slightly increase[1] T_N until magnetic order becomes unobservable near 16 kbar, at which point superconductivity appears at 2.1 K [3]. Specific heat measurements indicate an enhanced Sommerfeld coefficient of roughly 420 mJ/mole-K^2 below 10 K; [3] for a single

[1]Recent unpublished results appear to show that applied pressure causes T_N to decrease with increasing pressure[82]

impurity system [121], this corresponds to a Kondo temperature of roughly 10 K (see eq. 3.1.1).

$$\gamma = \frac{\pi R 2J}{6T_K} \tag{3.1.1}$$

where γ is the Sommerfeld parameter and J is the total angular momentum. The crystal structure of $CeRhIn_5$ is composed of alternating layers of the cubic heavy fermion antiferromagnet $CeIn_3$ and a transition-metal layer composed of $RhIn_2$. As such, dimensionality or anisotropy may play a role in the interactions that produce the unusual P-T phase diagram exhibited by $CeRhIn_5$. This is borne out by nuclear quadrupolar resonance [77] and neutron scatting measurements [1] which indicate that the magnetic moments lie in the basal plane of the tetragonal structure with a spiral along the c-axis, with a reduced magnetic moment of 0.75 Bohr magnetons (μ_B). However, recent inelastic neutron scattering experiments indicate the the inter- and intra-plane exchange are not very different indicating some degree of 3-dimensional behavior for $CeRhIn_5$ [122]. Further measurements are needed to fully elucidate the influence of dimensionality on the physical properties of $CeRhIn_5$.

In order to enhance our understanding of the ground state properties of $CeRhIn_5$, we have measured the anisotropic resistivity of this compound as a function of magnetic field and temperature. The resistivity is moderately anisotropic, with a room-temperature c-axis to in-plane resistivity ratio $\rho_c/\rho_a(300\text{ K}) = 1.7$. This ratio changes markedly with decreasing temperature, and at 4 K the in-plane resistivity is larger than the out-of-plane resistivity by a factor of 80 %. The antiferromagnetic transition at 3.8 K produces an inflection point in ρ. With application of magnetic field, the transition moves to slightly lower temperatures, with a different field-dependence for each direction of the applied field. The magnetoresistance (MR) also depends upon

the direction of the applied field, and it appears to be only moderately influenced by structural anisotropy. The MR is positive in the magnetically ordered state and shows little sign of saturating, except possibly at the lowest temperature for H||c. At moderate temperatures, we observe a positive contribution to the MR that is characteristic of a Kondo system in the coherent regime. At higher temperature, this positive MR gives way to a negative contribution characteristic of a single impurity Kondo system.

3.1.2 Experimental Details

Single crystals of $CeRhIn_5$ were grown from an In flux method [71] as described previously [37]. The deleterious influence of residual In flux on low-T transport measurements (the superconducting transition for In occurs at 3.4 K) necessitates careful sample surface polishing to remove any possible In contamination. The polished single crystal samples were orientated by using Laue x-ray diffraction to determine the crystallographic in-plane (a-axis) and out-of-plane (c-axis) directions. Finally, the resistance of each sample that was slated for use in MR measurements was measured down to 2 K to ensure that no extrinsic superconductivity contamination was evident at 3.4 K due to surface In. The samples that passed this screening process had residual resistivity ratios [RRR = $\rho(300K)/\rho(2K) \approx 100$] that were similar to those reported previously [72]. All in field resistivity measurements reported here were made with a conventional four-probe sample configuration in which silver conductive paint or epoxy was used to make sample contacts. Sample resistances were measured with a low-frequency ac bridge. The in-plane and out-of-plane resistivities were determined on oriented samples via the Montgomery[123] and anisotropic van

der Pauw methods[124, 125] by M.F. Hundley. The transverse magnetoresistance was measured with current applied along an a-axis, and the applied field oriented perpendicular to the measurement current (i.e., either in the other a-axis or along the c-axis). The transport measurements were carried out in a variable flow cryostat capable of producing temperatures from 1.4 K to 325 K. To avoid magnetoresistance effects in the Cernox thermometer used to determine and control sample temperature, temperatures below 3 K were stabilized by controlling the ^{4}He vapor pressure.

3.1.3 Results

The temperature-dependent resistivities of $CeRhIn_5$ and $LaRhIn_5$ in, and perpendicular to, the basal plane, are shown in Fig. 3.1a. The data for $CeRhIn_5$ indicate that this compound is moderately anisotropic; ρ_c is roughly 70 % larger than ρ_a at room temperature. Below 325 K the resistivity falls with decreasing temperature in both directions, and both ρ_a and ρ_c exhibit shoulder-like features between 50 and 100 K. Both resistivities fall-off more rapidly at lower temperatures. ρ_a and ρ_c cross at 30 K, and the a-axis resistivity is larger than the c-axis resistivity down to 1 K. In comparison, the resistivity of $LaRhIn_5$ (the non-magnetic analog of $CeRhIn_5$) varies linearly with temperature below 300 K, and saturates to a value near 1 $\mu\Omega cm$ below 20 K. The $LaRhIn_5$ c-axis resistivity is greater than the in-plane resistivity at all temperatures, and the anisotropy ratio ρ_c/ρ_a is nearly T-independent. The 300 K anisotropy ratio $\rho_c/\rho_a = 1.2$ for $LaRhIn_5$ suggests that the non-magnetic electronic anisotropy inherent to the $RMIn_5$ structure is relatively small.

The temperature-dependent magnetic scattering component ($\rho_{mag} = \rho_{Ce} - \rho_{La}$) of the $CeRhIn_5$ in-plane and c-axis resistivities are presented in Fig. 3.1b. After

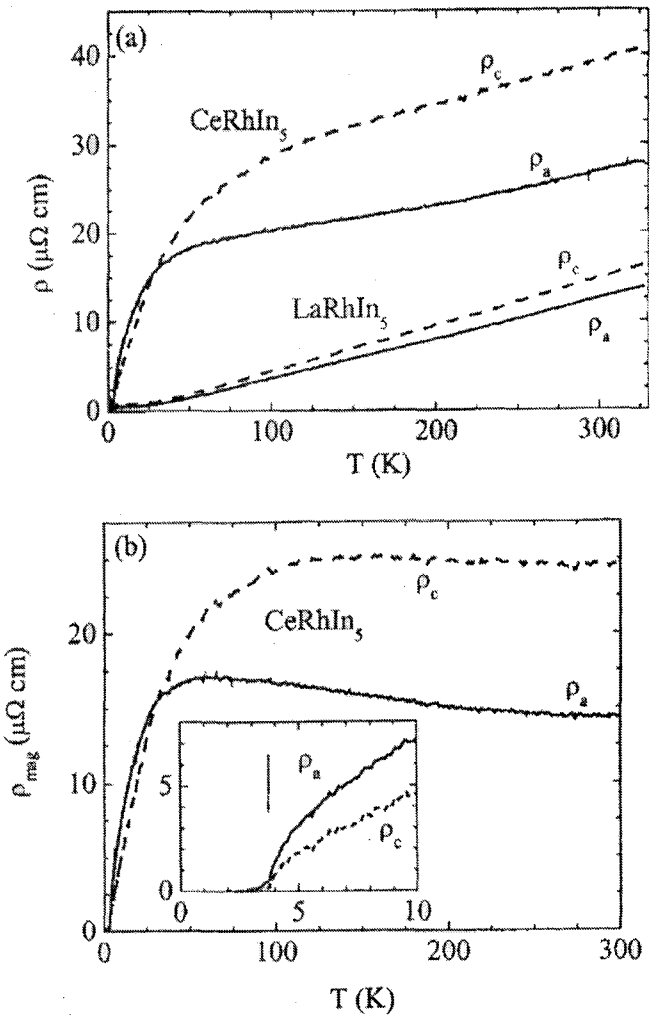

Figure 3.1: (a) In-plane (solid lines) and c-axis (dashed lines) temperature-dependent resistivities of $CeRhIn_5$ and the non-magnetic analog $LaRhIn_5$. (b) The in-plane (solid line) and c-axis (dashed line) magnetic resistivity ($\rho_{mag} = \rho_{Ce} - \rho_{La}$) of $CeRhIn_5$. The data near T_N are highlighted in the inset, with the arrow positioned at T_N.

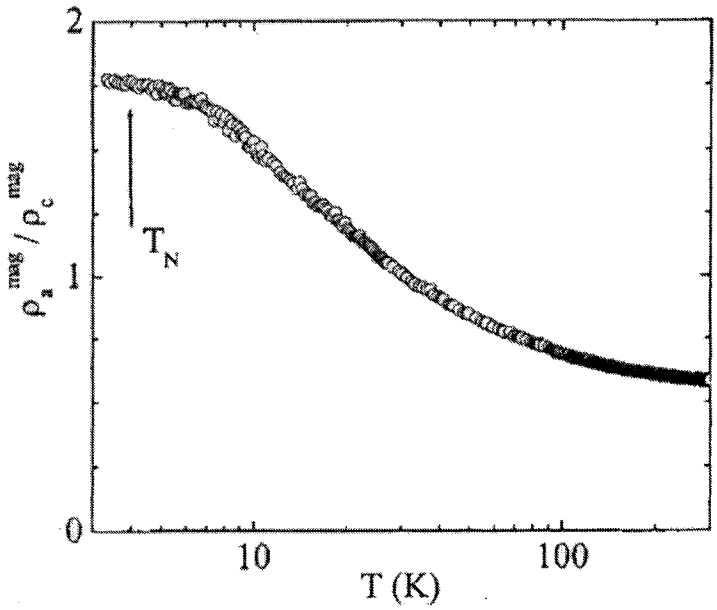

Figure 3.2: Temperature-dependent magnetic resistivity anisotropy ratio ($\rho_a^{mag}/\rho_c^{mag}$) of $CeRhIn_5$.

removing the electron-phonon scattering contribution to ρ_{Ce}, the magnetic resistivity in both crystallographic directions varies as $\rho \propto -\ln(T)$ at high temperatures and drops sharply below 50 K; this T-dependence is characteristic of Kondo lattice compounds [118]. The resistivity in the vicinity of the 3.8 K antiferromagnetic (AFM) transition is shown in the inset to Fig. 3.1b. A clear change in magnetic scattering is evident in both ρ_a and ρ_c near T_N. The transport anisotropy ratio is plotted as a function of temperature in Fig. 3.2. Near room temperature the magnetic resistivity is moderately anisotropic ($\rho_a^{mag}/\rho_c^{mag}$ at 300 K is 0.6), and the ratio exhibits a gradual evolution from a high-T regime where $\rho_a^{mag}/\rho_c^{mag} < 1$ to a low-T regime where $\rho_a^{mag}/\rho_c^{mag} > 1$. The magnetic resistivities cross at 30 K. ρ_c^{mag} is smaller than ρ_a^{mag}

down to the lowest measurement temperature (1.4 K), and there is no evidence for any change in $\rho_a^{mag}/\rho_c^{mag}$ at or below T_N.

We now turn to an examination of the influence of applied magnetic fields on the T-dependent in-plane resistivity. The resistivity as a function of temperature in a field of 18 tesla is displayed in Fig. 3.3, and compared to the zero-field ρ_a data. In Fig. 3.3(a) the magnetic field is applied parallel to the basal plane and perpendicular to the current. A positive MR is evident at low temperatures, with the magnitude of the effect diminishing with increasing temperature. Above roughly 50 K, no difference is discernable between $\rho(H = 0)$ and $\rho(18\ T)$. The inset to Fig. 3.3(a) shows $\rho(T)$ in fields of 0, 10, and 18 T in the vicinity of T_N; in this temperature regime the applied fields appear to uniformly increase the resistivity below 4 K. The H-dependent AFM ordering temperature can be determined by finding the location of the inflection point in ρ that marks T_N. The arrows in the inset denote $T_N(H)$. The transition moves downward monotonically with temperature; in 18 T the inflection point occurs at 3.35 K, corresponding to the rate $dT_N/dH_{\|} = -25$ mK/T. The a-axis resistivity for a field applied parallel to the c-axis is shown in Fig. 3.3(b). In this field orientation, the low-T magnetoresistance is also positive, but the 18 T MR crosses zero at 16 K, and becomes large and negative at higher temperatures. This negative MR effect reaches a maximum value at nearly 30 K. At higher temperatures the negative MR diminishes in magnitude, approaching zero at 100 K. The inset to Fig. 3.3(b) depicts $\rho(T)$ in fields of 0, 5, 10, 15, and 18 T in the vicinity of T_N; as with the in-plane field orientation, the applied field uniformly increases ρ_a below 5 K. The field also decreases the AFM transition temperature, but at a faster rate than for fields oriented in the basal plane. In 18 T the applied field drops T_N to 3.0 K; this corresponding

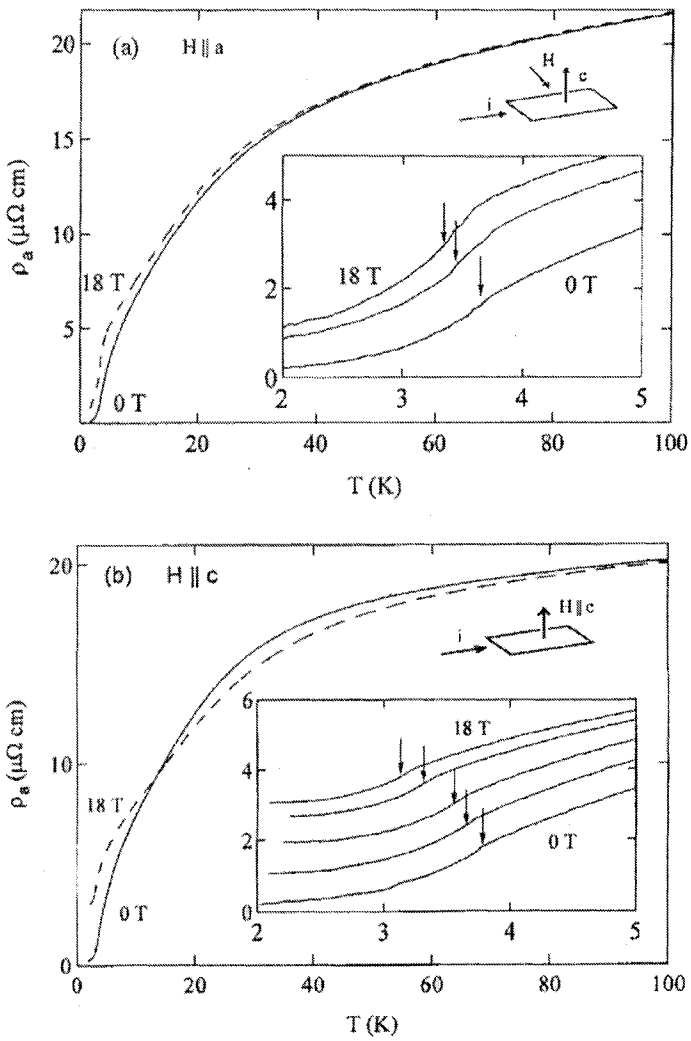

Figure 3.3: In-plane temperature-dependent resistivity in an applied magnetic field. In (a) the magnetic field is applied in the basal plane (perpendicular to the current). The inset displays an expanded view near the AFM transition (the curves correspond to μ_oH = 0, 10, and 18 T). The arrows mark the inflection point in r (located at 3.70, 3.45, and 3.35 K). In (b) the field is applied along the c-axis. The curves in the inset correspond to μ_oH = 0, 5, 10, 15, and 18 T, where the inflection points are located at 3.80, 3.70, 3.60, 3.30, and 3.10 K, respectively. For both field directions a small amount of scatter in the ρ(T) data leads to an uncertainty in determining T_N of $\pm$ 50 mK.

to a rate $dT_N/dH_\perp$ = -35 mK/T, a value that is in good agreement with previous Cp(H,T) measurements. [86, 6]

The field-dependent in-plane magnetoresistance $\Delta\rho_a(H) = \rho_a(H) - \rho_a(H=0)$ at constant temperature is depicted in Figures 3.4 (H || a) and 3.5 (H || c) for $CeRhIn_5$. With the field applied in the basal plane the MR below 10 K (Fig. 3.4a) exhibits two distinct regimes. At 1.4 K the $\Delta\rho_a(H)$ varies linearly with H throughout the measured field range ($H \leq 18$ T), while for $T > T_N$ the MR grows in magnitude and exhibits some curvature below 5 T. At 7.5 K the MR varies as $H^{\frac{1}{2}}$ above 1 T, and it saturates above 15 T. At still higher temperatures (Fig. 3.4b) $\Delta\rho_a(H)$ displays a broad maximum that occurs near $H_{max} = 12$ T. The rise in the MR at low fields is suppressed as the temperature is increased, and the overall magnitude of the magnetoresistance diminishes as well. The relative magnetoresistance in 18 T, defined as $[\rho_a(H) - \rho_a(H=0)]/\ \rho_a(H=0)$, is plotted as a function of temperature in the inset to Fig. 3.4a. The relative MR is nearly zero above 20 K, and grows markedly below 10 K in large measure due to the sharp drop in $\rho_a(T, H = 0)$ that stems from the onset of coherence. In contrast, the magnetoresistance of the non-magnetic analog $LaRhIn_5$ displays a standard metal-like positive MR that varies as H^2 and diminishes in magnitude with increasing temperature.

The in-plane magnetoresistance of $CeRhIn_5$ with H applied along the c axis is depicted in Fig. 3.5. For $T \leq 7.5$ K (Fig. 3.5a) the results are qualitatively similar to those for H || a. Below T_N $\Delta\rho_a(H)$ is positive, with a small change in slope evident near 2.5 T. There is little sign of saturation, except possibly the appearance of a feature of unknown origin at 17 T at 1.4 K. Above T_N the high-field MR grows as H^α with $\alpha < 1$. At 7.5 K $\Delta\rho_a(H)$ varies as $H^{1/2}$ throughout the measured field range and it

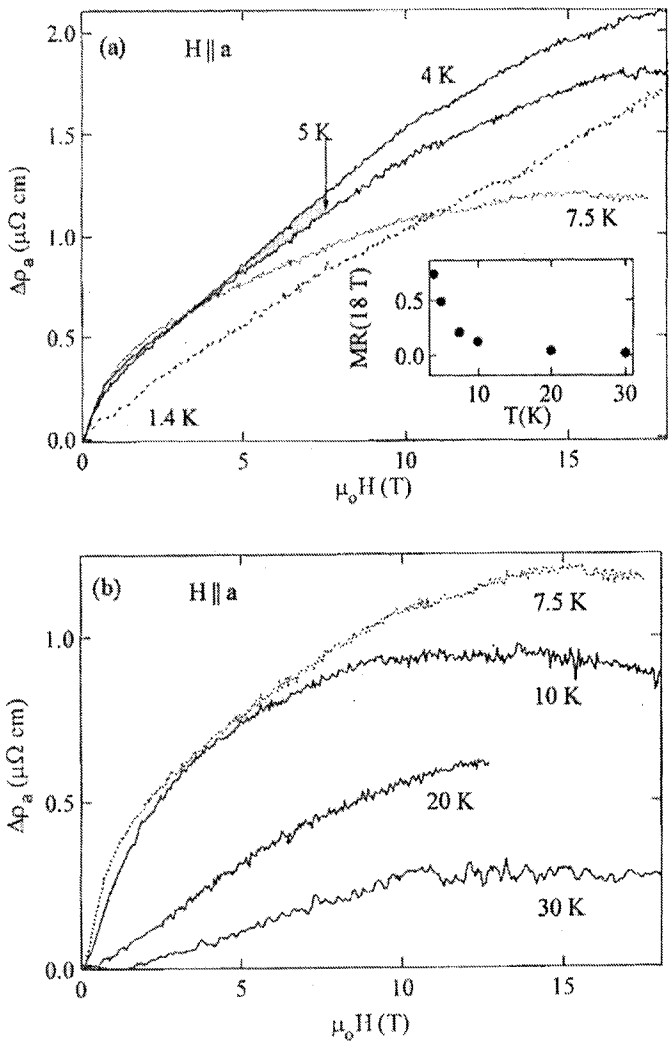

Figure 3.4: In-plane field-induced change in resistivity $\Delta\rho = (\rho(H) - \rho(0))(H \parallel a)$. The low-T behavior is featured in (a). The inset shows the magnetoresistance $\Delta\rho/\rho(0)$ at 18 T for T < 30 K. The value for the 1.4 K magnetoresistance at 18 T ($\Delta\rho/\rho(0) = 8.7$) is not displayed due to its large magnitude. The high temperature behavior of $\Delta\rho$ is displayed in (b).

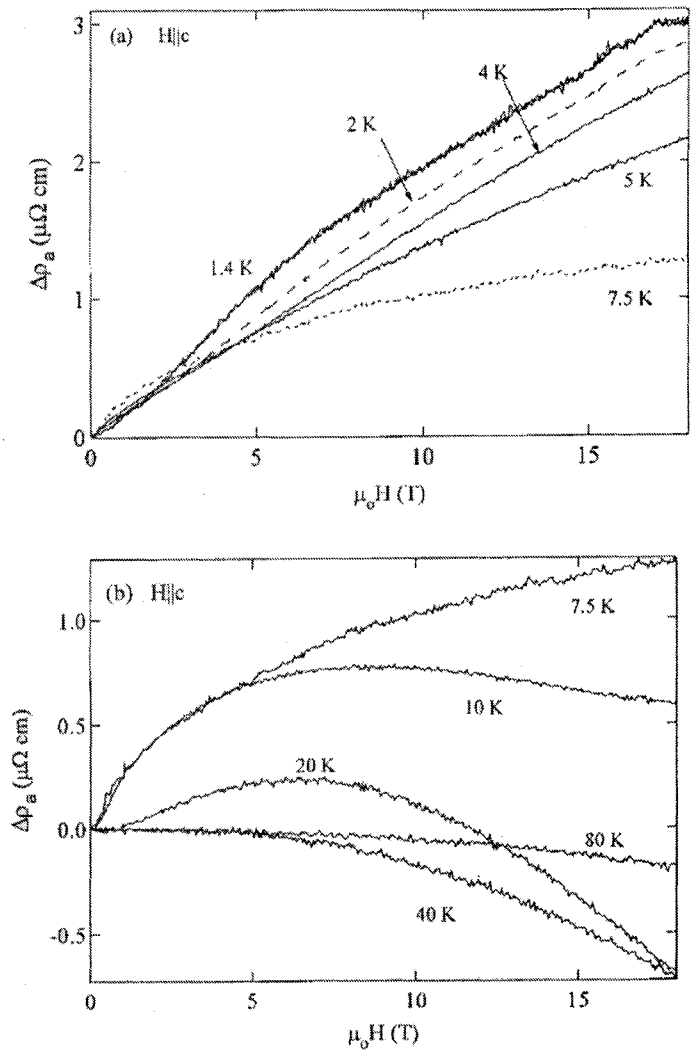

Figure 3.5: In-plane field-induced change in resistivity $\Delta\rho = (\rho(H) - \rho(0))$ (H $\|$ c). The low-T behavior is featured in (a). The high temperature behavior of $\Delta\rho$ is displayed in (b).

is approaching saturation at 18 T. For T $\geq$ 7.5 K (Fig. 3.5b) the MR is quite different from the low-T behavior. The $H^{1/2}$ behavior present at 7.5 K evolves into a peak in $\Delta\rho_a$(H) at 10 K that occurs between 5 and 10 T, and the MR decreases markedly at still higher fields. Above 20 K, the low-H positive MR is no longer in evidence and the negative MR contribution predominates. The MR is negative above 30 K at all fields, and the overall magnitude of the negative MR decreases with increasing temperature. Taken as a whole, the temperature and magnetic-field dependent ρ_a data presented in Figs. 3-5 suggest that there are three field-dependent transport regimes in $CeRhIn_5$. The first, in the magnetically ordered state, exhibits a large positive MR that shows little sign of saturation at 18 T (we note that at least 40 T is required to field-polarize the AFM state) [126]. The second regime resides in the paramagnetic state just above T_N. In this regime the MR is positive and exhibits a tendency to saturate near 20 T. The third regime occurs at temperatures above 10 K and at high fields where a negative MR contribution comes into play that initially produces a maximum in $\Delta\rho_a$(H). At still higher temperatures, the positive MR disappears and the negative contribution dominates the field-dependent transport. Magnetic anisotropy influences the detailed nature of the field-dependent transport. The influence of the high-T negative MR contribution is largest with the field applied perpendicular to the basal plane. As such, the peak field H_{max} is largest with the field applied in the basal plane, and the MR is more negative for H $\|$ c.

3.1.4 Discussion

The anisotropy in the zero-field resistivity data, and the complex H-field and T-dependence of the a-axis magnetoresistance are the most prominent features of these

$CeRhIn_5$ magnetotransport data. How do these features reflect the tetragonal crystal structure, the Kondo and crystal-field interactions, and the RKKY-mediated antiferromagnetic order? Before answering these questions, we first must examine the influence that lattice anisotropy has on the electronic and magnetic structure in the $CeRhIn_5$. The $CeRhIn_5$ unit cell is composed of cubic $CeIn_3$ building blocks that are separated by $RhIn_2$ layers. Full-potential band structure calculations [74] indicate that the electronic structure of $CeRhIn_5$ and $LaRhIn_5$ reflects the quasi-2D nature of the tetragonal unit cell. The band structure exhibits a number of bands that cross the fermi energy E_F, producing three fermi surfaces. Only the first, containing hole-like orbits, is relatively isotropic. Reflecting $CeRhIn_5$'s planar structure, the second and third surfaces are composed of corrugated cylindrical electron- and hole-like orbits that extend along the c-axis. de Haas-van Alphen (dHvA) measurements detect extremal orbits that are consistent with the band-structure calculations. [72, 74] In addition, the Hall effect in both $CeRhIn_5$ and $LaRhIn_5$ is anisotropic and strongly temperature dependent [127], providing clear evidence for competing electron and hole carriers. The fact that the Hall effect in $CeRhIn_5$ and $LaRhIn_5$ are quite similar indicates that they share the same anisotropic electronic structure, and that the f-electrons in $CeRhIn_5$ are localized. de Haas-van Alphen (dHvA) measurements [128], which observe similar frequencies throughout the entire $Ce_{1-x}La_xRhIn_5$ series, are consistent with this last conclusion. Hence, from both measurement and calculation, the layered structure of $CeRhIn_5$ is reflected in the compound's complex electronic structure.

The magnetic structure of the antiferromagnetic ground state also reflects $CeRhIn_5$'s

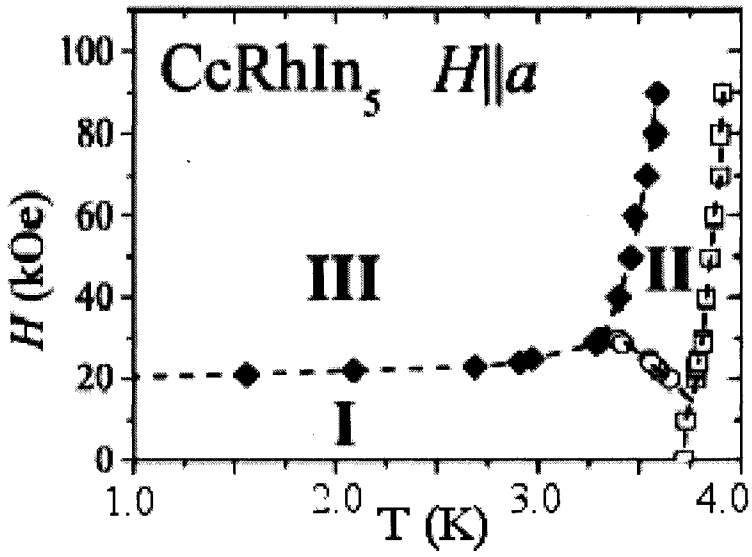

Figure 3.6: H-T phase diagram for $CeRhIn_5$ for H||a. There are three magnetically ordered portions of the phase diagram. I is the incommensurate structure at zero field; II is a commensurate structure; and III is a second incommensurate structure. [Source ref. [6]]

layered nature. The magnetic moments that order at $T_N = 10$ K in $CeIn_3$ are commensurate with the cubic lattice. [2] In contrast, the magnetic moments in $CeRhIn_5$ are found to lie completely within the basal plane, and they form an incommensurate spiral along the c-axis. [77, 1] Field-dependent specific-heat [6] and dHvA [72] measurements indicate that fields oriented along the c-axis gradually reduce the ordering temperature without altering this incommensurate structure. Fields applied within the basal plane strongly influence the magnetic structure, producing a complex H-T phase diagram (see figure 3.6) [126, 6, 87]. Below 3 K a field of 2 T transforms the magnetic structure to one that is commensurate with the lattice, while a third state is also present near 3.5 K. The onset ordering temperature is much less field-dependent

than for H || c. In the paramagnetic regime the magnetic susceptibility χ exhibits a factor-of-two anisotropy between χ_a and χ_c. [3] This anisotropy stems from the splitting of the J = 5/2 manifold under the influence of tetragonal crystalline electric fields. The crystal field level scheme that describes χ_a(T) and χ_c(T) in the paramagnetic state [129][2] includes a Γ_7 doublet groundstate (composed predominately of the $|\frac{5}{2}\rangle$ spin state), a first-excited Γ_7 doublet (predominately $|\frac{3}{2}\rangle$) at 7 meV, and the 2nd excitted state, a spin-$\frac{1}{2}$ Γ_6 doublet, located 24 meV above the Γ_7 groundstate. Taking into consideration $CeRhIn_5$'s electronic and magnetic structures, as well as the crystal-level scheme, we can now examine the underlying mechanisms responsible for the magnetotransport features exhibited by $CeRhIn_5$.

The modest transport anisotropy exhibited by $LaRhIn_5$ ($\rho_c/\rho_a \approx 1.2$) indicates that the quasi-2D electronic structure does not translate into transport anisotropy. Conventional electron-phonon scattering also appears to be weakly influenced by the planar 115 structure as well. The absence of significant anisotropy in the resistivity of $LaRhIn_5$ indicates that the anisotropy in the $CeRhIn_5$ resistivity stems from magnetic scattering. Both the a-axis and c-axis magnetic resistivities of $CeRhIn_5$ display temperature-dependencies that are characteristic of a Kondo-lattice compound. The complex T-dependent anisotropy between the a and c-axis magnetic resistivities is reminiscent of that seen in many other heavy-electron systems. For example, The a-axis and c-axis resistivities in the tetragonal compounds $CeRu_2Si_2$ and $CeNi_2Ge_2$ also cross in a manner reminiscent of $CeRhIn_5$. [130, 131] There are also a number of other f-electron compounds that exhibit an anisotropic ρ_{mag} but without any crossing of the ρ_a and ρ_c resistivities. Systems that fall into this second

[2]The crystal field level scheme will be described in more detail in chapter 5

class include orthorhombic $CeCu_6$ [132] and the tetragonal compounds $CePt_2Si_2$ [133], $CePd_2Si_2$ [134], and $CeCu_2Si_2$. [135] As with $CeRhIn_5$, ρ_a and ρ_c never differ by more than a factor of 2 in these systems. These resistivity anisotropies can be explained by considering the nature of the scattering relaxation rates that are produced when Kondo scattering is influenced by anisotropic crystal-field levels. [136, 137, 138, 139] This modelling successfully describes the anisotropy evidenced by a wide variety of Ce compounds. [133, 136, 137, 138, 139, 140, 141] As such, it seems reasonable to conclude that the magnetic resistivity anisotropy in $CeRhIn_5$ is a reflection of anisotropic carrier scattering due to the influence of the crystal fields.

The influence of an applied magnetic field on the resistivity near the antiferromagnetic transition is depicted in the insets to Figs. 3.3a and 3.3b. The zero-field AFM order at $T_N = 3.8$ K gives rise to an inflection point in the resistivity, indicating that magnetic order alters the transport in at most a modest way. The absence of any abrupt change in the ratio ρ_a/ρ_c at T_N indicates that the onset of magnetic order influences spin-wave scattering isotropically; this is consistent with inelastic neutron scattering measurements [122] which indicate that there is no 3-D to 2-D crossover prior the onset of long-range order and that the magnetic system is predominantly three-dimensional. Specific-heat [6] measurements show that a magnetic field applied in the basal plane will split the antiferromagnetic transitions into three separate transitions. Preliminary neutron-diffraction measurements [87] indicate that these transitions are associated with an evolution in the zero-field magnetic structure. No such splitting of the antiferromagnetic transition signature is evident in the resistivity data shown in the Fig. 3.3a inset. This may be due to the relatively small change in carrier scattering that will occur when the system is transformed from one magnetic

structure to the next; as such, the resistivity inflection points pertaining to the reorientation transitions may be unobservable. However, the inflection point (determined by finding the maximum of $d\rho(H,T)/dT$), as indicated by the arrows in the inset, decreases very gradually ($dT_N/dH_{\|}$ = -25 mK/T) with magnetic field. Specific-heat measurements [86, 6] with the magnetic field applied along the c-axis indicate that while the field does not alter the magnetic structure it does have a stronger influence on T_N; this is consistent with the more rapid field-induced decrease in the inflection-point temperature ($dT_N/dH_{\perp}$= -35 mK/T) evident in the data displayed in the Fig. 3.3b inset. We note that the inflection point at zero applied field occurs at 3.7 $\pm$ 0.05 K in one case (Fig. 3.3a inset) and at 3.8 $\pm$ 0.05 K (Fig. 3.3b inset). This difference is merely an indication of the error in determining the maximum in $d\rho/dT$. Despite this moderate error, the trend of T_N to lower temperature with increasing applied field emerges and is in agreement with previous thermodynamic measurements. [86, 6]

We now consider the magnetoresistance in the paramagnetic state. The data exhibit two field/temperature regimes: at low H and T the MR is positive, while at high H and T the MR exhibits a negative contribution. A similar low-T positive MR has been reported in both $CeAl_3$ [102, 103] and $CeRu_2Si_2$ [104] at low temperatures, and in UBe_{13} under pressure. [105] The similarity between $CeRhIn_5$ and these other compounds suggests that a low-temperature positive MR appears to be a common feature of Kondo systems that are in, or are approaching, a coherent fermi-liquid state. [109, 142] Despite many attempts [108, 109, 110] no satisfactory detailed theoretical explanation for the positive MR in the low-T paramagnetic state has been put forward. For now we can only say that this effect must reflect the influence of an

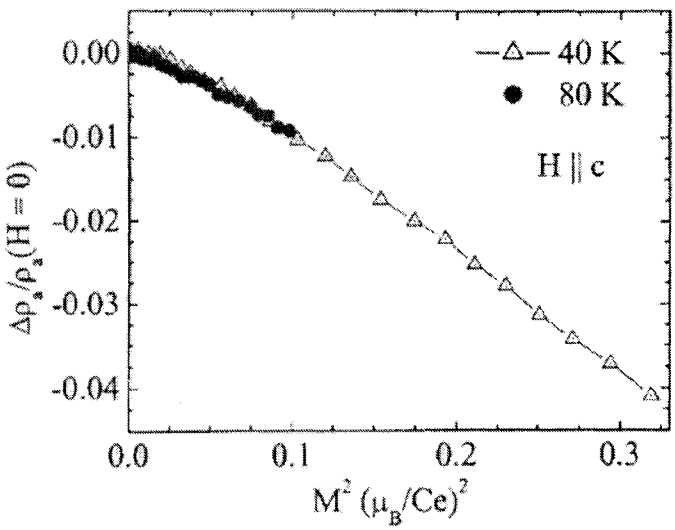

Figure 3.7: In-plane magnetoresistance $\Delta\rho_a/\rho_0$ at 40 and 80 K plotted as a function of the magnetization squared. H is applied along the c-axis, and the M^2 units are Bohr magnetons per Ce atom.

applied H-field on the Kondo-coherent state. In the single-impurity regime our understanding of MR effects rests on firmer ground. In this regime an applied field reduces incoherent Kondo scattering, producing a negative MR. [95, 96, 97, 98, 99, 100, 101] In this situation the MR is known to scale with the induced magnetization M as $\Delta\rho/\rho_o \propto -M^2$. [99, 100, 101] Hence, a plot of $\Delta\rho/\rho_o(M)$ for all H and T should fall onto a single, universal curve. A careful analysis of the magnetoresistance data for all temperatures that exhibit a hint of a negative MR is made problematic by the interaction between the low-H positive effect and the high-H negative contribution. Nonetheless, this single-impurity analysis is possible with H $\parallel$ c for T $\geq$ 40 K, as the MR shows no positive contribution in this temperature range. These data are plotted as a function of M^2 in Fig. 3.7. The data scale as expected, falling on a common line and varying as M^2. Hence, the negative high-temperature MR contribution appears to be a simple-impurity effect. At these temperature the applied field reduces incoherent Kondo scattering, giving rise to a negative MR. The detailed nature of the MR, and in particular the stronger negative contribution for H $\parallel$ c are an indication that the magnetic anisotropy evident in ρ_{mag} also influences the detailed balance between coherent and incoherent MR effects in $CeRhIn_5$. As such, the temperature-dependent $CeRhIn_5$ magnetotransport reflects the prevalent Kondo regime (coherent at low T, single-impurity at high-T) as well as the magnetic anisotropy stemming from the nature of the crystal-field levels.

3.1.5 Conclusions

Structural anisotropy influences the physical properties of $CeRhIn_5$ in a subtle but significant way. Tetragonal crystalline electric fields split the $J = \frac{5}{2}$ manifold into

three doublets whose anisotropy influences both the magnetic susceptibility [3] and the zero-field resistivity. The $RhIn_2$ spacer layer alters the c-axis magnetic exchange sufficiently to produce antiferromagnetism with an incommensurate spiral spin structure. [77, 1] Dimensionality effects are also evident in the way an applied H-field alters this spin arrangement. [6, 87] Both dHvA [72, 74] and Hall effect [127] measurements indicate that $CeRhIn_5$'s electronic structure has two-dimensional character. And, finally, while the overall field and temperature-dependent MR in the paramagnetic regime is predominantly determined by Kondo-lattice and single-impurity Kondo interactions, the detailed interplay between these positive and negative MR contributions indicate the impact of anisotropy on the magnetotransport. Magnetotransport measurements are presented in chapter 4 for the ambient-pressure superconducting members of the 115 series ($CeIrIn_5$ and $CeCoIn_5$) to determine the relative importance of structural and magnetic (CEF) anisotropy in these systems.

3.2 $Ce_{1-x}La_xRhIn_5$

In this section, we will further examine the high field magnetotransport behavior of $CeRhIn_5$ by tuning the interactions by chemical substitution of La onto the Ce site. Doping studies of the $CeMIn_5$ series have already proven to present interesting behavior, including possible coexistence of superconductivity and magnetism in $CeRh_{1-x}Ir_xIn_5$ [89] and $CeRh_{1-x}Co_xIn_5$ [143] and doping induced disordered short-range magnetism and non-fermi liquid behavior for $Ce_{1-x}La_xRhIn_5$[144].

To gain a better understanding of the unusual heavy fermion ground state in $CeRhIn_5$ we have measured the magnetotransport of the $Ce_{1-x}La_xRhIn_5$ series. We have performed our measurements from 1.4 to 300 K in applied magnetic fields to

18 T for samples x = 0.25 and x = 0.75. Substituting 25 % La increases the region in which the magnetoresistance is negative, and by 75 % La the magnetoresistance is positive at 18 T over the entire measured temperature range. At 1.4 K a positive magnetoresistance is observed for x = 0, 0.25, 0.75. The magnitude of the magnetoresistance is nearly the same for x = 0.25 and 0.75 and slightly reduced from that of the pure compound. The samples were grown using a flux growth technique as detailed in Moshopoulou, et al.[37] The samples have Residual Resistivity Ratios (RRR) (300 to 2 K) of 4 for x = 0.25 and 22 for x = 0.75. For comparison, samples of $CeRhIn_5$ have RRR values in the range 50 - 100, while $LaRhIn_5$ has a RRR of 22. The measurements were performed in similar experiential conditions as those in the previous section and as described in Chapter 2. In all cases the current was placed in the basal plane and the field applied along the c-axis.

An overview of the magnetotransport is displayed in fig. 3.8: (a) displays the resistivity at 0 and 18 T for $CeRhIn_5$. A rapid decrease occurs with decreasing temperature in the resistivity at 40 K signaling the onset of coherence. The resistivity at 18 T crosses below the zero field data at 20 K. The inset displays the low temperature behavior in which the resistive signature of the antiferromagnetic transition may be observed as slight downturn in the resistivity. In (b) the resistivity is displayed for x = 0.25. The negative magnetoresistance (at 18 T) persists over a broad range of temperature down to 10 K. The inset displays the magnetoresistance at 1.4 K for x = 0.25 and x = 0.75. Both are positive; the x = 0.25 is close to linear except at low and high fields. For applied fields above 15 T the magnetoresistance behaves as if it is approaching a maximum suggesting the magnetic field is starting to significantly affect the coherent regime. A rapid increase in the magnetoresistance of the x = 0.75 data is

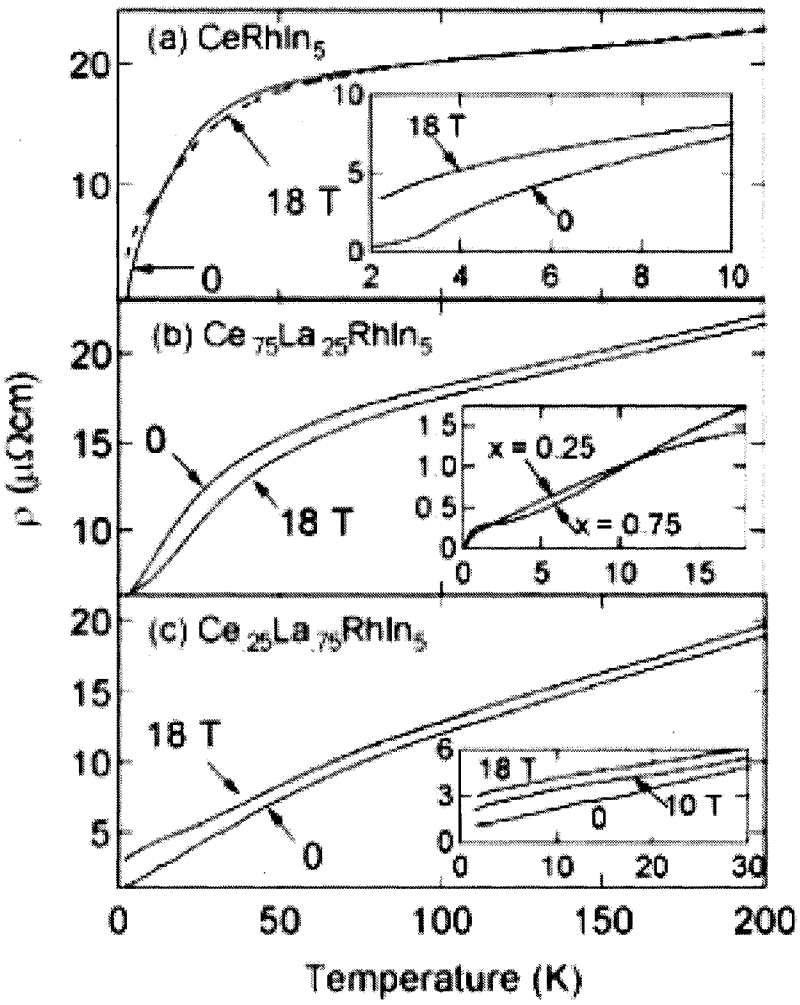

Figure 3.8: Resistivity (ρ) versus Temperature at 0 and 18 T for $CeRhIn_5$ (a), $Ce_{.75}La_{.25}RhIn_5$ (b), and $Ce_{.25}La_{.75}RhIn_5$ (c). The inset in (a) shows the resistive signature of the antiferromagnetic transition. The inset in (b) shows the magnetoresistance, $\frac{\Delta\rho}{\rho_o} = (\rho(T, H) - \rho(T, 0))/\ \rho(T, 0)$ at 1.4 K for x = 0.25 and 0.75. The inset in (c) shows the development of a broad maximum at low temperature for x = 0.75 for applied fields of 0, 10, 18 T.

seen at low field. This may be a signature of the broad feature in the resistivity, which will be discussed in conjunction with (c). Power law fits above 2 T yield poor fits to the data. It is possible the slight upturn in the magnetoresistance may indicate that part of the magnetoresistance is due to normal metal positive magnetoresistance. (c) displays the resistivity at 0 and 18 T for x = 0.75. The magnetoresistance is positive (at 18 T) from 1.5 to 200 K. Fitting the zero field data with a power law between 1.5 and 30 K and yields a power of slightly greater than 1. At low temperature a broad feature appears in the resistivity in applied fields. The origin of this feature is unknown, but may be related to a doping induced short-range magnetism which persists to higher La-concentration[4].

The data presented lead to a general picture in which there are two contributions to the magnetoresistance. One is due to the positive magnetoresistance of the coherent regime of a Kondo Lattice and the other a negative contribution due to a single impurity-like regime. The latter contribution dominates for sufficiently large La concentrations where the Ce ions are well separated. For the x = 0.75 compound a positive contribution is observed over the whole temperature and field range in this study. Another mechanism is needed to describe this positive magnetoresistance; some possibilities include a positive normal metal magnetoresistance, interactions among single impurity like Ce atoms, and disorder effects.

3.2.1 Conclusions

In conclusion, we have given an overview of the magnetotransport for a variety of La substitutions for Ce in $CeRhIn_5$. In particular there is a sign change in the magnetoresistance at high temperature which is reached by La concentration of 75.

Future work should include a more detailed study of the concentration range as well as an attempt to understand the broad bump which appears in the resistivity for the x = 0.75. The overall picture from magnetotransport studies of $Ce_{1-x}La_xIn_5$ is that the anisotropy of $CeRhIn_5$ is typical of other heavy fermion compounds indicating that, at least from the standpoint of transport measurements, $CeRhIn_5$ is not unusually anisotropic. Additionally, we find a high temperature single impurity regime, while at lower temperatures we find behavior characteristic of a Kondo lattice. The single impurity regime extends to lower temperatures with the substitution of La for Ce.

Chapter 4

Magnetotransport studies of $CeIrIn_5$ and $CeCoIn_5$

In this chapter we report magnetotransport measurements on $CeCoIn_5$ and $CeIrIn_5$. In contrast to $CeRhIn_5$, these materials exhibit superconductivity at ambient pressure. The measurements are reported in the temperature range 1.4 K to 300 K and in magnetic fields to 18 T. The high temperature magnetotransport behavior is similar to that of $CeRhIn_5$ in several ways. (1) A drop in the resistance as a function of temperature is observed which is indicative of the formation of a coherent Kondo lattice. (2) At high temperatures a negative magnetoresistance is observed which conforms to the expectation of a high temperature single impurity regime. In contrast to $CeRhIn_5$, a peak in the resistivity is observed at the onset of coherence in both $CeCoIn_5$ and $CeIrIn_5$. This is likely related to the different crystal field splitting exhibited by the different members of the $CeMIn_5$ family. At intermediate temperature we observe a positive peak in the magnetoresistance of all three compounds, with the magnitude of the magnetoresistance being largest in $CeRhIn_5$ and least in $CeIrIn_5$. Below the

superconducting transition temperature in $CeCoIn_5$ a negative magnetoresistance is observed above the critical field required to destroy superconductivity.

4.1 $CeIrIn_5$ and $CeCoIn_5$

4.1.1 Introduction

There are a number of strategies that may be employed to investigate the nature of the unconventional ground states found in heavy fermion materials. The most prevalent tactic is to investigate the normal state out of which the superconductivity grows. The procedure used is to explore the behavior of the normal state at temperatures above the superconducting transition temperature. However, even more information can be gleaned concerning the normal state by looking in regions only accessible by driving the system normal by tuning an intensive variable other than temperature. An example of this is application of magnetic fields. Furthermore, examining the interactions in non-superconducting materials which are closely related to the superconducting material can provide insight into the nature of the superconductivity. In the studies presented in this chapter, the aim is not only to understand similarities and differences between two closely related heavy fermion superconductors, but more importantly to understand any systemic difference or similarities to antiferromagnetic $CeRhIn_5$.

This chapter is organized as follows. First an overview of the the behavior of $CeIrIn_5$ and $CeCoIn_5$ will be given. Following this, the magnetoresistance will be discussed for three temperature regimes. The discussion for the high temperature regime will concentrate on further strengthening the case for a single impurity regime

at high temperature in both $CeIrIn_5$ and $CeCoIn_5$. Next, the magnetoresistance at intermediate temperatures will be examined in the context of the formation of a coherent regime. The low temperature behavior will be discussed in the context of the formation of a coherent regime as well as speculation regarding the promotion of a fermi liquid regime by applied magnetic fields. Finally, a general discussion will be given which compares the magnetotransport behavior of $CeRhIn_5$ to that of $CeIrIn_5$ and $CeCoIn_5$.

4.1.2 Results and Discussion

Overview

We start with an overview of the magnetotransport properties of $CeIrIn_5$ and $CeCoIn_5$. The resistivity measurements reported in this chapter were performed at the National High Magnetic Field Laboratory Los Alamos facility. The experimental conditions were similar to those described in chapters 2 and 3. All of the magnetoresistance measurements are transverse magnetoresistance where the magnetic field is applied parallel or perpendicular to the c-axis and always perpendicular to the current.

Fig. 4.1 displays ρ at zero and 18 T for the temperature range 2 - 300 K for $CeIrIn_5$. The resistivity increases from 100 K until a broad maximum is reached at about 40 K. This broad maximum is interpreted to represent the onset of coherence. As expected, for $T > T^*$ (the coherence temperature) the resistivity displays a logarithmic increase, which is characteristic of the the single impurity Kondo effect. Fits utilizing a logarithmic term (for at temperature range on order of 60 K) yield χ^2s at least an order of magnetic smaller than simple linear fits. Notice that for the magnetic field applied in the basal plane the magnetoresistance is unobservable on the

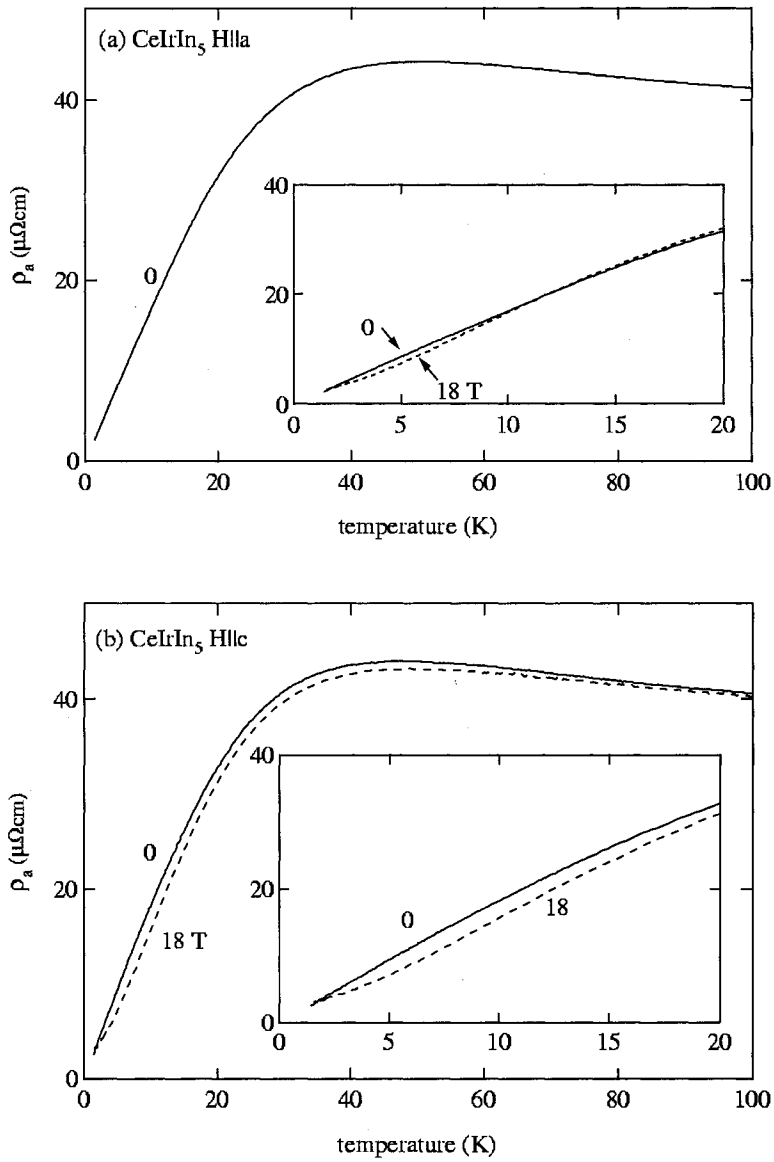

Figure 4.1: ρ for current in the basal plane with applied magnetic fields of 0 and 18 T for fields applied perpendicular to the current in the basal plane and along the c-axis. Note that for magnetic fields applied in the basal plane the magnetoresistance at 18 T is too small to be observed in (a). The insets display the low temperature behavior.

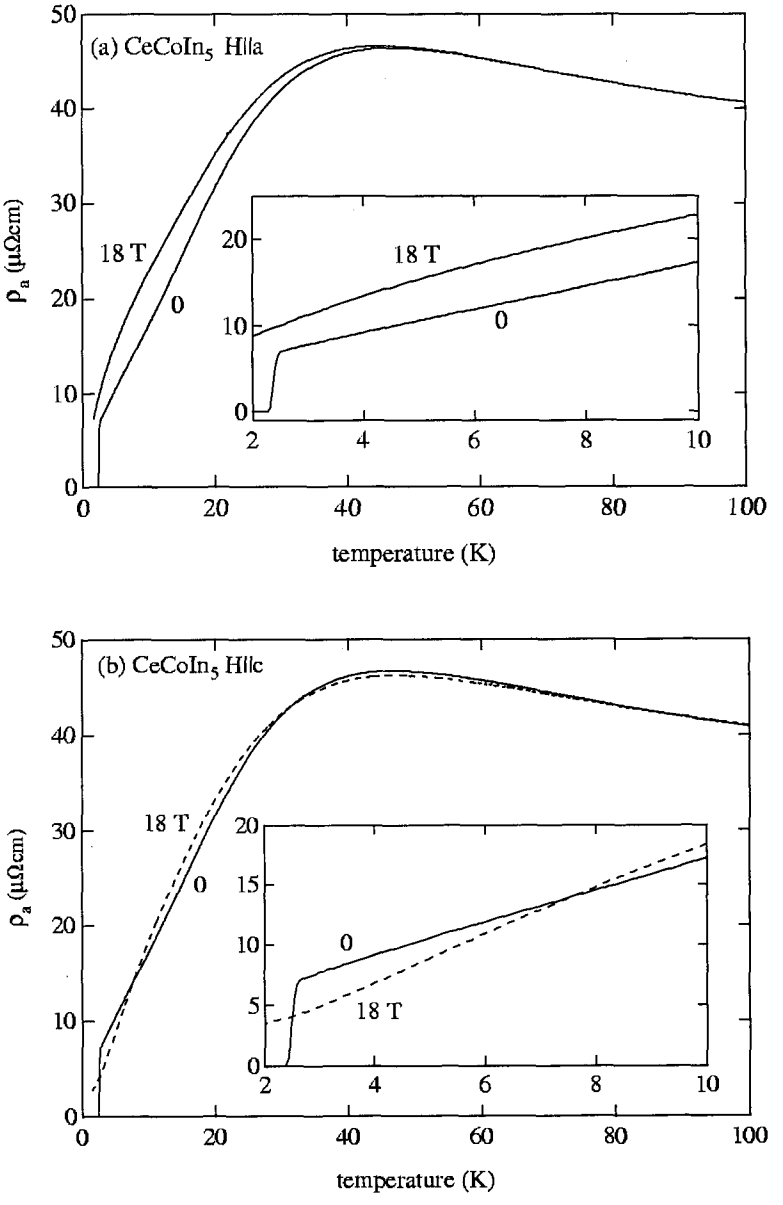

Figure 4.2: ρ for current in the basal plane with applied magnetic fields of 0 and 18 T for fields applied perpendicular to the current in the basal plane and along the c-axis. The insets display the low temperature behavior.

scale show in fig. 4.1(a). In both of the insets of fig. 4.1 the magnetoresistance at 18 T is negative and appears to be more characteristic of a fermi liquid than the zero field data. The magnetotransport data for $CeCoIn_5$ shown in fig. 4.2 bear many similarities to that of $CeIrIn_5$ including: a logarithmic divergence of the resistivity above the onset of coherence, In both, the onset of coherence appears at approximately 40 K. However in contrast to $CeIrIn_5$, he magnetoresistance appears to be stronger for field applied in the plane in $CeCoIn_5$. However, in both materials the promotion of a fermi liquid regime appears to be stronger for field applied along the c-axis. This point will be discussed in more detail in the low temperature section.

High Temperature Regime

The magnetoresistance of $CeIrIn_5$ is shown in fig. 4.3. For magnetic fields applied along the c-axis the most prominent feature is the negative magnetoresistance present at temperatures from 15 to 60 K. Similar behavior is manifested for magnetic fields applied perpendicular to the c-axis. However, a positive contribution to the magnetoresistance is evident at much higher temperatures than for magnetic fields applied along the c-axis. The observation of negative magnetoresistance is consistent with the notion that a single impurity regime exists at high temperature in $CeIrIn_5$. To further examine the conclusion that the high temperature resistivity behaves as a single impurity in figure 4.4 we show that the magnetoresistance scales as the magnetization squared (M^2)[99, 100, 101]. The scaling is reasonable, but in comparison to the high temperature scaling observed in $CeRhIn_5$ the collapse of the magnetoresistance at different temperatures is not as good at high magnetic fields, suggesting that nonlinear effects are slightly more important in $CeIrIn_5$. Curiously, the scaling

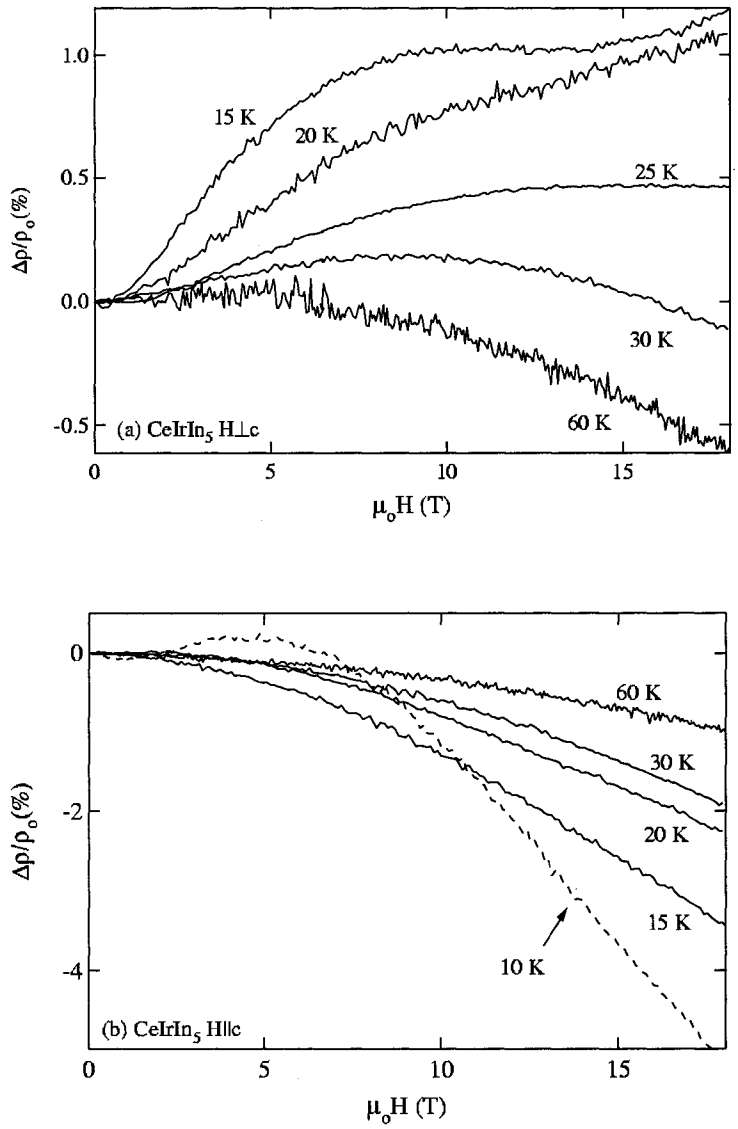

Figure 4.3: Magnetoresistance (in units of percent) versus applied magnetic fields for $CeIrIn_5$ at high temperature. (a) displays the magnetoresistance for applied fields perpendicular to the c-axis and (b) displays the magnetoresistance for fields parallel to the c-axis.

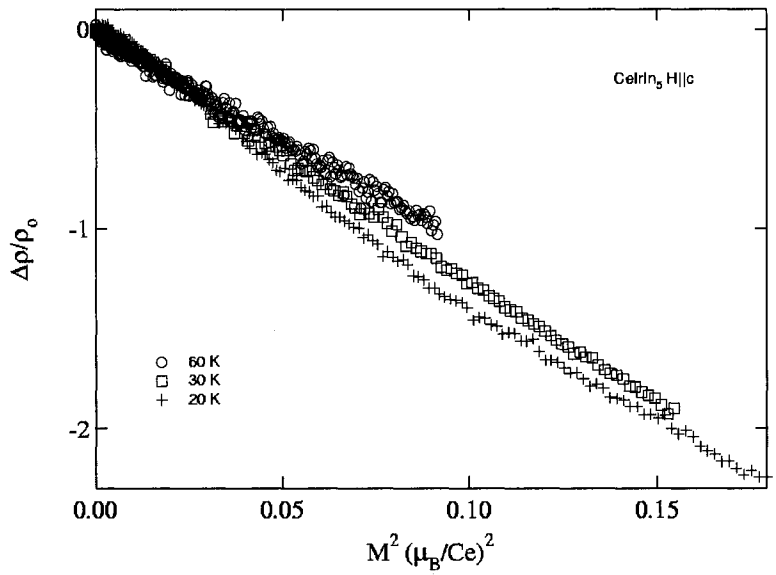

Figure 4.4: The magnetoresistance of $CeIrIn_5$ plotted versus magnetization squared (M^2). The field is applied along the c-axis.

produces a slightly more linear result at low fields for $CeIrIn_5$ than for $CeRhIn_5$.

Intermediate Temperature Regime

Up to this point the discussion of the magnetoresistance in $CeCoIn_5$ and particularly in the case of $CeIrIn_5$ has concentrated on the establishing that a single impurity regime exists at high temperatures. However, it is important to consider the formation of the coherent regime as temperature is lowered. As is the case in $CeRhIn_5$, a positive contribution begins to emerge as coherence sets in for both $CeIrIn_5$ (fig. 4.5) and $CeCoIn_5$ (fig. 4.6). The positive contribution is due to the destruction of the coherent state by the applied magnetic field(see section 3.1.4). There appears to be no simple scaling between the magnetoresistance for field applied parallel and perpendicular to the c-axis in $CeIrIn_5$. For example, within the simplest picture it would be reasonable for the magnetoresistance to scale as the magnetization for the two different field directions. However, in $CeIrIn_5$ this type of scaling fails, suggesting that the scattering mechanisms are influenced more profoundly by the direction of an applied magnetic field than simply the response characterized by the magnetization. The fact that the scaling fails at even low magnetic fields suggests that more than simply high field nonlinearity of the magnetic susceptibility is to blame. In $CeCoIn_5$, this type of scaling is successful for magnetic fields where the scattering due to the destruction of the Kondo coherent state is dominant(fig. 4.7). Above this field, the scaling breaks down, perhaps reflecting the complicated interplay of the scattering caused by both single impurity type scattering and Kondo coherent type scattering. This is a distinction between $CeIrIn_5$ and $CeCoIn_5$. Evidently, the anisotropy as reflected in the magnetoresistance of $CeIrIn_5$ is not represented well by the anisotropy

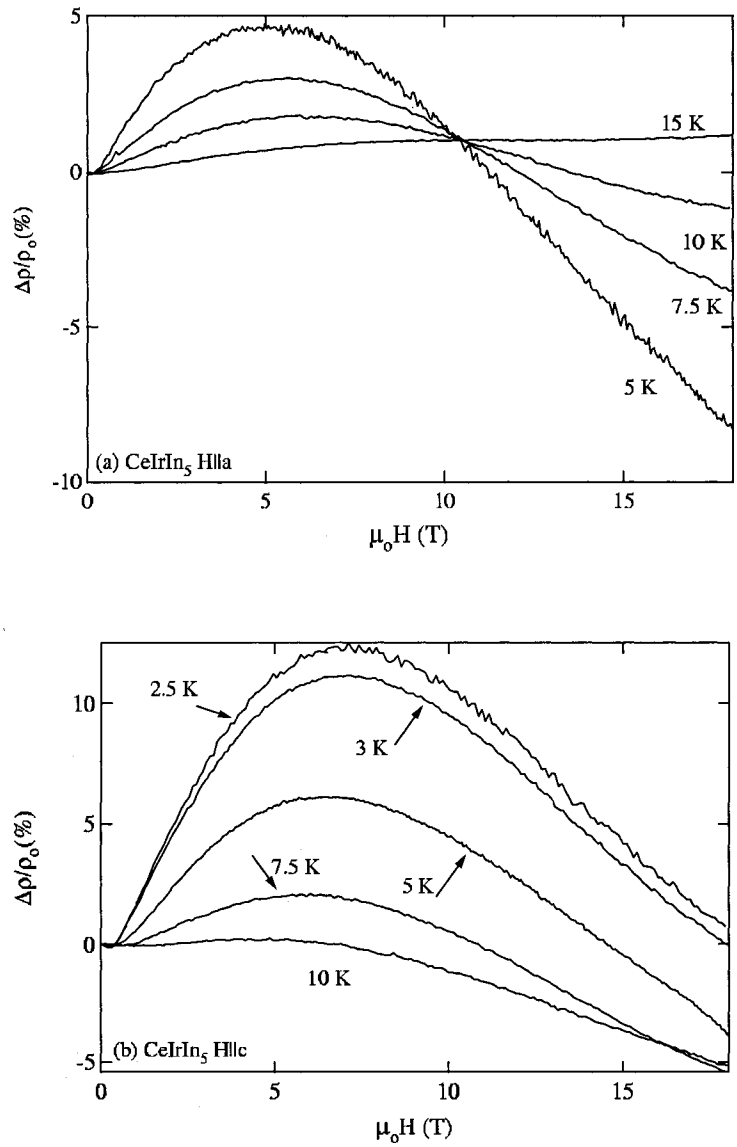

Figure 4.5: Magnetoresistance (in units of percent) versus applied magnetic fields for $CeIrIn_5$ at intermediate temperatures. (a) displays the magnetoresistance for applied fields perpendicular to the c-axis and (b) displays the magnetoresistance for fields parallel to the c-axis.

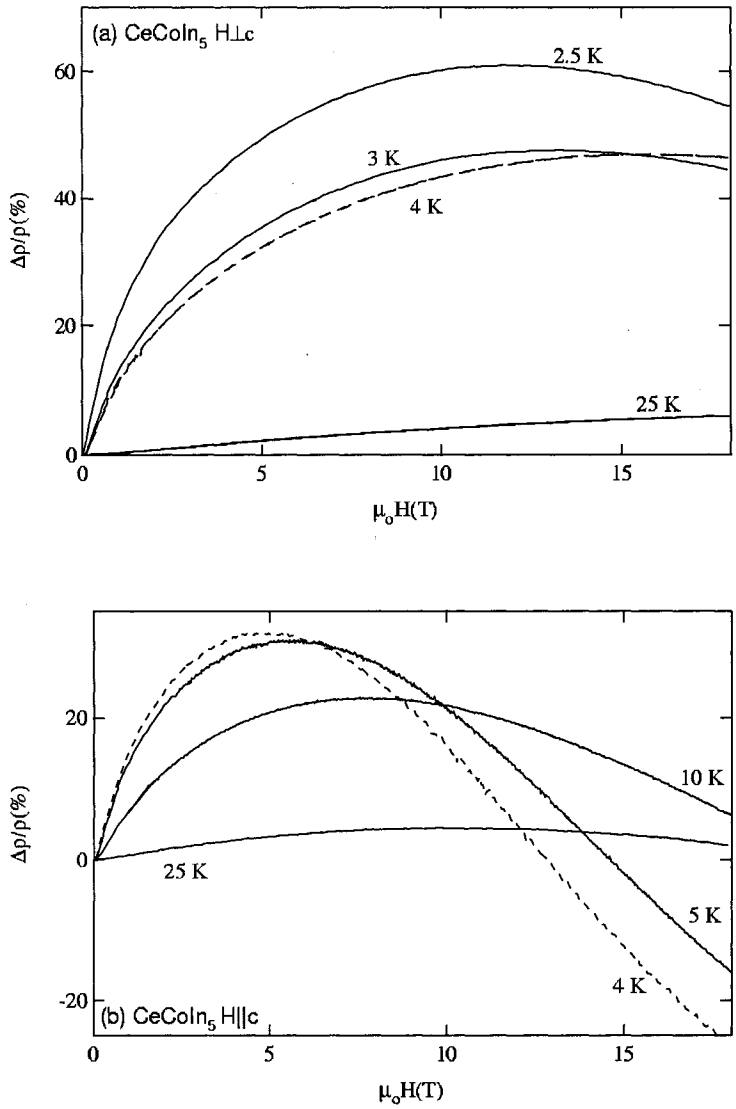

Figure 4.6: Magnetoresistance (in units of percent) versus applied magnetic fields for $CeCoIn_5$ at intermediate temperatures. (a) displays the magnetoresistance for applied fields perpendicular to the c-axis and (b) displays the magnetoresistance for fields parallel to the c-axis.

reflected in the magnetic susceptibility. In contrast, this appears to be the case for fields to 5 or 10 T depending on the temperature range for $CeCoIn_5$.

Low Temperature Regime

The low temperature magnetoresistance for $CeIrIn_5$ with applied magnetic field parallel and perpendicular to the c-axis is shown in fig. 4.8. The most prominent change from the intermediate temperature regime is that the magnetoresistance at the lowest temperatures (1.4 and 2 K) displays an upturn starting at around 15 T. This upturn may be related to the low magnitude of the magnetoresistance due to Kondo scattering, coupled with the increasing effect of a positive normal metal magnetoresistance. This speculation is consistent with the idea the magnetic fields tend to promote the formation of a fermi liquid regime in this material. To quantify the statement in the previous sentence further, power law fits to the resistivity of the form $\rho = xT^y + z$ have been performed and are summarized in table 4.1. It is important to note that while the power appears to be approaching 2 at 18 T, measurements at lower temperature are required to further understand this detail and will be the subject of future work.

The magnetoresistance of $CeCoIn_5$ at low temperatures is displayed in fig. 4.9. For magnetic field applied both parallel and perpendicular to the c-axis it appears that the superconducting transition appears at fields where the coherent Kondo scattering is no longer dominant, suggesting a relation between the formation of a Kondo coherent state and heavy fermion superconductivity in $CeCoIn_5$. In fact, magnetoresistance measurements for fields applied along the c-axis appear to support this hypothesis as identification of a crossover to a fermi liquid regime[145]. We have performed similar

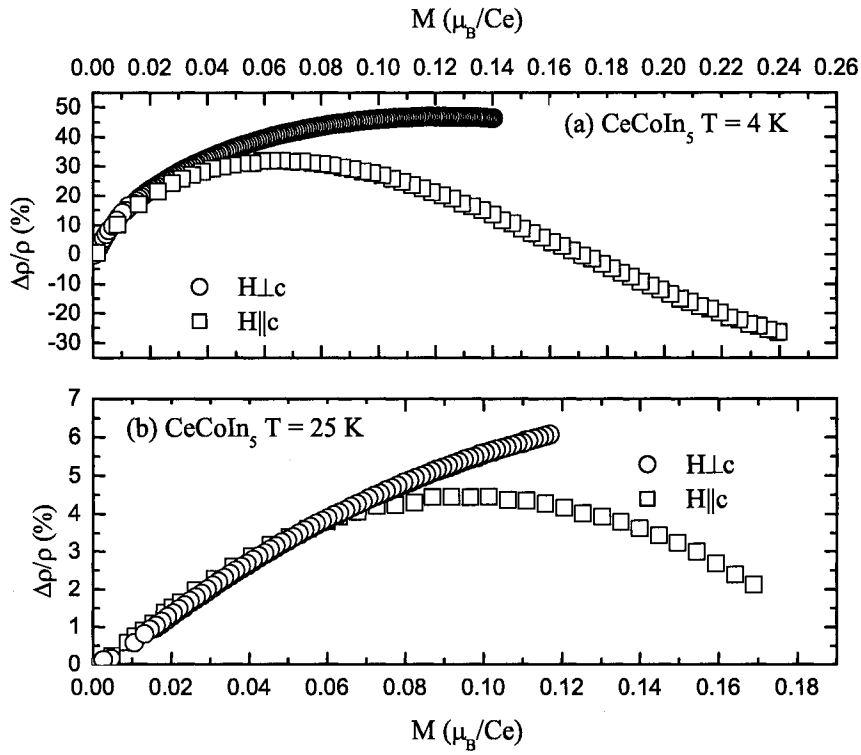

Figure 4.7: Magnetoresistance versus Magnetization for $CeCoIn_5$. (a) displays the scaled data at 4 K for magnetic field applied parallel (squares) and perpendicular (circles) to the c-axis. (b) displays the scaled data at 25 K for magnetic field applied parallel (squares) and perpendicular (circles) to the c-axis.

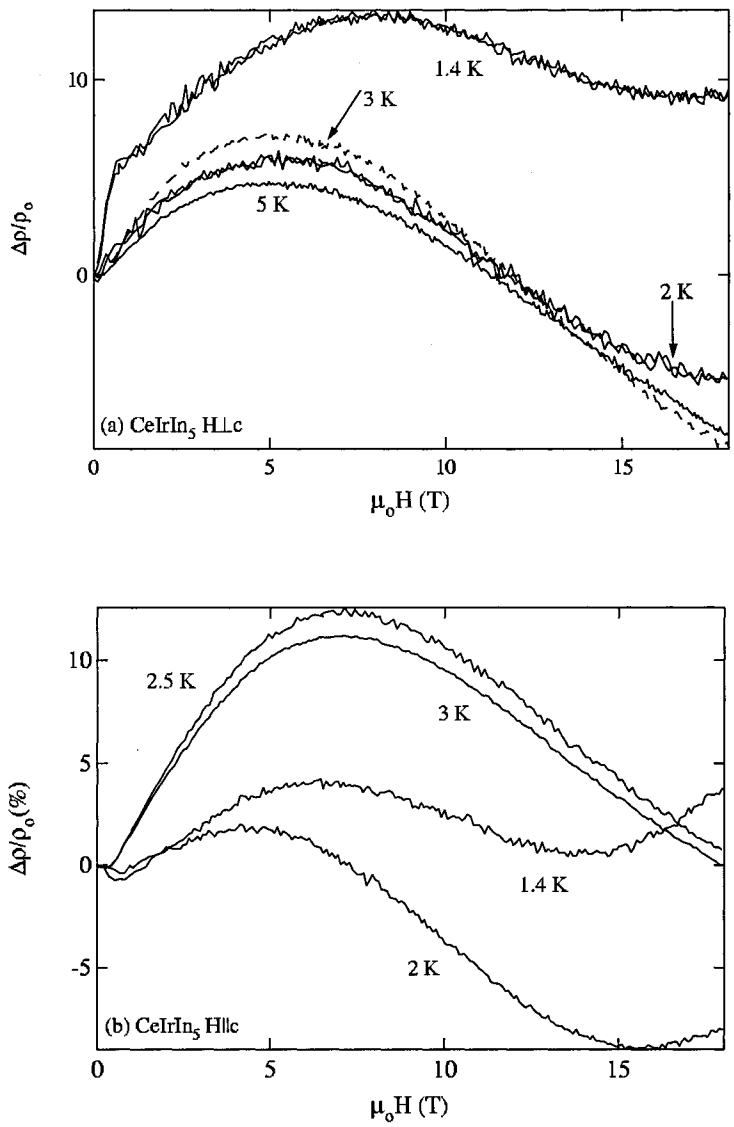

Figure 4.8: Magnetoresistance (in units of percent) versus applied magnetic fields for $CeIrIn_5$ at low temperatures. (a) displays the magnetoresistance for applied fields perpendicular to the c-axis and (b) displays the magnetoresistance for fields parallel to the c-axis.

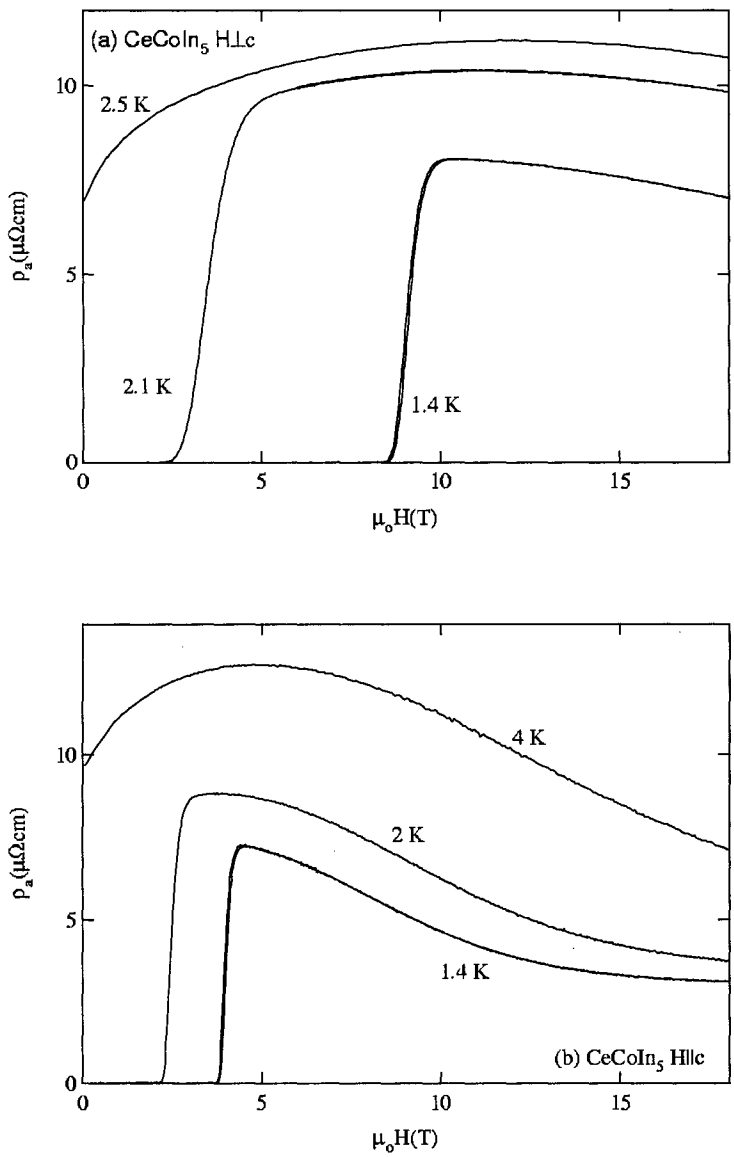

Figure 4.9: Resistivity (ρ) versus applied magnetic fields for $CeCoIn_5$ at low temperatures. (a) displays ρ for applied fields perpendicular to the c-axis and (b) displays ρ for fields parallel to the c-axis.

$\rho = xT^y + z$	$CeIrIn_5$		$CeCoIn_5$	
H‖c	0	18 T	0	18 T
x $((\mu\Omega cm)/K^y)$	1.83 ± 0.05	0.35 ± 0.01	1.44 ± 0.01	1.32 ± 0.03
y	1.01 ± 0.01	1.61 ± 0.02	0.975 ± 0.003	1.17 ± 0.01
z $(\mu\Omega cm)$	0.10 ± 0.08	2.51 ± 0.03	3.63 ± 0.02	0.12 ± 0.06
H⊥c				
x $((\mu\Omega cm)/K^y)$	1.83 ± 0.05	0.46 ± 0.02	1.44 ± 0.01	8.82 ± 0.09
y	1.01 ± 0.01	1.55 ± 0.02	0.975 ± 0.003	0.476 ± 0.003
z $(\mu\Omega cm)$	0.10 ± 0.08	1.86 ± 0.05	3.63 ± 0.02	-3.6 ± 0.1

Table 4.1: Parameters for power law fits ($\rho = xT^y + z$) to the resistivity for the temperature range 2.5 - 6 K for $CeCoIn_5$ and for 2 to 6 K for $CeIrIn_5$. This fits are found to be dependent on the temperature range selected.

power law fits for $CeCoIn_5$ and for fields along the c-axis support the conclusions of ref. [145]. It appears that fermi liquid behavior is promoted by a magnetic field, though the present measurements suffer from lack of low temperature data. For fields applied perpendicular to the c-axis the situation appears to be somewhat different, indicating that future work should concentrate on low temperature measurements to determine if a fermi liquid regime is promoted by applied fields in the basal plane.

4.1.3 Conclusions

The are a number of properties common to all of the members of $CeMIn_5$ as revealed by magnetotransport studies. First, all of the materials exhibit a single impurity regime at high temperature and show signs of developing Kondo lattice behavior at lower temperatures. As in $CeRhIn_5$, the anisotropy observed in the magnetoresistance is not large and is typical of other heavy fermion materials. The magnitude of the magnetoresistance is largest in $CeRhIn_5$, probably due to the the presence of

magnetic fluctuations in addition to the Kondo fluctuations present in all members of the $CeMIn_5$ series. The magnitude of the magnetoresistance of $CeCoIn_5$ is intermediate between that of $CeRhIn_5$ and $CeIrIn_5$. This indicates that in addition to the scattering due to Kondo fluctuations, the scattering caused by magnetic fluctuations are crucial for explaining the magnetotransport properties of $CeMIn_5$. Furthermore, the intermediate amount of magnetic fluctuations present in $CeCoIn_5$ may be further evidence that $CeCoIn_5$ is near a quantum critical point while $CeRhIn_5$ and $CeIrIn_5$ are farther from a quantum critical point on the magnetic and nonmagnetic side respectively. This is consistent with studies which argue that $CeCoIn_5$ is very near to a quantum critical point [146, 147]. In $CeCoIn_5$, it appears that the anisotropy in the magnetoresistance is reflected in the anisotropy in the magnetization. This feature is not present in $CeRhIn_5$ and $CeIrIn_5$. Although in $CeRhIn_5$ the scaling appears to fail less drastically than in $CeIrIn_5$. Ultimately, a description of the magnetotransport in the $CeMIn_5$ series requires the inclusion of the Kondo effect, crystal field effects and magnetic interactions.

Chapter 5

Crystal field studies of $CeRhIn_5$ and $CeIrIn_5$

In this chapter we report the determination of the crystal field levels and parameters which generate them in $CeRhIn_5$ as well as suggestions for the crystal field level splitting in $CeIrIn_5$. In section 5.2, we describe the measurement of the crystal field level scheme in $CeRhIn_5$ with inelastic neutron scattering. Subsequently, we calculate the magnetic susceptibility and specific heat with the results of our studies. In an attempt to further understand the influence of Kondo spin fluctuations upon the behavior of $CeRhIn_5$ calculations have been performed employing the non-crossing approximation (NCA) to the Anderson impurity model. Finally, we show that our investigations produce a crystal field level scheme that is superior to previous attempts that used thermodynamic measurements alone. In section 5.3 we describe attempts to determine the crystal fields levels of $CeIrIn_5$. To date, these attempts have been only partially successful, but do provide guidance as to the appropriate experimental conditions for a successful determination of the crystal level scheme.

5.1 Introduction

Almost all of the thermodynamic properties of materials, especially those at low temperatures, are determined by the characteristics of the lowest-lying electronic states of the system. In 4f systems the spin-orbit interaction generally acts to separate the J-multiplets of the free ion by hundreds, even thousands, of Kelvin. Therefore it is the ground state multiplet that is of greatest interest. When a 4f ion is placed in a crystal, its surroundings both interact directly with the unpaired electrons and impose a lower symmetry than that of the perfectly spherical one of free space. Crystal field theory is the usual method of addressing the description of the splitting of the states of the lowest lying multiplet and allows us to calculate the energies and eigenvectors of the resulting crystal field states.

5.2 $CeRhIn_5$

Recently, it has become apparent that crystal field (CF) effects strongly influence the properties of the $CeMIn_5$ family of heavy fermion superconductors[58, 148, 149](see also chapters 3 and 4), underscoring the fact that the ultimate ground state achieved by a particular member of the family must grow out of a ground state crystal field doublet. Thus a careful determination of both the CF splitting and wave functions of the ground state multiplet is important. To that end we have begun to directly probe the CF energy level splitting in the $CeMIn_5$ family using inelastic (IE) neutron scattering. The first step in our investigations has been determining the crystal field levels in $CeRhIn_5$.

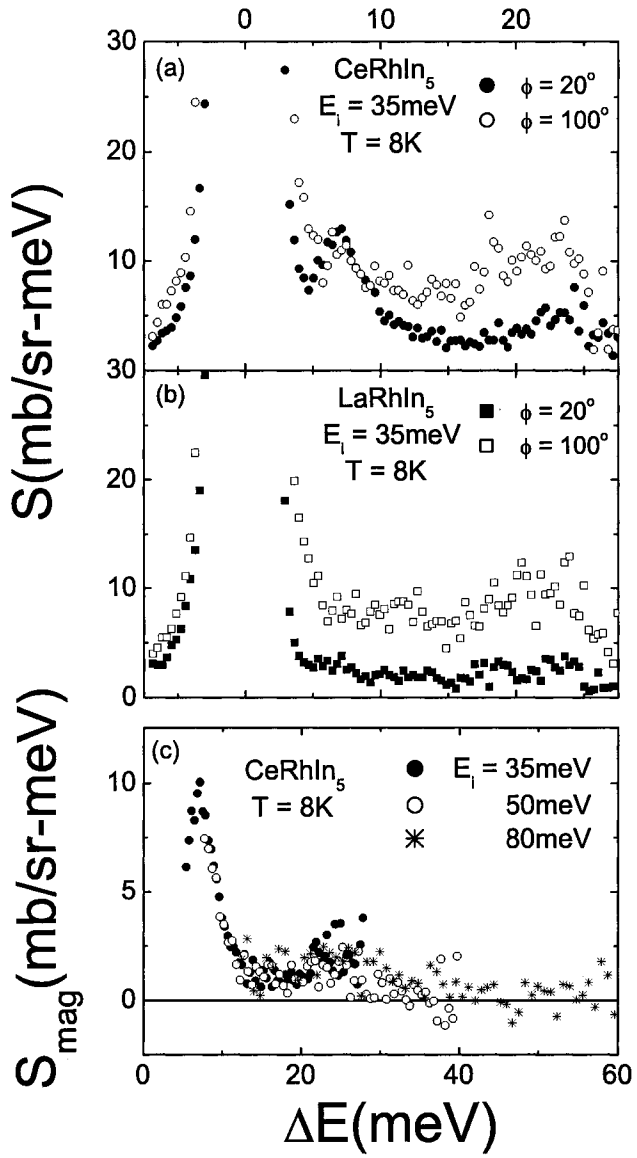

Figure 5.1: Neutron energy spectra of (a) $CeRhIn_5$ and (b) $LaRhIn_5$ at an initial energy E_i = 35 meV, at 8 K and for two mean scattering angles, 20° and 100°. The data have been corrected for neutron absorption and the scattering from the sample holder has been subtracted from the data. (c) The Q=0 magnetic scattering, determined as described in the text, in $CeRhIn_5$ at 8K and for three incident energies E_i.

In $CeRhIn_5$, as in the other members of $CeMIn_5$ family, the crystal field Hamiltonian in tetragonal symmetry can be written

$$H_{CF} = B_2^0 O_2^0 + B_4^0 O_4^0 + B_4^4 O_4^4 \tag{5.2.1}$$

where O_l^m and B_l^m are the Stevens operators, which represent the Ce^{3+} ion symmetry, and CF parameters, which determine the strength of the crystal field, respectively. The Ce^{3+} $J = 5/2$ wave function splits into three doublets, $\Gamma_{7t}^{(1)} = \{\alpha[\pm 5/2\rangle + \beta[\mp 3/2\rangle\}$, $\Gamma_{7t}^{(2)} = \{\beta[\pm 5/2\rangle - \alpha[\mp 3/2\rangle\}$ and $\Gamma_{6t} = [\pm 1/2\rangle$[58]. An analysis of susceptibility and thermal expansion results[126] suggested crystal field levels $\Gamma_7^{(2)}$, $\Gamma_7^{(1)}$ and Γ_6 at E=0, 5.86 meV (68 K) and 28.43 meV (300 K) respectively, with $\beta = 0.969$ (yielding a nearly pure $[\pm 5/2\rangle$ ground state). A subsequent study[58] based on an analysis of the susceptibility and specific heat suggested a similar scheme, but with splittings 6 and 12 meV (70 and 140 K). In this paper we report the results of an analysis of neutron scattering data for $CeRhIn_5$ which indicate that these initial estimates are incorrect; our results have different values for the splittings and a smaller value for the mixing parameter β, i.e., a greater admixture of $[\mp 3/2\rangle$ into the $[\pm 5/2\rangle$ ground state. To assist in comparison of our results to those of previous work [126, 58], we report calculations of the specific heat and magnetic susceptibility based on our CF parameters which include the Kondo effect in an *ad hoc* manner similar to those of refs. [58] and [126]. We also present more sophisticated calculations that employ the non-crossing approximation (NCA)[56, 150] to the Anderson model in order to estimate the effect of Kondo spin fluctuations on the susceptibility, specific heat and IE neutron spectra.

Large high quality single crystals of $CeRhIn_5$ and $LaRhIn_5$ were obtained using

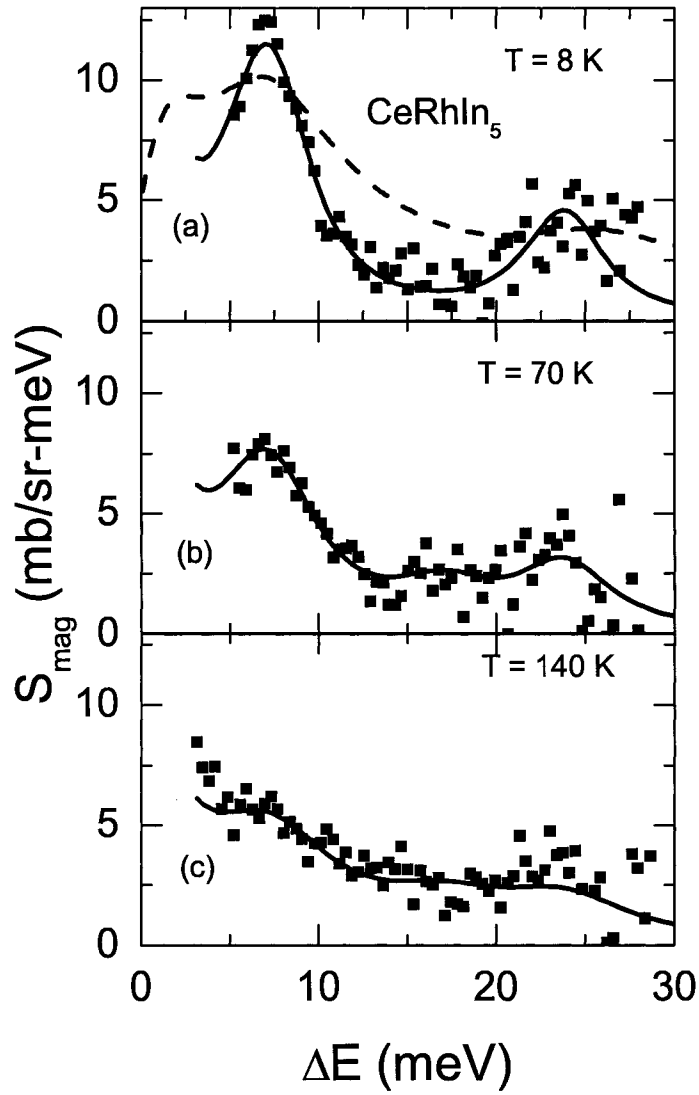

Figure 5.2: Temperature dependence of the magnetic part of the IE neutron scattering response of $CeRhIn_5$ for $E_i = 35$ meV. The scattering dependence due to the Ce^{3+} form factor has been removed as in the previous figure. The data at all three temperatures ((a) 8 K, (b) 70 K, and (c) 140 K) have been fit simultaneously (solid lines) with a least squares fitting routine to determine the crystal field parameters. The results of the fitting parameters including the crystal field parameters are displayed in table 5.1. We have included in (a) the results of the NCA calculation (dashed line).

methods described previously. For the magnetic susceptibility and specific heat measurements, single crystals were carefully prepared which were free of residual In flux; in the case of the neutron scattering measurements, ~50 g of single crystals for both $CeRhIn_5$ and $LaRhIn_5$ were powdered. The neutron scattering experiments were performed in time-of-flight mode using LRMECS at IPNS (Argonne National Laboratory) with experimental conditions that were similar to that of an earlier report[151] (see also section 2.2.2). A key problem in our investigations was the high neutron absorption of both In and Rh. In initial experiments the standard LRMECS sample holder was used; however, in subsequent experiments a new sample holder was designed to maintain a more uniform sample thickness than the standard holder, thus allowing for a more accurate absorption correction. The results for both the standard LRMECS holder and the newer holder were similar, indicating that the absorption correction was appropriate. Neutron scattering spectra were collected for several different incident energies (E_i) and temperatures between 8 and 140 K with counting times ranging from 24 to 48 hours. To improve statistics, we were able to take advantage of the nondispersive nature of the CF scattering and group detectors into three bins with mean scattering angle 20^o (low Q), 60^o and 100^o (high Q). A vanadium standard was utilized to put the scattering on an absolute scale.

Data for $CeRhIn_5$ and $LaRhIn_5$ (measured to help identify the nonmagnetic scattering in $CeRhIn_5$) at 8 K and $E_i = 35$ meV for low and high Q are shown in Fig. 5.1. The data were corrected for absorption assuming a uniformly thick flat-plate sample as well as the scattering due to the empty sample holder. Direct comparison of low angle scattering (where magnetic scattering is strongest) for $CeRhIn_5$ (Fig. 5.1a) and $LaRhIn_5$ (Fig. 5.1b) shows two additional peaks near 7 and 23

meV. In order to interpret the IE neutron scattering spectra it is important to determine the part of the scattering that is magnetic and is thus related to the crystal field excitations. The standard technique is to subtract out the nonmagnetic part of the scattering. The nonmagnetic scattering can be determined in a number of ways, the best method being to compare the scattering of a nonmagnetic analog to the scattering of the material in question. There are a number of methods to do this. All of the methods suffer from the ambiguity introduced by difference of the scattering cross section (σ) of the magnetic and nonmagnetic analog. In particular, we determine the nonmagnetic scattering in $CeRhIn_5$ in two ways: 1) By using the expression $S_{mag}(20°) = S(Ce, 20°) - fS(La, 20°)$ where we choose the factor f as the ratio (0.75) of the total scattering cross-sections $\sigma(CeRhIn_5)/\sigma(LaRhIn_5)$. 2) By determining the ratio $R = S(La, 100°)/S(La, 20°)$ from scaling the high angle nonmagnetic scattering to that of low angle[152]. Excellent agreement with 1) is obtained using $S_{mag}(20°) = S(Ce, 20°) - FS(Ce, 100°)/R$ with inclusion of an additional factor F = 0.75 to account for the difference in Q-scaling of the La and Ce compounds. The value of F is similar to the one used in a recent study of $YbXCu_4$[150]; it can be justified on the basis that for high angle scattering the data are predominantly single-phonon, and proportional to σ, while the low angle scattering contains a significant contribution from multiple scattering (one elastic and one phonon) proportional to σ^2, so that the cross section does not cancel in the ratio. Results of this analysis for three different E_i are shown in Fig. 1c. The dependence of the scattering on the Ce^{3+} form factor has been removed in this plot, so the data represent the $Q = 0$ scattering. The assumption is made that the crystal fields are purely local and uncoupled entities. The data have been truncated below $0.15E_i$ (where the elastic line dominates

B_2^0	B_4^0	B_4^4
-1.03±0.02	0.044±0.001	0.122±0.003
$E(\Gamma_7^1)$	$E(\Gamma_6)$	β
6.9±0.3	23.6±0.5	0.80±0.02
$\Gamma(8K)$	$\Gamma(70K)$	$\Gamma(140K)$
2.3±0.1	2.9±0.2	4.2±0.4

Table 5.1: Crystal field parameters B_l^m, splittings and Lorentzian halfwidths Γ of the IE excitations at four temperatures for $CeRhIn_5$ and the wave function mixing parameter β. The units of all quantities (except for β, which is unitless) are meV. The reduced Chi-square for the fit was $\chi^2 = 0.69$

the scattering) and above $0.8E_i$, where statistics are small due to the k_f/k_i factor present in the scattering cross section (eq. 2.2.9). Good agreement is evident for data taken at three different E_i, with all of the data sets displaying magnetic excitations at approximately 7 and 24 meV.

In Fig. 5.2 we plot the $Q = 0$ (form factor removed) magnetic scattering (method 1), determined at $E_i = 35$ meV, for three different temperatures. We have performed a simultaneous least squares fit to four data sets (8 K, 70 K and 140 K at $E_i = 35$ meV and 8 K at $E_i = 80$ meV) to determine the CF parameters. The fit includes the effects of instrumental resolution. Variables of the fit include B_2^0, B_4^0, B_4^4 and an overall scale factor (which four parameters were constrained to the same values for all data sets) and the Lorentzian halfwidth Γ of the IE excitations which was allowed to vary with temperature. The changes in the Lorentzian halfwidth account for changes in the effective f-conduction electron hybridization as a function of temperature. Due to the limitations imposed by the resolution of LRMECS we were are unable to resolve the

quasi-elastic (QE) contribution to IE spectrum. Therefore, to prevent proliferation of fitting parameters we constrained the quasi-elastic (QE) halfwidth to 1/2 Γ. Results of the fit are shown in Table 5.1 and plotted in Fig. 5.2.

To compare our results to those of Refs. [58] and [126], we have calculated the susceptibility and specific heat (Fig. 5.3). The susceptibility includes a positive molecular field contribution $\lambda = 35$ mol/emu, where λ represents contributions to $1/\chi$ from AF and Kondo fluctuations. At high T these contribute to $1/\chi$ as $(T_K+T_N)/C_J$; with $C_J = 0.807$ emu-K/mol for $J = 5/2$ and $T_N = 3.8$ K. This gives $T_K \sim 25$ K. We note that this value of $k_B T_K$ is similar to the width of the 7 meV IE excitation at 8 K. The calculation for the specific heat contains both a Schottky term due to the excited levels and a Kondo doublet term[121] with $T_K = 25$ K for the ground state level, which puts the calculated specific heat in the range 20-50 K in better agreement with measured value – without this, the calculated value due only to the Schottky contribution is smaller by a factor of 0.8. The Kondo doublet term characterizes the Kondo broadening of the ground state doublet. However, the effect of Kondo spin fluctuations upon the higher crystal field doublets is not included. We have not attempted to fit for the effects on C_{mag} and χ of the AF transition at 3.8 K.

A more sophisticated way to calculate the influence of Kondo spin fluctuations is through the Anderson model (see section 1.2.3. We present results obtained using the non-crossing approximation (NCA) [56, 150]. We have used a Gaussian background band with density of states $N(\varepsilon) = e^{-(\varepsilon/W)^2}/\sqrt{\pi}W$ with $W = 3$ eV, and set the $4f$ level position at $E_f = -2$ eV and the spin-orbit splitting at $E_{so} = 0.273$ eV, which are standard values for Ce. Since the Kondo physics renormalizes the CF levels upward in energy by an amount approximately equal to the Kondo temperature the bare level

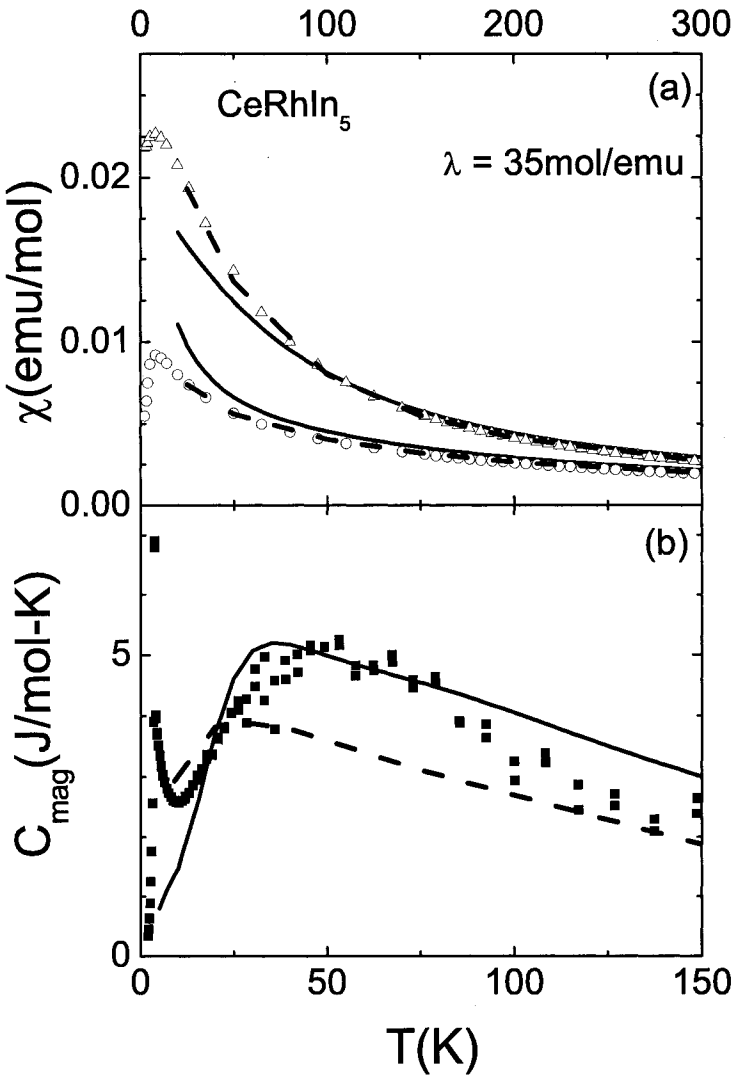

Figure 5.3: (a) Measured anisotropic susceptibilities χ^{zz} (triangles) and χ^{xx} (circles) for $CeRhIn_5$ compared to the value calculated for the CF parameters of Table 5.1 with a molecular field contribution $\lambda = 35$ mol/emu (solid lines) and compared to the results of the NCA calculation (dashed lines). (b) Magnetic specific heat compared to the value calculated for a Schottky contribution from the excited levels and a Kondo contribution from the ground state doublet (solid line) and to the results of the NCA calculation (dashed line).

energies were chosen to be $E_b = 5.3$ meV and $E_c = 23$ meV which are smaller than the measured level energies. The mixing parameter $\beta = 0.80$ was chosen to be similar to that obtained in Table 5.1. The hybridization, V, was then varied until a good fit to the anisotropic susceptibility was obtained for $V = 0.4665$ eV. The results for S_{mag}, χ and C_{mag} are given in Figs. 5.2a and 5.3.

We now turn to the discussion of the effect of systematic errors on our conclusions. As mentioned previously, the neutron absorption of In and Rh is an important consideration. Comparison of the data for two different sample holders (which exhibited small differences in sample thickness and distribution) indicated similar results, augmenting our belief that the absorbtion correction employed is correct. If the nonmagnetic background subtraction is varied by varying f (method 1) or F/R (method 2), the scattering at 7 meV is relatively unaffected, but the strength of the 24 meV scattering, and hence β, is affected somewhat. Given the consistency between results at different E_i and T we think that our CF scheme is correct. We were unable to observe quasi-elastic (QE) scattering, due to the requirement that to obtain the resolution necessary a small E_i is required which causes the effects of neutron absorption, which varies as $1/\sqrt{E}$, to become large. In our fits we constrained the QE halfwidth to half the value of the IE width to prevent proliferation of fit parameters. Constraining to other values (e.g. $\Gamma_{QE} = \Gamma_{IE}$) leads only to minor variation in the final fits.

Our fits to χ using the CF parameters and a molecular field term are not as good as those of Refs. [58] and [126]. A possible reason that our fits are not as good as those of refs. [58] and [126] is that we do not include the effect of exchange anisotropy, which should only be important below 20 K. Such anisotropy can be mimicked as in

[58] through inclusion of an anisotropic mean field parameter, which we have chosen not to do for the sake of simplicity. The inclusion of a mean field parameter in addition to the crystal field parameters, in our opinion, leads to a proliferation of fit parameters which has the potential to generate incorrect results. To further emphasize this point, the fits of refs. [58] and [126] produce a value of β very close to unity, indicating essentially no $[\mp 3/2\rangle$ admixture into $[\pm 5/2\rangle$ ground state. In this case there would be no observable amplitude for the $\Delta m_z = 1$ transition to $[\pm 1/2\rangle$ state at 24 meV. This cannot be correct as we clearly observe this transition in the neutron scattering data. Comparison to the ordered moment of $CeRhIn_5$ observed by neutron diffraction yields further insight. $CeRhIn_5$ is found to exhibit a spiral structure with the magnetic moment lying completely in the basal plane of the tetragonal structure. The value of the moment is $0.75\mu_B$ [1]. The ordered moment must arise from the ground state doublet. Calculations of the in-plane and z-axis moments are shown in table 5.2. The results of Refs. [58] and [126] clearly cannot account for the observed ordered moment and must be discarded on these grounds alone.

On the other hand, the NCA calculations based on our CF scheme and a Kondo temperature of order 25 K does an excellent job reproducing χ. However, it overestimates the width of the 7 meV excitation as seen in Fig. 2a and underestimates the temperature of the peak in the specific heat (Fig. 3b). These deviations from the data may reflect the fact that we have neither included antiferromagnetic exchange, exchange anisotropy, nor anisotropic hybridization (i.e., different hybridization of the different CF states) in the NCA fits.

In summary, we find a more significant $[\mp 3/2\rangle$ admixture into $[\pm 5/2\rangle$ ($\beta = 0.80$) ground state than found earlier by Refs. [126] ($\beta = .969$) or [58] ($\beta \sim 1$). Moreover,

	This Study (neutron scattering)	Ref. [58] (magnetic susceptibility and specific heat)	Ref. [126] (magnetic susceptibility and specific heat)
1^{st} excited splitting	79 K	70 K	68 K
2^{nd} excited splitting	274 K	140 K	330 K
Admixture of $\frac{5}{2}$ and $\frac{3}{2}$	0.8	$\sim$1	0.969
Magnetic Moment (in plane)	$0.92\mu_B$	$\sim 0\mu_B$	$0.46\mu_B$
Magnetic Moment (z)	$0.91\mu_B$	$\sim 2.14\mu_B$	$1.93\mu_B$

Table 5.2: Comparison to other attempts to determine the crystal field level schemes in $CeRhIn_5$. Note that the ordered magnetic moment determined by neutron diffraction is $0.75\mu_B$[1].

only the parameters obtained in this study can properly account for the ordered moment observed in neutron diffraction experiments. To emphasize this last point table 5.2 shows the calculated magnetic moments for the different determinations of the crystal field splitting. Most importantly, the calculated in-plane magnetic moment of refs. [58] and [126] is simply to low to account for the ordered moment. The resulting CF level parameters provide reasonable fits to both the magnetic susceptibility and specific heat with the inclusion of a mean field parameter and a Kondo doublet respectively. In addition, NCA fits the susceptibility remarkably well with some deficiencies in both the specific heat and neutron scattering linewidths. Taken together the NCA calculations and the fits to specific heat and susceptibility all indicate a $T_K \sim 25$ K. We note that the ordered moment $g\mu_B\langle J_x\rangle = 0.92\mu_B$ deduced for β =0.80 is larger than the value $0.75\mu_B$ needed to fit the diffraction pattern in the ordered state[1]. This is a common feature of magnetically ordered heavy fermion materials where the ordered moment is reduced from that expected for the ground state by the Kondo effect[117].

5.3 $CeIrIn_5$

In order to determine if there is a systematic relationship between the crystal level schemes in the $CeMIn_5$ family of compounds and the ground state realized by a particular member it is important to determine the CF energy level splitting in several members. We have attempted to identify the CF level scheme in $CeIrIn_5$, but owing to the simultaneous limitations imposed by the poor resolution of LRMECS and the high (larger than $CeRhIn_5$) neutron absorption we have been unable to definitively observe any crystal field excitation in $CeIrIn_5$. However, from the experiments that

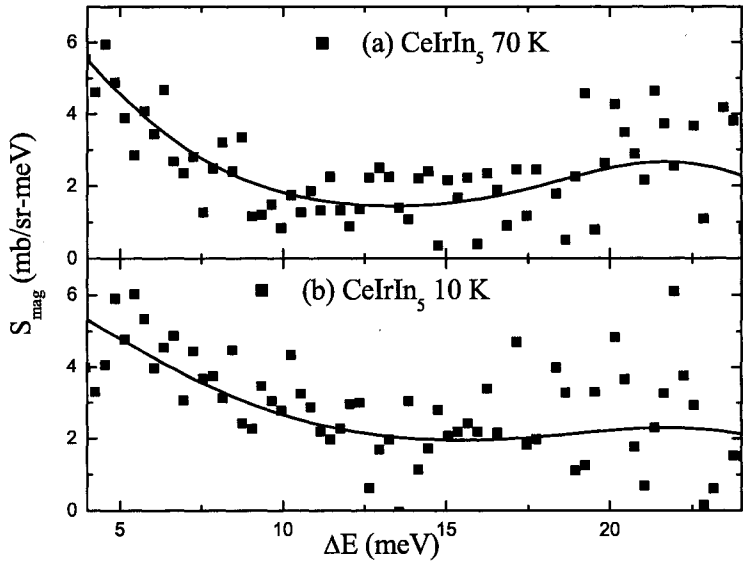

Figure 5.4: Temperature dependence of the magnetic part of the IE neutron scattering response of $CeIrIn_5$ for $E_i = 30$ meV. The raw data (solid squares) is show at (a) 70 K and (b) 10 K. The line is a guide to the presence of possible crystal field excitations at 3 and 23 meV.

have been performed we are now in a position to predict the energy range where CF excitations are likely to be observed as well as select the appropriate experimental conditions required.

Figure 5.4 shows several spectra taken for $CeIrIn_5$ which show that an instrument possessing higher resolution is needed in order to resolve scattering at low energies. The line in both (a) and (b) emphasizes a possible excitation at $\sim$ 3 meV as well as a very weak excitation at $\sim$ 23 meV. More solid conclusions require that an instrument with high resolution be used with a larger incident energy so that conditions to observed the 3 and 23 meV features are optimized.

	$CeRhIn_5$	$CeIrIn_5$	$CeIrIn_5$	$CeCoIn_5$	$CeCoIn_5$
	This Work	Ref. [58]	Ref. [126]	Ref. [148]	Ref. [149]
1^{st} excited splitting	79 K	45 K	61 K	34 K	148 K
2^{nd} excited splitting	274 K	125 K	300 K	102 K	197 K
ground state wave function	$0.80\left\|\pm\frac{5}{2}\right\rangle$ $-0.60\left\|\mp\frac{3}{2}\right\rangle$	$0.66\left\|\pm\frac{5}{2}\right\rangle$ $+0.76\left\|\mp\frac{3}{2}\right\rangle$	$-0.98\left\|\pm\frac{5}{2}\right\rangle$ $+0.20\left\|\mp\frac{3}{2}\right\rangle$	$\left\|\pm\frac{1}{2}\right\rangle$	$-0.39\left\|\pm\frac{5}{2}\right\rangle$ $+0.92\left\|\mp\frac{3}{2}\right\rangle$

Table 5.3: The various proposed crystal field level schemes for the $CeMIn_5$ family. All of the measurements, except those for $CeRhIn_5$, have been performed utilizing a combination of magnetic susceptibility, specific heat, nuclear magnetic resoance, and thermal expansion.

5.4 Conclusions

Table 5.3 shows various crystal field parameters for the members of the $CeMIn_5$ series. Notice that the only determination using neutron scattering is that described in section 5.2 for $CeRhIn_5$ (we have shown that the other determinations of the crystal field are unlikely to be correct and therefore have not been included in this table). Furthermore, there is significant disagreement between the different determinations for $CeCoIn_5$ and $CeIrIn_5$. Before rigorous conclusions may be drawn regarding the systematic influence of crystal field splitting on the heavy fermion ground state in the $CeMIn_5$ series the conflicts must be resolved. The best way to resolve these discrepancies is through inelastic neutron scattering and future work should be concentrated in that direction.

Chapter 6

Conclusions

This thesis has investigated several aspects of the exotic magnetic and superconducting ground states found in heavy fermion materials. Here we have chosen as examples the recently discovered $CeMIn_5$ family. This family provides a unique opportunity for systematic study of the magnetic and superconducting ground states due to the high quality of the samples, the presence of magnetic and superconducting ground states in the same crystal structure with the only difference being a different transition metal from the same column of the periodic table.

We have found that all of the members of the $CeMIn_5$ series exhibit a high temperature single impurity-like regime and a low temperature Kondo lattice regime. Magnetotransport measurements of $CeMIn_5$ family further indicate a moderate degree of anisotropy consistent with the influence of the effect of crystal field splitting. These measurements further augment the conclusion that two different Kondo regimes are present in these materials. At lower temperatures application of magnetic fields along the c-axis of $CeRhIn_5$ show that the magnetically ordered state is remarkably stable to large values of magnetic field, which is consistent with previous work. In the

superconducting members of $CeMIn_5$ (M = Co and Ir), the application of magnetic fields appears to promote the formation of a fermi liquid regime. Future work should concentrate on exploring this in further detail

To further understand the influence of crystal field splitting to the ground state properties of $CeMIn_5$ we have determined the crystal field level scheme of $CeRhIn_5$. Comparison to the value of the ordered magnetic moment obtained from neutron diffraction measuremnets indicate that our results are superior to previous work in this regard. Moreover, we are able to produce reasonable fits to the specific heat and magnetic susceptibility. To look for systematic correlations between crystal field splitting and the ground state in the different members of $CeMIn_5$ we have attempted to determine the crystal level scheme in $CeIrIn_5$ with inelastic neutron scattering as we have done in $CeRhIn_5$. These experiments were at best partially suscessful, but they do provide guidance for future experiments. A comparison of the crystal field splitting as determined by bulk measurements for $CeIrIn_5$ and $CeCoIn_5$ indicates large discrepancies. Thus reliable conclusions pertaining to the influence of crystal field splitting upon the exotic ground states in the $CeMIn_5$ family await a sound determination of the crystal field splitting with a direct technique such as neutron scattering.

Bibliography

[1] Wei Bao, P.G. Pagliuso, J.L. Sarrao, J.D. Thompson, Z. Fisk, J.W. Lynn, and R.W. Erwin, "Incommensurate Magnetic Structure of $CeRhIn_5$," *Phys. Rev. B*, vol. 62 and 63, p. 14621 and 219901(E), 2000 and 2001.

[2] N.D. Mathur, F.M. Grosche, S.R. Julian, I.R. Walker, D.M. Freye, R.K.W. Haselwimmer, and G.G. Lonzarich, "Magnetically Mediated Superconductivity in Heavy Fermion Compounds," *Nature*, vol. 394, p. 39, 1998.

[3] H. Hegger, C. Petrovic, E.G. Moshopoulou, M.F. Hundley, J.L. Sarrao, Z. Fisk, and J.D. Thompson, "Pressure-Induced Superconductivity in Quasi-2D $CeRhIn_5$," *Phys. Rev. Lett.*, vol. 84, p. 4986, 2000.

[4] Y. Haga, Y. Inada, H. Harima, K. Oikawa, M. Murakawa, H. Nakawaki, Y. Tokiwa, D. Aoki, H. Shishido, S. Ikeda, N. Watanabe, and Y. Onuki, "Quasi-two-dimensional Fermi Surfaces of the Heavy Fermion Superconductor $CeIrIn_5$," *Phys. Rev. B*, vol. 63, p. 060503(R), 2001.

[5] D.L. Cox and N. Grewe, "Transport Porperties of the Anderson Lattice," *Z. Phys. B-Condensed Matter*, vol. 71, p. 321, 1988.

[6] A.L. Cornelius, P.G. Pagliuso, M.G. Hundley, and J.L. Sarrao *Phys. Rev. B*, vol. 64, p. 144411, 2001.

[7] K. Andres, J.E. Graebner, and H.R. Ott, "4f-Virtual-Bound-State Formation in $CeAl_3$ at Low Temperatures," *Phys. Rev. Lett.*, vol. 35, p. 1779, 1975.

[8] F. Steglich, J. Aarts, C.D. Bredl, W. Lieke, D. Meschede, W. Franz, and H. Schäfer, "Superconductivity in the Presence of strong Pauli Paramagnetism: $CeCu_2Si_2$," *Phys. Rev. Lett.*, vol. 43, p. 1892, 1979.

[9] H.R. Ott, H. Rudiger, Z. Fisk, and J.L. Smith, "UBe_{13}: An Unconventional Actinide Superconductor," *Phys. Rev. Lett.*, vol. 52, p. 1595, 1983.

[10] G.R. Stewart, Z. Fisk, J.O. Willis, and J.L. Smith, "Possibility of Coexistence of Bulk Superconductivity and Spin Fluctuations in UPt_3," *Phys. Rev. Lett.*, vol. 52, p. 679, 1984.

[11] G. Aeppli, E. Bucher, C. Broholm, J.K. Kjems, J. Baumann, and J. Hufnagl, "Magnetic Order and Fluctuations in Superconducting UPt_3," *Phys. Rev. Letts.*, vol. 60, p. 615, 1988.

[12] T.T.M Palstra, A.A. Menovsky, J. van den Berg, P.J. Dirkmaat, P.H. Kes, G.J. Nieuwenhuys, and J.A. Mydosh, "Superconducting and Magnetic Transitions in the Heavy-Fermion System URu_2Si_2," *Phys. Rev. Lett.*, vol. 55, p. 2727, 1985.

[13] P. Chandra, P. Coleman, J.A. Mydosh, and V. Tripathi, "Hidden orbital order in the heavy fermion metal URu_2Si_2," *Nature*, vol. 417, p. 831, 2002.

[14] P. Haen, J. Flouquet, F. Lapierre, and P. Lejay, "Metamagnetic-Like Transition in $CeRu_2Si_2$," *J. Low Temp. Phys.*, vol. 67, p. 391, 1987.

[15] A. Lacerda, A. de Visser, P. Haen, P. Lejay, and J. Flouquet, "Thermal Properties of Heavy-Fermion $CeRu_2Si_2$," *Phys. Rev. B*, vol. 40, p. 8759, 1989.

[16] A de Visser, F.R. de Boer, A.A. Menovsky, and J.J.M. Franse, "High-field transitions in URu_2Si_2 observed by magnetoresistivity and magnetization experiments," *Solid Sate Commun.*, vol. 64, p. 527, 1987.

[17] P.H. Frings and J.J.M. Franse, "Susceptibility of Spin-fluctuation Compounds in High Magnetic Fields," *Phys. Rev. B*, vol. 31, p. 4355, 1985.

[18] J.A. Detwiler, G.M. Schmiedeshoff, N. Harrison, A.H. Lacerda, J.C. Cooley, and J.L. Smith, "Magnetization of UBe_{13} to 60 T," *Phys. Rev. B*, vol. 61, p. 402, 2000.

[19] M.K. Wu, J.R. Ashburn, C.J. Torng, P.H. Hor, R.L. Meng, L. Gao, Z.J. Huang, Y.Q. Wang, and C.W. Chu, "Superconductivity at 93 K in a New Mixed-Phase Y-Ba-Cu-O Compound System at Ambient Pressure," *Phys. Rev. Lett.*, vol. 58, p. 908, 1987.

[20] R.J. Cava, B. Batlogg, R.B. van Dover, D.W. Murphy, S. Sunshine, T. Siegrist, J.P. Remeika, E.A. Rietman, S. Zahurak, and G.P. Espinosa, "Bulk Superconductivity at 91 K in Single-Phase Oxygen-Deficient Perovskite $Ba_2YCu_3O_{9-\delta}$," *Phys. Rev. Lett.*, vol. 58, p. 1676, 1987.

[21] For example, A.J. Millis, H. Monien, D. Pines, "Phenomenlogical Model of Nuclear Relaxation in the Normal State Of $YBa_2Cu_3O_7$," *Phys. Rev. B*, vol. 42, p. 167, 1990.

[22] K. Miyake, S. Schmitt-Rink, and C.M. Varma, "Spin-fluctuation-meadiated Even-parity Pairing in Heavy Fermion Superconductors," *Phys. Rev. B*, vol. 34, p. 6554, 1986.

[23] P. Monthoux and D. Pines, "$YBa_2Cu_3O_7$: A Nearly Antiferromagnetic Fermi Liquid," *Phys. Rev. B*, vol. 47, p. 6069, 1993.

[24] T. Moriya, Y. Takahashi, and K. Ueda, "Antiferromagnetic Spin Fluctuations and Superconductivity in Two-Dimensional Metals - Possible Model for High T_c Oxides," *J. Phys. Soc. Jap.*, vol. 59, p. 2905, 1990.

[25] H. Takagi, B. Batlogg, H.L. Kao, J. Kwo, R.J. Cava, J.J. Krajewski, and W.F. Peck Jr., "Systematic Evolution of Temperature-Dependent Resistivity in $La_{2-x}Sr_xCuO_4$," *Phys. Rev. Lett.*, vol. 69, p. 2975, 1992.

[26] T. Ito, H. Takagi, S. Ishibashi, T. Ido, S. Uchida, Uchida S, "Normal-state Conductivity Between CuO_2 Planes In Copper-Oxide Superconductors," *Nature*, vol. 350, p. 596, 1991.

[27] P. Monthoux and G.G. Lonzarich, "p-Wave and d-Wave Superconductivity in Quasi-two-dimensional Metals," *Phys. Rev. B*, vol. 59, p. 14598, 1999.

[28] W. Lieke, U. Rauchschwable, C.B. Bredl, and F. Steglich, "Superconductivity in $CeCu_2Si_2$," *J. of Appl. Phys.*, vol. 53, p. 2111, 1982.

[29] C.D. Bredl, H. Spille, U. Rauchschwalbe, W. Lieke, F. Steglich, G. Cordier, W. Assmus, M. Herrmann, and J. Aarts, "Gapless Superconductivity and Variation of T_c in the Heavy-Fermion System $CeCu_2Si_2$," *J. Magn. Magn. Mater.*, vol. 31-34, p. 373, 1983.

[30] D. Jaccard, K. Behnia, and J. Sierro *Phys. Lett. A*, vol. 163, p. 475, 1992.

[31] R. Movshovich, T. Graf, D. Mandrus, J.D. Thompson, J.L. Smith, and Z. Fisk, "Superconductivity in heavy-fermion $CeRh_2Si_2$," *Phys. Rev. B*, vol. 53, p. 8241, 1996.

[32] M.F. Hundley, J.L. Sarrao, J.D. Thompson, R. Movshovich, M. Jaime, C. Petrovic, Z. Fisk, "Unusual Kondo Behavior in the Indium-rich Heavy-Fermion Antiferromagnet $Ce_3Pt_3In_13$," *Phys. Rev. B*, vol. 65, p. 24401, 2002.

[33] S. Quezel, P. Burlet, J.L. Jacoud, L.P. Regnault, J. Rossat-Mignod, C. Vettier, P. Lejay, and J. Flouquet, "Magnetic-Ordering in $Ce_xLa_{1-x}Ru_2Si_2$ Solid-Solutions," *J. Magn. Magn. Mater.*, vol. 76 & 77, p. 403, 1988.

[34] I.R. Walker, F.M. Grosche, D.M. Freye, and G.G. Lonzarich, "The Normal and Superconducting States of $CeIn_3$ Near the Border of Antiferromagnetic Order," *Physica C*, vol. 282-287, p. 303, 1997.

[35] C. Petrovic, R. Movshovich, M. Jaime, P.G. Pagliuso, M.F. Hundley, J.L. Sarrao, J.D. Thompson, and Z. Fisk, "A New Heavy-fermion superconductor $CeIrIn_5$: A Relative of the Cuprates?," *Europhys. Lett.*, vol. 84, p. 354, 2001.

[36] C. Petrovic, P.G. Pagliuso, M.F. Hundley, "R. Movshovich, J.L. Sarao, J.D. Thompson, and Z. Fisk, "Heavy-fermion Superconductivity in $CeCoIn_5$ at 2.3 K," *J. Phys. Condens. Matter*, vol. 13, p. L337, 2001.

[37] E.G. Moshopoulou, Z. Fisk, J.L. Sarrao, and J.D. Thompson, "Crystal Growth and Intergrowth Structure of the New Heavy Fermion Materials $CeIrIn_5$ and $CeRhIn_5$," *J. Solid State Chem.*, vol. 158, p. 25, 2001.

[38] Y. Kohori, Y. Yamato, Y. Iwamoto, and T. Kohara, "Appearence of Anisotropic non s-wave Superconductivity Above the Critical Pressure of Antiferromagnetic $CeRhIn_5$," *Eur. Phys. J. B*, vol. 18, p. 601, 2000.

[39] T. Mito, S. Kawasaki, G.-q. Zheng, Y. Kawasaki, K. Ishida, Y. Kitaoka, D. Aoki, Y. Haga, and Y. Onuki, "Pressure-induced Anomalous Magnetism and Unconventional Superconductivity in $CeRhIn_5$: ^{115}In-NQR study under pressure," *Phys. Rev. B*, vol. 63, p. 220507(R), 2001.

[40] R. Movshovich, M. Jaime, J.D. Thompson, C. Petrovic, Z. Fisk, P.G. Pagliuso, and J.L. Sarrao, "Unconventional Superconductivity in $CeIrIn_5$ and $CeCoIn_5$: Specific Heat and Thermal Conductivity Studies," *Phys. Rev. Lett.*, vol. 86, p. 5152, 2001.

[41] N. Ashcroft and N. Mermin, *Solid State Physics*. Forth Worth: Saunders College Publishing, 1976.

[42] E.A. Goremychkin, R. Osborn, A. Yu. Muzychka, "Crystal-field effects in $PrCu_3Si_2$: An evaluation of evidence for heavy-fermion behavior," *Phys. Rev. B*, vol. 50, p. 13863, 1994.

[43] S. Doniach and S. Engelsberg, "Low-Temperature Properties of Nearly Ferromagnetic Fermi Liquids," *Phys. Rev. Letts.*, vol. 17, p. 750, 1966.

[44] L.D. Landau, "The Theory of a Fermi Liquid," *Eksp. Teor. Fiz. [Sov. Phys. JETP3, 920 (1957)]*, vol. 30, p. 1058, 1957.

[45] L.D. Landau, "Oscillations in a Fermi Liquid," *Eksp. Teor. Fiz. [Sov. Phys. JETP **5**, 101 (1957)].*, vol. 32, p. 59, 1957.

[46] A. Abrikosov, *Fundamentals of the Theory of Metals.* Amsterdam: North-Holland, 1988.

[47] Z. Fisk, P.C. Canfield, W.P. Beyermann, J.D. Thompson, and M.F. Hundley, M.B. Maple, M.A. Lopez de la Torre, P. Visani, and C.L. Seaman, "Massive Electron State in YbBiPt," *Phys. Rev. Lett.*, vol. 67, p. 3310, 1991.

[48] S. Kondo, D.C. Johnston, C.A. Swenson, F. Borsa, A.V. Mahajan, L.L. Miller, T. Gu, A.I. Goldman, M.B. Maple, D.A. Gajewski, E.J. Freeman, N.R. Dilley, R.P. Dickey, J. Merrin, K. Kojima, G.M. Luke, Y.J. Uemura, O. Chmaissen, and J.D. Jorgensen, "LiV_2O_4: A Heavy Fermion Transition Metal Oxide," *Phys. Rev. Lett.*, vol. 78, p. 3729, 1997.

[49] A. Hewson, *The Kondo Problem to Heavy Fermions, Cambridge Studies in Magnetism vol. 2.* Cambridge: Cambridge University Press, 1997.

[50] K. Yosida, *Theory of Magnetism, Springer Series in Solid-State Sciences vol. 122.* Berlin: Springer, 1998.

[51] W.J. de Haas, J. de Boer, G.J. van den Berg, "The Electrical Resistance of Gold, Copper, and Lead at Low Temperatures," *Physica*, vol. 1, p. 1115, 1933-34.

[52] J. Kondo, "Resistance Minimum in Dilute Magnetic Alloys," *Prog. Theoret. Phys.*, vol. 32, p. 37, 1964.

[53] S. Doniach, in *Valence Instabilities and Related Narrow Band Phenomena*, ed. R.D. Parks (Plenum, New York, 1977), p. 169, "Phase Diagram for the Kondo Lattice,"

[54] S. Doniach, "The Kondo Lattice and Weak Antiferromagnetism," *Physica B*, vol. 91, p. 231, 1977.

[55] P.W. Anderson, "Localized Magnetic States in Metals," *Phys. Rev.*, vol. 124, p. 41, 1961.

[56] N.E. Bickers, D.L. Cox, and J.W. Wilkins, "Self-consistent Large-N Expansion for Normal-state Properties of Dilute Magnetic Alloys," *Phys. Rev. B*, vol. 36, p. 2036, 1987.

[57] Y. Kuramoto, "Self-Consistent Perturbation Theory for Dynamics of Valence Fluctuations: I. Single-Site Theory," *Z. Phys. B*, vol. 53, p. 37, 1983.

[58] P.G. Pagliuso, N.J. Curro, N.O. Moreno, M.F. Hundley, J.D. Thompson, J.L. Sarrao, and Z. Fisk, "Structurally Tuned Superconductivity in Heavy-Fermion $CeMIn_5$ (M=Co, Ir, Rh)," *Physica B*, vol. 320, p. 370, 2002.

[59] T. Takimoto, T. Hotta, T. Maehira, and K. Ueda, "Spin-fluctuation-induced Superconductivity Controlled by Orbital Fluctuation," *J. Phys. Condens. Matter*, vol. 14, p. L369, 2002.

[60] M.T. Hutchings, "Point-Charge Calculations of Energy Levels of Magnetic Ions in Crystalline Electric Fields," *Solid State Physics*, vol. 16, p. 277, 1965.

[61] K.R. Lea, M.J.M Leask, and W.P. Wolf, "The Raising of Angular Momentum Degeneracy of f-Electron Terms by Cubic Fields," *J. Phys. Chem. Solids*, vol. 23, p. 1381, 1962.

[62] K.W.H. Stevens, "Matrix Elements and Operator Equivalents Connected with the Magnetic Properties of Rare Earth Ions," *Proc. Phys. Soc. Lond.*, vol. A65, p. 209, 1952.

[63] H.A. Kramers, "General Theory of a Paramagnetic Rotation in Crystals," *Pro. Acad. Amsterdam*, vol. 33, p. 959, 1930.

[64] U. Walter, "Treating Crystal Field Parameters in Lower Than Cubic Symmetries," *J. Phys. Chem. Solids*, vol. 45, p. 401, 1984.

[65] P. M. Levy and S. Zhang, "Crystal-Field Splitting in Kondo Systems," *Phys. Rev. Lett.*, vol. 62, p. 78, 1989.

[66] A.P. Murani, A.D. Taylor, R. Osborn, and Z.A. Bowden, "Evolution of the Spin-Orbit Excitaion with Increasing Kondo Energy in $CeIn_{3-x}Sn_x$," *Phys. Rev. B*, vol. 48, p. 10606, 1993.

[67] M.S.S. Brooks, O. Eriksson, J.M. Wills, and B. Johansson, "Density Functional Theory of Crystal Field Quasiparticle Excitations and the Ab Initio Calculation of Spin Hamiltonian Parameters," *Phys. Rev. Letts.*, vol. 79, p. 2546, 1997.

[68] J.D. Thompson, R. Movshovich, Z. Fisk, F. Bouguet, N.J. Curro, R.A. Fisher, P.C. Hammel, H. Hegger, M.F. Hundley, M. Jaime, P.G. Pagliuso, C. Petrovic, N.E. Phillips, and J.L. Sarrao, "Superconductivity and Magnetism in a New Class of Heavy-Fermion Materials," *J. Mag. Mag. Mater.*, vol. 226, p. 5, 2001.

[69] P.G. Pagliuso, J.D. Thompson, M.F. Hundley, J.L. Sarrao, and Z. Fisk, "Crystal Structure and Low-temperature Magnetic Properties of R_mMIn_{3m+2} Compounds (M = Rh or Ir; m = 1,2; R = Sm or Gd)," *Phys. Rev. B*, vol. 63, p. 054426, 2001.

[70] Z. Fisk, J.P. Remeika, "Growth of Single Crystals From Molten Metal Fluxes," in: K.A. Gschneidner Jr., L. Eyrig (Eds.), Handbook on the Physics and Chemistry of Rare Earths, Vol 12, Elsevier, Amsterdam, 1989, p. 53.

[71] P.C. Canfield and Z. Fisk, "Growth of Single Crystals From Metallic Fluxes," *Philos. Mag. B*, vol. 65, p. 1117, 1992.

[72] A.L. Cornelius, A.J. Arko, J.L. Sarrao, M.F. Hundley, and Z. Fisk, "Anisotropic Electronic and Magnetic Properties of the Quasi-two-dimensional Heavy-fermion Antiferromagnet $CeRhIn_5$," *Phys. Rev. B*, vol. 62, p. 14181, 2000.

[73] A.D. Christianson, A.H. Lacerda, M.F. Hundley, P.G. Pagliuso, and J.L. Sarrao, "Magnetotransport of $CeRhIn_5$," *Phys. Rev. B*, vol. 66, p. 054410, 2002.

[74] D. Hall, E.C. Palm, T.P. Murphy, S.W. Tozer, C. Petrovic, E. Miller-Ricci, L. Peabody , C.Q Huei-Li, U. Alver, R. G. Goodrich, J.L. Sarrao, P.G. Pagliuso, J.M. Wills, and Z. Fisk, "Electronic Structure of $CeRhIn_5$: de Haas-van Alphen and Energy Band Calculations," *Phys. Rev. B*, vol. 64, p. 064506, 2001.

[75] D. Hall, E.C. Palm, T.P. Murphy, S.W. Tozer, Z. Fisk, U. Alver, R.G. Goodrich, J.L. Sarrao, P.G. Pagliuso, and T. Ebihara, "Fermi Surface of the Heavy-fermion Superconductor $CeCoIn_5$: The de Haas-van Alphen Effect in the Normal State," *Phys. Rev. B*, vol. 64, p. 212508, 2001.

[76] R. Settai, H. Shishido, S. Ikeda, Y. Murakawa, M. Nakashima, D. Aoki, Y. Haga, H. Harima, and Y. Onuki, "Quasi-two-dimensional Fermi surfaces and the de Haas-van Alphen Oscillation in Both the Normal and Superconducting Mixed States of $CeCoIn_5$," *J. Phys. Condens. Matter*, vol. 13, p. L627, 2000.

[77] N.J. Curro, P.C. Hammel, P.G. Pagliuso, J.L. Sarrao, J.D. Thompson, and Z. Fisk, "Evidence for Spiral Magnetic Order in the Heavy Fermion Material $CeRhIn_5$," *Phys. Rev. B*, vol. 62, p. 6100, 2000.

[78] K.H.J. Buschow, H.W. de Wijn, and A.M. van Diepen, "Magnetic Susceptibilities of Rare-Earth-Indium Compounds: RIn_3," *J. Chem. Phys.*, vol. 50, p. 137, 1969.

[79] J.M. Lawrence and S.M. Shapiro, "Magnetic Ordering in the Presence of Fast Spin Fluctuations: A Neutron Scattering Study of $CeIn_3$," *Phys. Rev. B*, vol. 22, p. 4379, 1980.

[80] A. Benoit, J.X. Boucherle, P. Convert, J. Flouquet, J. Palleau, and J. Schweizer, "Magnetic Structure of the Compound $CeIn_3$," *Solid State Commun.*, vol. 34, p. 293, 1980.

[81] R.A. Fisher, F. Bouquet, N.E. Phillips, M.F. Hundley, P.G. Pagliuso, J.L. Sarrao, Z. Fisk, and J.D. Thompson, "Specific Heat of $CeRhIn_5$: Pressure-driven Evolution of the Ground State from Antiferromagnetism to Superconductivity," *Phys. Rev. B*, vol. 65, p. 224509, 2002.

[82] M. Nicklas *et al.*, "unpublished,"

[83] W. Bao, S.F. Trevino, J.W. Lynn, P.G. Pagliuso, J.L. Sarrao, J.D. Thompson, and Z. Fisk, "Effect of Pressure on Magnetic Structure in Heavy Fermion $CeRhIn_5$," *Appl. Phys. A*, vol. 74, p. S557, 2002.

[84] W. Bao, A.D. Christianson, P.G. Pagliuso, J.L. Sarrao, J.D. Thompson, A.H. Lacerda, J.W. Lynn, "Effect of La Doping on Magnetic Structure in Heavy Fermion $CeRhIn_5$," *Physica B*, vol. 312-313, p. 120, 2002.

[85] A.D. Christianson and A. Lobet *et al.* in preperation

[86] J.S. Kim, J. Alwood, G.R. Stewart, J.L. Sarrao, and J.D. Thompson, "Specific Heat in High Magnetic Fields and non-Fermi-liquid Behavior," *Phys. Rev. B*, vol. 64, p. 134524, 2001.

[87] W. Bao, G. Aeppli, A.D. Christianson, Z. Fisk, M.F. Hundley, A.H. Lacerda, J.W. Lynn, P.G. Paglisuo, J.L. Sarrao, and J.D. Thompson, "Magnetic Properties of Heavy Fermion Superconductors $CeRhIn_5$ and Ce_2RhIn_8," *Int. J. Mod. Phys.*, vol. 16, p. 3244, 2002.

[88] G.-q. Zheng, K. Tanabe, T. Mito, S. Kawasaki, Y. Kitaoka, D. Aoki, Y. Haga, and Y. Onuki, "Unique Spin Dynamics and Unconventional Superconductivity in the Layered Heavy Fermion Compound $CeIrIn_5$: NQR Evidence," *Phys. Rev. Lett.*, vol. 86, p. 4664, 2001.

[89] P.G. Pagliuso, C. Petrovic, R. Movshovich, D. Hall, M.F. Hundley, J.L. Sarrao, J.D. Thompson, and Z. Fisk, "Coexistance of Magnetism and Superconductivity in $CeRh_{1-x}Ir_xIn_5$," *Phys. Rev. B*, vol. 64, p. 100503(R), 2001.

[90] P.G. Pagliuso, R. Movshovich, A.D. Bianchi, M. Nicklas, N.O. Moreno, J.D. Thompson, M.F. Hundley, J.L. Sarrao, and Z. Fisk, "Multiple Phase Transitions in Ce(Rh,Ir,Co)In_5," *Physica B.*

[91] J. Bass, W.P. Pratt Jr., and P.A. Schroeder, "The Temperature-dependent Electrical Resistivities of the Alkali Metals," *Rev. Mod. Phys.*, vol. 62, p. 645, 1990.

[92] A.J. Dekker, "Electrical Resistivity of Metals and Alloys Containing Localized Magnetic Moments," *J. Appl. Phys.*, vol. 36, p. 1965, 1965.

[93] V.U.S. Rao and W.E. Wallace, "Calculation of the Influence of the Crystalline Electric Field on the Spin-Disorder Resistivity of Rare-Earth Alloys and Comparison with Results on $CeAl_2$," *Phys. Rev. B*, vol. 2, p. 4613, 1970.

[94] A. Pippard, *Magnetoresistance in Metals.* Cambridge: Cambridge University Press, 1989.

[95] M.D. Daybell and W.A. Steyert, "Observation of Nagoaka's Bound State for Conduction Electrons in Dilute Magnetic Alloys," *Phys. Rev. Lett.*, vol. 18, p. 398, 1967.

[96] M.D. Daybell and W.A. Steyert, "Thermal and Magnetic Degradation of the Quasibound State in Dilute Magnetic Copper-Chromium Alloys," *Phys. Rev. Lett.*, vol. 20, p. 195, 1968.

[97] E.T. Hedgcock, W.B. Muir, T.W. Raudorf, and R. Szmidt, "Magnetoresistance and Magnetization in Cu:Fe Alloys Below 4.2 K," *Phys. Rev. Lett.*, vol. 20, p. 457, 1968.

[98] H. Rohrer, "Magnetoresistance of Dilute Alloys," *Phys. Rev.*, vol. 174, p. 583, 1968.

[99] P. Monod, "Magnetic Field Dependence of the Kondo Resistivity Minimum in CeFe and CuMn Alloys," *Phys. Rev. Lett.*, vol. 19, p. 1113, 1967.

[100] R. More and H. Suhl, "Magnetoresistance of Dilute Magnetic Alloys," *Phys. Rev. Lett.*, vol. 20, p. 500, 1968.

[101] M.-T Béal-Monod and R,A. Weineré, "Negative Magnetoresistivity in Dilute Alloys," *Phys. Rev.*, vol. 170, p. 552, 1968.

[102] U. Rauchschwalbe, "Magnetic Properties of Heavy-Fermion Superconductors," *Physica B*, vol. 147, p. 1, 1987.

[103] G.M. Roesler, Jr. and P.M. Tedrow, "Scaling Behavior of the Giant Anisotripic Magnetoresistance in Thin Films of the Heavy Fermion $CeAl_3$," *Phys. Rev. B*, vol. 45, p. 12893, 1992.

[104] J. Flouquet, P. Haen, F. Lapierre, D. Jaccard, and G. Remenyi, "Experimental Aspects of Heavy Fermions," *J. Magn. Magn. Mater.*, vol. 54-57, p. 322, 1986.

[105] M.C. Aronson, J.D. Thompson, J.L. Smith, Z. Fisk, and M.W. McElfresh, "Kondo Coherence in UBe_{13}: Magnetoresistance at High Pressure," *Phys. Rev. Lett.*, vol. 63, p. 2311, 1989.

[106] J.M. Lawrence, T. Graf, M.F. Hundley, D. Mandrus, J.D. Thompson, A. Lacerda, M.S. Torikachvili, J.L. Sarrao, and Z. Fisk, "Kondo Hole Behavior in $Ce_{0.97}La_{0.03}Pd_3$," *Phys. Rev. B*, vol. 53, p. 12559, 1996.

[107] A.L. Cornelius, J.M. Lawrence, T. Ebihara, P.S. Riseborough, C.H. Booth, M.F. Hundley, P.G. Pagliuso, J.L. Sarrao, J.D. Thompson, M.H. Jung, A.H. Lacerda, and G.H. Kwei, "Two Energy Scales and Slow Crossover in $YbAl_3$," *Phys. Rev. Lett.*, vol. 88, p. 117201, 2002.

[108] F.J. Ohkawa, "Magnetoresistance of Kondo Lattices," *Phys. Rev. Lett.*, vol. 64, p. 2300, 1990.

[109] A. Lorek, N. Grewe, and F.B. Anders, "Magnetotransport in Heavy Fermion Compounds," *Solid State Commun.*, vol. 78, p. 167, 1991.

[110] F.B.Anders and M. Huth, "The Influence of the Dynamics of Ionic Multiplets onto Electronic Transport Properties of Heavy-Fermion Systems: a Semi-Phenomenological Approach," *Eur. Phys. J. B*, vol. 19, p. 491, 2001.

[111] G. Squires, *Introduction to the Theory of Thermal Neutron Scattering.* Mineola: Dover, 1986.

[112] J. T. G. Shirane, S.M. Shapiro, *Neutron Scattering with a Triple-Axis Spectrometer.* Cambridge: Cambridge University Press, 2002.

[113] A.J. Freeman and J.P. Desclaux, "Dirac-Fock Studies of Some Electronic Properties of Rare-Earth Ions," *J. Magn. Magn. Mater.*, vol. 12, p. 11, 1979.

[114] K.C. Tuberfield, L. Passell, R.J. Birgeneau, and E. Bucher, "Neutron Crystal-Field Spectroscopy in Rare-Earth Metallic Compounds," *J. Applied Phys.*, vol. 42, p. 1746, 1971.

[115] C. Kittel and H. Kroemer, *Thermal Phyiscs 2nd ed.* New York: Freeman, 1980.

[116] J. Griffith, *The Theory of Transition-Metal Ions.* Cambridge: Cambridge University Press, 1961.

[117] Z. Fisk, D.W. Hess, C.J. Pethick, D. Pines, J.L. Smith, J.D. Thompson, J.O. Willis, "Heavy-Electron Metals: New Highly Correlated States of Matter," *Science*, vol. 239, p. 33, 1988.

[118] Z. Fisk, J.L. Sarrao, J.L. Smith, and J.D. Thompson, "The Physics and Chemistry of Heavy Fermions," *Proc. Natl. Acad. Sci.*, vol. 92, p. 6663, 1995.

[119] J.J.M. Franse, "High-Magnetic-Field Experiments in Heavy-Fermion Systems," *Physica B*, vol. 155, p. 236, 1989.

[120] U. Rauchschwalbe, F. Steglich, and H. Rietschel, "Low-Temperature Resistivity of UBe_13 in High Magnetic Fields," *Europhysics. Lett.*, vol. 1, p. 71, 1986.

[121] V.T. Rajan, "Magnetic Susceptibility and Specific Heat of the Coqblin-Schrieffer Model," *Phys. Rev. Lett.*, vol. 51, p. 308, 1983.

[122] Wei Bao, G. Aeppli, J.W. Lynn, P.G. Pagliuso, J.L. Sarrao, M.F. Hundley, J.D. Thompson, and Z. Fisk, "Anisotropic Three-Dimensional Magnetic Fluctuations in Heavy Fermion $CeRhIn_5$," *Phys. Rev. B*, vol. 65, p. 100505, 2002.

[123] H.C. Montgomery, "Method for Measuring Electrical Resistivity of Anisotropic Materials," *J. Appl. Phys.*, vol. 42, p. 2971, 1971.

[124] L.J. van der Pauw, "A Method of Measuring Specific Resistivity and Hall Effect of Dics of Arbitrary Shape," *Philips Research Reports*, vol. 13, p. 1, 1958.

[125] W.L.V. Price, "Electric Potential and Current Distribution in a Rectangular Sample of Anisotropic Material with Application to the Measurement of the Principal Resistivities by an Extension of van der Pauw's Method," *Solid-State Elect.*, vol. 16, p. 753, 1973.

[126] T. Takeuchi, T. Inoue, K. Sugiyama, D. Aoki, Y. Tokiwa, Y. Haga, K. Kindo, and Y. Onuki, "Magnetic and Thermal Properties of $CeIrIn_5$ and $CeRhIn_5$," *J. Phys. Soc. Japan*, vol. 70, p. 877, 2001.

[127] M.F. Hundley, P.G. Pagliuso, J.L. Sarrao, T.A. Brandman, J.M. Wills, and J.D. Thompson, "unpublished,"

[128] U. Alver, R.G. Goodrich, N. Harrison, D.W. Hall, E.C. Palm, T.P. Murphy, S.W. Tozer, P.G. Pagliuso, N.O. Moreno, J.L. Sarrao, and Z. Fisk, "Localized f electrons in $Ce_xLa_{1-x}RhIn_5$," *Phys. Rev. B*, vol. 64, p. 180402(R), 2001.

[129] A.D. Christianson, J.M. Lawrence, P.G. Pagliuso, N.O. Moreno, J.L. Sarrao, J.D. Thompson, P.S. Riseborough, S. Kern, E.A. Goremychkin, and A.H. Lacerda, "Neutron Scattering Study of Crystal Fields in $CeRhIn_5$," *Phys. Rev. B*, vol. 66, p. 193102, 2002.

[130] F. Lapierre and P. Haen, "Resistivity Anisotropy in $CeRu_2Si_2$," *J. Magn. Magn. Mater.*, vol. 108, p. 167, 1992.

[131] T. Fukuhara, K. Maezawa, H. Ohkuni, J. Sakurai, and H. Sato, "Anisotropic Transport and Magnetic Properties of $CeNi_2Ge_2$," *J. Magn. Magn. Mater.*, vol. 140-144, p. 889, 1995.

[132] A. Amato, D. Jaccard, E. Walker, and J. Flouquet, "Transport Properties of $CeCu_6$ Single Crystals," *Solid State Commun.*, vol. 55, p. 1131, 1985.

[133] A.K. Bhattacharjee, B. Coqblin, M. Raki, L. Forro, C. Ayache, and D. Schmitt, "Anisotropy of Transport Properties in the Kondo Compound $CePt_2Si_2$: Experiments and Theory," *J. Phys. (France)*, vol. 50, p. 2781, 1989.

[134] R.A. Steeman, E. Frikkee, R.B. Helmholdt, A.A. Menovsky, J. van den Berg, G.J. Nieuwenhuys, and J.A. Mydosh, "$CePd_2Si_2$: A Reduced-Moment Antiferromagnetic," *Solid State Commun.*, vol. 66, p. 1988, 1988.

[135] W. Assmus, M. Herrmann, U. Rauchschwalbe, S. Rigel, W. Lieke, H. Spille, S. Horn, G. Weber, F. Steglich, and G. Cordier, "Superconductivity in $CeCu_2Si_2$ Single Crystals," *Phys. Rev. Lett.*, vol. 52, p. 469, 1984.

[136] S. Kashiba, S. Maekawa, S. Takahashi, and M. Tachiki, "Effect of Crystal Field on Kondo Resistivity in Ce Compounds," *J. Phys. Soc. Jpn.*, vol. 55, p. 1341, 1986.

[137] N. Kawakami, A. Nakamura, and A. Okiji, "Crystal-Field Effects on Thermoelectic Power and Resistivity for the Ce-Kondo System," *J. Phys. Soc. Jpn.*, vol. 57, p. 4359, 1988.

[138] S.M.M. Evans, A.K. Bhattacharjee, and B. Coqblin, "A Theoretical Study of the Anisotropic Susceptibility and Resistivity in Heavy Fermion Compounds," *Physica B*, vol. 165&166, p. 413, 1990.

[139] S.M.M. Evans, A.K. Bhattacharjee, and B. Coqblin, "Anisotropic Transport Properties of Cerium Kondo Compounds," *Phys. Rev. B*, vol. 45, p. 7244, 1992.

[140] B. Coqblin, A.K. Bhattacharjee, and S.M.M. Evans, "Anisotropy Effects in Cerium Kondo Compounds," *J. Magn. Magn. Mater.*, vol. 90&91, p. 393, 1990.

[141] M. Raki, L. Forro, C. Ayache, D. Schmitt, A.K. Bhattacharjee, and B. Coqblin, "Anisotropic Transport Properties of Cerium Kondo Compounds," *Physica B*, vol. 163, p. 93, 1990.

[142] U. Rauchsschwalbe, F. Steglich, and H. Rietschel, "Magneto-Resistance of Heavy-Fermion Compounds," *Physica B*, vol. 148B, p. 33, 1987.

[143] V.S. Zaph, E.J. Freeman, E.D. Bauer, J. Petricka, C. Sirvent, N.A. Frederick, R.P. Dickey, and M.B. Maple, "Coexistance of Superconductivity and Antiferromagnetism in $CeRh_{1-x}Co_xIn_5$," *Phys. Rev. B*, vol. 65, p. 14506, 2001.

[144] P.G. Pagliuso, N.O. Moreno, N.J. Curro, J.D. Thompson, M.F. Hundley, J.L. Sarrao, Z. Fisk, A.D. Christianson, A.H. Lacerda, B.E. Light, and A.L. Cornelius, "Ce-site Dilution Studies in the Antiferromagnetic Heavy Fermions $Ce_mRh_nIn_{3m+2n}$ (m=1,2;n=0,1)," *Phys. Rev. B*, vol. 66, p. 54433, 2002.

[145] J. Paglione, *et al. unpublished.*

[146] M. Nicklas, R. Borth, E. Lengyel, P.G. Pagliuso, J.L. Sarrao, V.A. Sidorov, G. Sparn, F. Steglich, and J.D. Thompson, "Response of the Heavy-Fermion Superconductor $CeCoIn_5$ to Pressure: Roles of Dimensionality and Proximity to a Quantum-Cirtical Point," *J. Phys. Condens. Matter*, vol. 13, p. L905, 2001.

[147] V.A. Sidorov, M. Nicklas, P.G. Pagliuso, J.L. Sarrao, Y. Bang, A.V. Balatsky, and J.D. Thompson, "Superconductivity and Quantum Criticality in $CeCoIn_5$," *Phys. Rev. Lett.*, vol. 89, p. 157004, 2002.

[148] N.J. Curro, B. Simovic, P.C. Hammel, P.G. Pagliuso, J.L. Sarrao, J.D. Thompson, "Anomalous NMR Magnetic Shifts in $CeCoIn_5$," *Phys. Rev. B*, vol. 64, p. 180514(R), 2001.

[149] S. Nakatsuji, S. Yeo, L. Balicas, Z. Fisk, P. Schlottmann, P.G. Pagliuso, N.O. Moreno, J.L. Sarrao, and J.D. Thompson, "Intersite Coupling Effects in a Kondo Lattice," *Phys. Rev. Letts.*, vol. 89, p. 106402, 2002.

[150] J.M. Lawrence, P.S. Riseborough, C.H. Booth, J.L.Sarrao, J.D. Thompson and R. Osborn, "Slow Crossover in $YbXCu_4$ (X=Ag, Cd, In, Mg, Tl, Zn) Intermediate-Valence Compounds," *Phys. Rev. B*, vol. 63, p. 054427, 2001.

[151] J.M. Lawrence, R. Osborn, J.L. Sarrao, Z. Fisk, "Time-of-flight Neutron-scattering Study of $YbInCu_4$ and $YbIn_{0,3}Ag_{0.7}Cu_4$," *Phys. Rev. B*, vol. 59, p. 1134, 1999.

[152] E.A. Goremychkin and R. Osborn, "Crystal-field Excitations in $CeCu_2Si_2$," *Phys. Rev. B*, vol. 47, p. 14280, 1993.